https://theses.gla.ac.uk/

Theses Digitisation:

https://www.gla.ac.uk/myglasgow/research/enlighten/theses/digitisation/

This is a digitised version of the original print thesis.

Copyright and moral rights for this work are retained by the author

A copy can be downloaded for personal non-commercial research or study, without prior permission or charge

This work cannot be reproduced or quoted extensively from without first obtaining permission in writing from the author

The content must not be changed in any way or sold commercially in any format or medium without the formal permission of the author

When referring to this work, full bibliographic details including the author, title, awarding institution and date of the thesis must be given

Enlighten: Theses
https://theses.gla.ac.uk/
research-enlighten@glasgow.ac.uk

A METHOD FOR THE DESIGN OF MULTIRATE SAMPLED-DATA DIGITAL FLIGHT CONTROL SYSTEMS OF PILOTED AIRCRAFT

By

Colin Goodchild C.Eng MIEE.

Dissertation submitted to the Faculty of Engineering, University of Glasgow, for the Degree Doctor of Philosophy.

September 1990

© C Goodchild 1990

ProQuest Number: 10983750

All rights reserved

INFORMATION TO ALL USERS
The quality of this reproduction is dependent upon the quality of the copy submitted.

In the unlikely event that the author did not send a complete manuscript
and there are missing pages, these will be noted. Also, if material had to be removed,
a note will indicate the deletion.

ProQuest 10983750

Published by ProQuest LLC (2018). Copyright of the Dissertation is held by the Author.

All rights reserved.
This work is protected against unauthorized copying under Title 17, United States Code
Microform Edition © ProQuest LLC.

ProQuest LLC.
789 East Eisenhower Parkway
P.O. Box 1346
Ann Arbor, MI 48106 – 1346

ABSTRACT

The initial flight-test operations of piloted aircraft, in which Digital Flight Control (DFC) systems were first employed, exposed handling qualities problems that were not predicted during the design stage. Subsequent studies attributed the cause of these problems to the techniques used in the design of the digital control systems. The particular feature which unites the reported difficulties is that, an infinite-resolution sampled-data model is assumed for the design process but the practical DFC implementation is realised as an amplitude-quantised sampled-data system.

A modern DFC system exemplifies the concept of a mixed-data, digital control system. In the case of an aircraft, a mixed-data flight control system is a configuration of the following data domains: The Continuous-Amplitude, Continuous-Time (CACT) domain of the basic aircraft model; the Discrete-Amplitude, Discrete-Time (DADT) domain of the flight control computer; and the Discrete-Amplitude, Continuous-Time (DACT) domain of the basic aircraft's control data. This observation, which defines the data-domains of a DFC system, exposes an interesting paradox; viz. the theoretical techniques for mixed-data system design are defined in a domain that does not exist in a modern DFC system. This non-existent domain is the Continuous Amplitude, Discrete Time (CADT) domain and is usually referred to as the sampled-data domain. In addition to the mixed-data issue, a modern DFC system communicates with other aircraft-subsystems using a wide variety of data formats and information bandwidths. Consequently the DFC system must combine these various data

structures into a unified flight-control data-set.

This dissertation describes a DFC system design methodology. The rationale of the methodology is to unify the flight control data types and give contemporaneous consideration to the quantisation issue of the implementation domain, within a framework of familiar CADT domain techniques. The basis of the methodology is a multirate sampled-data model and a direct digital design approach. A general feature of multirate sampled-data systems is the rapid expansion of the model complexity. To minimise the possibility of model assembly errors, an effective assembly-management technique is required. This requirement is satisfied in the proposed multirate sampled-data design model through a systematic assembly procedure.

In contrast to the normal qualitative practice of selecting a practical sampling-rate for a unirate system, the proposed multirate sampled-data DFC design methodology incorporates an analytical selection technique for the sampling policy. The technique has the facility of directly referring the sampling-rate of a given state element to a specification of an aircraft's handling qualities, as embodied in the military standard MIL-F-8785C.

Extensions of both the w- and w'-plane design methods to the multivariable, multirate sampled-data domain are developed. Although both the w- and in particular the w'-plane are established techniques for the design of unirate sampled-data DFC systems, their widespread adoption is impeded by the need to map a w plane design

model from a z-plane transfer-function description. Algorithms are described which avoid the transfer-function mapping route and allow an easy transition between the CADT state-space and the w planes. Apart from yielding a less cumbersome symbolic form of a w plane transfer-function representation, the proposed algorithms have the facility to model multivariable systems.

Parameters to assess the performance of the direct digital design and multirate sampled-data models are also developed. These parameters are derived directly from a discrete system description and therefore contrast with the usual s- to z-plane parameter maps. The assessment of multirate sampled-data systems is facilitated through the development of a two parameter root-locus diagram.

The proposed DFC design methodology is tested through a case study. Although relatively simple, the case study exercises most of the techniques developed in this dissertation.

ACKNOWLEDGEMENTS

During the research and preparation of this dissertation I have received advice and encouragement from many of my colleagues in the Faculty of Engineering. In particular, I place on record my gratitude to John Anderson, for his counselling and conscientious reviews of my work. I also acknowledge the advocacy of my Head of Department, Dr. R. A. McD. Galbraith, whose valuable comments have galvanised my efforts on many occasions. In addition, my gratitude is extended to the University of Glasgow and the Department of Aerospace Engineering for the resources and services made available to complete this dissertation.

C.G. September 1990.

GLOSSARY

CHAPTER ONE

INTRODUCTION

1.1 THE FUTURE REQUIREMENTS AND CURRENT PROBLEMS OF DFC SYSTEMS 1-1

1.2 THE CASE FOR DIGITAL FLIGHT CONTROL RESEARCH 1-3

1.3 THE PROPOSED DFC SYSTEM DESIGN METHODOLOGY 1-5

1.4 ORGANISATION OF THE DISSERTATION 1-4

CHAPTER TWO

MODELLING AIRCRAFT DYNAMICS FOR DIGITAL FLIGHT CONTROL

2.1 INTRODUCTION 2-1

2.1.1 A Generic Aircraft Model For DFC Design 2-1

2.2 THE ANALOGUE-DATA MODEL OF THE BASIC AIRCRAFT 2-3

2.3 PRELIMINARY ISSUES 2-5

2.3.1 Definitions of Continuous and Discrete Systems 2-5

2.3.2 The Mixed-Data Configuration of a DFC Aircraft 2-7

2.3.3 Data Domain Conversion 2-8

2.3.4 The Proposed Route for DFC Design 2-9

2.3.5 The Case for DFC Design in the CADT Domain 2-10

2.4 DISCRETE-DATA MODELS OF CONTINUOUS-TIME SYSTEMS 2-12

2.4.1 Transfer Function Methods 2-14

2.4.2 State-Space Mapping Methods 2-17

2.4.3 Mapping a CACT Model into the CADT Domain 2-21

2.5 SUMMARY 2-27

CHAPTER THREE

A SAMPLED-DATA AIRCRAFT MODEL FOR DFC DESIGN

3.1 INTRODUCTION 3-1

3.2 THE SAMPLING RATE SELECTION PROBLEM 3-3

3.2.1 Sampling Rate and Digital Processing Wordlength 3-4

3.3 SELECTING A SAMPLING POLICY 3-6

3.3.1 Sampling Policy Selection Procedure 3-8

3.3.2 The Presentation of a Multirate Sampling Policy 3-14

3.4 A MULTIRATE SAMPLED-DATA MODEL FOR DFC DESIGN 3-15

3.4.1 A Review of Multirate Sampled-Data Modelling Methods 3-16

3.4.2 A Development of a Multirate Sampled-Data System Model 3-17

3.4.3 A Proposed Model of a Multirate Sampled-Data System 3-18

3.4.4 Multirate Sampling with State-Feedback 3-26

3.4.5 An Alternative Form of the Multirate Sampling Model 3-32

3.5 ACCOUNTING FOR COMPUTATIONAL DELAY IN THE DFC CONTROLLER 3-35

3.6 SUMMARY 3-37

CHAPTER FOUR

DESIGN AND ANALYSIS OF DFC SYSTEMS

4.1 INTRODUCTION 4-1

4.2 w-PLANE AND w'-PLANE DESIGN AND ANALYSIS 4-3

4.2.1 Properties of the w-Plane 4-4

4.2.2 The w-Plane Analogue of Frequency 4-5

4.2.3 Properties of the w'-Plane 4-6

4.2.4 Frequency Response Plots in the w- and w'-Planes 4-9

4.2.5 Mapping the State Equations to the w- and w'-Planes 4-14

4.3 ANALYSIS PARAMETERS FOR CADT DIRECT DIGITAL DESIGN 4-19

4.3.1 Envelope-Frequency and Samples-per-Envelope-Cycle 4-20

4.3.2 Decrement-per-Envelope-Cycle 4-22

4.3.3 Natural Frequency and Resonance Magnification 4-23

4.3.4 The Two Parameter Root-Locus 4-25

4.4 SUMMARY 4-31

CHAPTER FIVE

A DIGITAL FLIGHT CONTROL DESIGN CASE STUDY

5.1 INTRODUCTION 5-1

5.2 A STATEMENT OF THE FLIGHT CONTROL PROBLEM 5-2

5.3 THE SAMPLING POLICY 5-6

5.4 THE MULTIRATE SAMPLED-DATA MODEL 5-11

5.5 THE DIGITAL DESIGN PROCEDURE 5-13

5.5.1 The Design of a Stability Augmentation System 5-14

5.5.2 The Design of a Speed-Attitude Decoupling Law 5-16

5.5.3 The Digital Flight Controller 5-17

5.5.4 Test Results 5-19

5.6 SUMMARY 5-22

CHAPTER SIX

CONCLUSIONS AND RECOMMENDATIONS FOR FURTHER RESEARCH

6.1 GENERAL CONCLUSIONS 6-1

6.2 TOPICS FOR FURTHER RESEARCH 6-6

APPENDIX ONE

A BASIC AIRCRAFT MODEL FOR DFC DESIGN

A1.1 INTRODUCTION A1-1

A1.2 A METHOD OF ASSEMBLING THE BASIC AIRCRAFT MODEL A1-1

A1.3 REASONS FOR THE PROPOSED MODELLING METHOD A1-6

A1.4 A CADT MAPPING METHOD FOR RANK DEFICIENT SYSTEMS A1-7

A1.5 SUMMARY A1-10

APPENDIX TWO

A STUDY OF DIGITAL DESIGN METHODS

A2.1 INTRODUCTION A2-1

A2.2 A COMPARISON OF DIGITAL SYSTEM DESIGN METHODS A2-2

A2.2.1 Experiments to Compare Digital Design Methods A2-3

A2.3 THE EXPERIMENTS IN DIGITAL DESIGN METHODS A2-5

A2.3.1 Stability Measured Against Sampling Period A2-9

A2.3.2 Disturbance Measured Against Sampling Period A2-11

A2.4 SUMMARY A2-13

APPENDIX THREE

SAMPLING, QUANTISATION AND DATA RESOLUTION

A3.1 INTRODUCTION A3-1

A3.2 THE PROBLEM STATEMENT A3-1

A3.3 SAMPLING, QUANTISATION AND DATA RESOLUTION COMPROMISES A3-2

A3.4 SUMMARY A3-4

APPENDIX FOUR

NOISE PROCESSES AND SAMPLED-DATA SYSTEMS

A4.1 INTRODUCTION A4-1

A4.2 NOISE PROCESSES IN CONTINUOUS-TIME SYSTEMS A4-1

A4.3 NOISE PROCESSES IN DISCRETE-TIME SYSTEMS A4-3

A4.4 THE EQUIVALENT DISCRETE MODEL FOR A SAMPLED-DATA SYSTEM A4-4

A4.4.1 The Covariance Matrix of a Sampled-Data Noise A4-7

A4.5 SUMMARY A4-9

APPENDIX FIVE

MODELLING A MULTIRATE SAMPLED-DATA SYSTEM

A5.1 INTRODUCTION A5-1

A5.2 THE PROBLEM STATEMENT A5-1

A5.2.1 The Assembly of the Closed-Loop Sampled-Data Model A5-2

A5.3 SUMMARY A5-6

APPENDIX SIX

MULTIVARIABLE w-PLANE AND w'-PLANE MODELS

A6.1 INTRODUCTION A6-1

A6.2 MAPPING THE CADT STATE-SPACE MODEL TO THE w-PLANE A6-1

A6.3 MAPPING THE CADT STATE-SPACE MODEL TO THE w'-PLANE A6-5

A6.4 SUMMARY A6-6

APPENDIX SEVEN

ANALYSIS TECHNIQUES FOR DIRECT DIGITAL DESIGN

A7.1 INTRODUCTION A7-1

A7.2 A REVIEW OF CACT DOMAIN DESIGN AND ANALYSIS CRITERIA A7-1

A7.3 THE DEVELOPMENT OF CADT DOMAIN DESIGN AND ANALYSIS CRITERIA A7-3

A7.3.1 Damping Factor in the CADT Domain A7-6

A7.3.2 Natural-Frequency and Resonance in the CADT Domain A7-9

A7.4 SUMMARY A7-12

REFERENCES

GLOSSARY

LIST OF SYMBOLS

$\mathbf{A}$	Continuous data domain state matrix.
$\mathbf{A}_w$	w Domain state matrix.
$\mathbf{A}_{w'}$	w' Domain state matrix.
$\mathbf{B}$	Continuous data controls input matrix.
$\mathbf{B}_w$	w Domain controls input matrix.
$\mathbf{B}_{w'}$	w' Domain controls input matrix.
$\mathbf{C}$	Continuous data state output matrix.
$\mathbf{C}_D$	Discrete data domain state output matrix.
$\mathbf{C}_w$	w Domain state output matrix.
$\mathbf{C}_{w'}$	w' Domain state output matrix.
$\mathbf{D}$	Continuous data domain direct matrix.
$\mathbf{D}_D$	Discrete data domain direct matrix.
$\mathbf{D}_w$	w Domain direct matrix.
$\mathbf{D}_{w'}$	w' Domain direct matrix.
$\mathbf{F}_{x,y,u}$	Coefficients of a linearised state equation.
$\mathbf{G}_C$	Continuous domain state covariance matrix.
$\mathbf{G}_K$	Discrete domain state covariance matrix.
$\mathbf{G}_{x,y,u}$	Coefficient matrices of a linearised output equation.
$\mathbf{H}$	State feedback matrix.
$\mathbf{H}_{x,y,u}$	Coefficient matrices of a linearised auxiliary equation.
$\mathbf{I}$	Identity matrix.
$\mathbf{M}$	General matrix expression.
$\mathbf{N}$	General matrix expression.
$\mathbf{Q}_C$	Covariance matrix of continuous input disturbances.
$\mathbf{U}(s)$	Vector of Laplace transformed open-loop control inputs.

$\mathbf{U}(z)$	Vector of z transformed open-loop control inputs.
$\mathbf{a}(t)$	Vector of a state-space system's auxiliary functions.
$\mathbf{u}(*)$	Vector of *-domain open-loop control inputs.
$\mathbf{v}(*)$	Vector of *-domain closed-loop inputs.
$\mathbf{w}_Q$	Vector of quantisation noise functions.
$\mathbf{x}(*)$	Vector of *-domain state functions
$\mathbf{y}(*)$	Vector of *-domain output functions.
C	Transfer function controlled variable, s,z,w, or w'-plane.
D	Transfer function denominator variable, s,z,w, or w'-plane.
G	Open-loop transfer function, s,z,w, or w'-plane.
H	Transfer function feedback variable, s,z,w, or w'-plane.
K	Transfer function gain, s,z,w, or w'-plane.
M_E	Aerodynamic moment about y-axis due to η (Appendix One).
$M_{\dot{\alpha}}$	Aerodynamic moment about y-axis due to $\dot{\alpha}$ (Appendix One).
M_α	Aerodynamic moment about y-axis due to α (Appendix One).
M_θ	Aerodynamic moment about y-axis due to θ (Appendix One).
R	Transfer function reference input, s,z,w, or w'-plane.
U_o	Aircraft equilibrium speed.
Z_α	Aerodynamic force along z-axis due to α (Appendix One).
Z_E	Aerodynamic force along z-axis due to η (Appendix One).
d_i	i-th Indexed denominator component of a transfer function.
g_{ij}	Element ij of the matrix $\mathbf{G}_c$.
h, h_i	Sampling period, general and i-th, respectively.
i	The i-th member of a discrete sequence.
m	General dimension of a state vector.
m_z	Resonance magnification on the z-plane.
n	A general number.
n_i	i-th Index numerator component of a transfer function.

n_z	Aircraft normal acceleration (Appendix One).
q	General dimension of a control input vector
q	Aircraft pitch-rate (Chapter Five) (Radians-per-second).
r	General dimension of a state output vector
r	z-Plane Radial (Chapter Four).
s_k	k-th sampling switch.
T	Time period of a periodic function.
t	Time.
t_0	Initial time.
u(*)	Scalar element of **u**(*).
u	Aircraft forward (x-axis) speed,(Chapter Five)(Metres/sec).
v(*)	Scalar element of **v**(*).
W	Digital-data wordlength, number of binary digits.
w	Aircraft normal (z-axis) speed, (Chapter Five)(Meters/sec).
Γ	A matrix function of the state matrix, **A**.
Δ	A time period < h.
Δ_P	A multirate discrete system controls input matrix.
Θ_P	A multirate discrete system direct matrix.
Λ_D	A diagonal form of Φ.
Λ_P	A multirate discrete system input matrix.
Π	Submatrix of a closed-loop multirate state matrix.
Φ	Discrete data domain state matrix.
Φ_P	A multirate discrete system state matrix.
X_P	A multirate discrete system state output matrix.
Ψ	Discrete data domain controls input matrix.
α	Matrix dimension.
α	Aircraft angle of attack (Appendix One).
β	Matrix dimension.

γ	Matrix dimension (Chapter Three).
γ	Decrement-per-cycle (Chapter Four) (z-plane parameter).
$\delta(t)$	Small time interval.
ε	Aircraft thrust. (Newtons) (Chapter Five).
ζ	Damping factor.
ζ_{PH}	Aircraft phugoid mode damping.
ζ_{SP}	Aircraft short period mode damping.
η	Aircraft elevator angle (Radians) (Chapter Five).
θ	Aircraft pitch attitude (Radians) (Chapter Five).
λ	Arbitrary time parameter.
λ_i	i-th eigenvalue.
μ	Samples-per-envelope-cycle (z-plane parameter).
π	Symbolic pi, numerical 3.142.
ρ	The lowest common denominator of sampling periods.
$\rho(s)$	Characteristic equation s-plane.
σ_x	Variance of a state element.
σ_w	Variance of a disturbance signal.
$\sigma_{s,w,z}$	Real component of s, w, or z, respectively.
τ, τ_n	Arbitrary time parameters.
ϕ	Angle parameter of a radial on the z-plane.
ϕ_n	Angle of natural frequency z-plane radial.
ϕ_m	Angle of resonance magnification z-plane radial.
ω_{PH}	Aircraft phugoid mode frequency.
ω_{SP}	Aircraft short period mode frequency.
$\omega_{s,w,z}$	Imaginary component of s, w, or z, respectively.

MATHEMATICAL OPERATORS

arc*trig*	The inverse trigonometry operator for sin, cos, tan, etc.
det[*]	The determinant of *
exp(*)	Exponential operation on *.
$\mathcal{E}$	Expectation operator.
j	$\sqrt{-1}$.
ln(*)	Natural logarithm of (*)
log	Logarithm to base ten.
S_Σ	Notation of a continuous system.
s	Laplace transform operator
w	w Transform operator.
w'	w' Transform operator.
z	z Transform operator.
$[*]^{-1}$	Matrix inverse.
$[*]^T$	Matrix transpose.
$\|*\|$	A matix norm, defined at the point of application.
Σ_s	Notation of a discrete system.
$\dot{*}$	Time differential of *.

ABBREVIATIONS

ADC, AD	Analogue to Digital Converter.
CACT	Continuous-Amplitude, Continuous-Time.
CADT	Continuous-Amplitude, Discrete-Time.
CDC	Continuous to Discrete Conversion.
DAC, DA	Digital to Analogue Converter.
DACT	Discrete-Amplitude, Continuous-Time.
DADT	Discrete-Amplitude, Discrete-Time.

DCC	Discrete to Continuous Conversion.
DFC	Digital Flight Control.
DLY	Delay.
LCM	Lowest Common Multiple.
ZOH	Zero-Order-Hold.

CHAPTER ONE

INTRODUCTION

1.1 THE FUTURE REQUIREMENTS AND CURRENT PROBLEMS OF DFC SYSTEMS

In 1985 Fraser [1.1] described the type of aircraft that could be produced by the year 2000. Fraser's description is based on the deliberations of a committee, set-up under the auspices of the National Research Council (NRC) in the United States. The National Aeronautics and Space Administration (NASA) requested the committee to consider the following question; "if resources were not an issue, what developments would be made in aircraft systems by the end of this century?" The committee answered the question by describing what can be regarded as an Information Technology (IT) aircraft. The committee asserted that the enabling technology for realising the IT aircraft would be digital computing coupled with real-time control.

At the same time as the ambitious predictions of an IT aircraft were being advanced, Moran [1.2] described the problems that were experienced with the DFC system used for the McDonnell Douglas F/A-18A combat aircraft. The difficulties with the F/A-18A DFC system exemplified the problems that were being exposed in a number of other aircraft DFC development programmes. In 1987, Tischler [1.3] gave a succinct account of digital fly-by-wire aircraft developments and the problems encountered with their DFC systems.

Tischler noted that the DFC problems were associated with the design method. Tischler's conclusions were confirmations of earlier work reported by McRuer *et-al* [1.4] and Goodchild [1.5]. The problems associated with DFC design methods, cited in the open literature, are summarised by the following three statements:

(i) Initial DFC design studies have consistently over-estimated the bandwidth achieved in the implementation. As Tischler [1.6] observes, this over-estimation is generally not exposed until after hardware implementation and the initial flight test.

(ii) Time delays between pilot initiated commands and the aircraft response are a significant problem in digital computer controlled aircraft. These delays tend to cause pilot induced oscillations. Powers [1.7] noted that a similar problem had been experienced in the pitch axis control of the Space Shuttle. Burton *et-al* [1.8] observed the same effect occurring in both longitudinal and lateral axes of the digitally controlled F/A-18A .

(iii) Neuromuscular interference from the pilot can be coupled into the high bandwidth DFC. This phenomenon is called "roll ratchet" [1.9] and is particularly noticeable to pilots during lateral control activity. Johnston *et-al* [1.10] reported the occurrence of the problem in the AFTI F-16 research aircraft. Smith *et-al* [1.11] described a similar effect occurring in the digital fly-by-wire Jaguar.

In all the cases cited above, the problems with the DFC performance were reported to have been overcome. However, the the problems were not exposed until the aircraft had reached their initial operational status. The reports also imply that the problems with these DFC systems were finally resolved by heuristic design methods. The reported inadequacy of the current approach to the design of DFC systems produced the conclusion that a better method of DFC system design is needed, particularly if the ideas for the information technology aircraft, described by Fraser, are to be realised.

1.2 THE CASE FOR DIGITAL FLIGHT CONTROL RESEARCH

The general conclusion that emerges from the references cited above, is that a digital flight control system design methodology is required which addresses the implementation issue of data amplitude quantisation. The research, reported in this dissertation, focuses of the notion that the data amplitude quantisation should be considered during the preliminary design stage of the DFC system. Data amplitude quantisation is a feature which distinguishes a digital control system from the classical concept of a sampled-data system. A relationship between data amplitude quantisation and sampling imposes an upper bound on the sampling-rate for a given Continuous-Amplitude, Continuous-Time system. This observation is considered in detail in Appendix Three.

The following observations provide the basis of the digital flight control system design methodology which is described in this

dissertation:

(i) The design of a digital flight control system must be undertaken in a domain in which the continuous-data basic aircraft system and the digital-data flight controller can be unified for the purpose of design, analysis and implementation modelling.

(ii) Amplitude quantisation of the basic aircraft's flight control data imposes an upper-bound on the sampling-rate, for a given characteristic frequency. For the same characteristic frequency, the Sampling Theorem defines a lower-bound on the sampling-rate. Thus for each characteristic frequency in a high order system, there exists a limited range of appropriate sampling-rates.

(iii) Control data is produced by merging the information from a wide range of aircraft mission and flight sensors. These sensors produce information in different data formats with different data-rates or bandwidths.

Consideration of the first observation leads to the conclusion that the design of a digital flight control system should be undertaken in the discrete-data domain, employing a sampled-data description of the basic aircraft's dynamics. The arguments that support this view are presented in Chapter Two and Appendix Two. Although the nature of the second and third observations is fundamentally different, a consideration of both issues produces the same conclusion; viz, the

design methodology of a digital flight control system must, in general, accommodate a multirate sampling policy. The arguments that underpin this assertion are presented in Chapter Three.

1.3 THE PROPOSED DFC SYSTEM DESIGN METHODOLOGY

A digital flight control system design methodology is the subject of this dissertation. The objective is to define an approach to digital flight control system design which takes account of the issues associated with mixed-data flight control systems. The thesis is formulated within a framework of requirements that are identified as essential attributes of a practical digital flight control system design philosophy.

The first requirement is generated by the National Research Council's (NRC) prediction, [1.12], of developments in the technology of aircraft flight systems. The NRC predicts a growth in airborne capabilities that will encourage advances in operational requirements and involve the integration of aircraft systems to an extent where the classical division of functions will disappear. For example, the aircraft structure, its propulsion and aerodynamics will be integrated with the mission, navigation and guidance functions in a general flight control system architecture. The enabling technologies for this total integration concept will be digital computer architectures and control system design methodologies.

As noted in Section 1, the reported inadequacies of current digital flight control systems are generally attributed to the control system design approach. A design methodology which implicitly addresses the mixed-data issues of digital flight control systems is required if the ambitious predictions for the integrated systems aircraft are to be realised.

The second requirement of a practical digital flight control system design methodology is concerned with the integrity of aircraft flight control systems. The design methodology of a flight control system is as important as the hardware, software and system configuration in establishing the integrity of the implemented system. Four aerospace system design maxims are defined by Mulcare *et-al* [1.13]. These maxims provide the fundamental guidance for the establishment of the design methodology proposed in this dissertation; Mulcare defined the maxims as:

(i) **Simplicity:** Within a framework that encompasses all the relevant design issues, the objective of the simplicity maxim is to enhance confidence in both the control function and its implementation.

(ii) **Visibility:** A compact and precise model description possesses visibility in the sense that a clear perspective of the physical problem is maintained throughout the development of a control system.

(iii) **Consistency:** The development of a large scale flight control system inevitably requires a design methodology that allows an incremental approach to modelling and conceptual verification. A design methodology possessing this property has consistency.

(iv) **Conclusiveness:** A design methodology which permits the analysis (validation) of the most critical functions with the highest degree of confidence possess conclusiveness.

The digital flight control system design methodology proposed in this dissertation is constructed to meet the above requirements and address the pragmatic needs of flight control system designers. To achieve these objectives, the digital flight control system model builds on the established and proven concepts of analogue flight control system design. Thus, the linear aircraft model and the gain scheduling strategies of flight control are the fundamental assertions on which the proposed design methodology is built.

The principle of the proposed digital flight control system design methodology is the recognition that a basic continuous-data aircraft model must be recast in different data domains as the the control system evolves through the design, modelling and implementation process. The data-domains associated with digital flight control systems are identified and defined. The current methods of digital flight control system design appear to adopt an ad-hoc approach to this important issue. The proposed methodology establishes the appropriate data-domains for the modelling, design and analysis of

digital flight control systems.

The DFC design methods described in this dissertation focus on the direct digital design approach. Direct digital design adopts the policy of control system design in the discrete-data domain. The basis of the direct digital design method is to recast a continuous-time plant as an equivalent, discrete-time system. In the flight control case, the continuous-time plant represents the basic aircraft, the control actuators and the data sensors etc. Direct digital design contrasts with the widely used emulation design methods. With the emulation approach, a digital control system is realised by designing the controller as a continuous-time system and then mapping the resulting continuous-time control law equations to the discrete-time domain for purposes of implementing the digital controller. An example of the emulation method in the design of a DFC system is provided by Joshi *et-al* [1.14]

The direct digital design method has, for some time, been recognised as the appropriate domain for DFC design. Kidd [1.15] and Goodchild [1.16] identified this fact during their studies into DFC systems for remotely piloted aircraft. Tischler [1.17] observed that emulation methods are useful for preliminary design and performance trade-off studies but direct digital methods are necessary to accurately evaluate the many important high-frequency dynamic characteristics of a modern digital system. Oz *et-al* [1.18] observed that the results produced by direct digital design can be significantly different to the results produced by emulation design. Oz concluded that the common blithe assumption of simplistic

interchangeability between discrete and continuous control design techniques should be given careful scrutiny and perhaps discarded. A cornerstone of a successful development of a digital flight control system is the selection of the control-data and measurement-data sampling rate or rates [1.19]. The appropriate sampling rate is determined from an analysis of the associated dynamics and the implementation environment. In general, this leads to a multirate sampling policy. The proposed design methodology includes a utility to model and analyse multirate sampled-data flight control systems. The four design methodology maxims are major factors in the proposed multirate sampled-data model.

The proposed design methodology of an aircraft's digital flight control system is described in the subsequent chapters of this dissertation. The problems associated with digital flight control are classified as handling qualities issues. The proposed design methodology is directed towards the design of the inner control-loops and autopilot functions, because the primary purpose of these inner-loop functions is to control and modify the handling qualities of a basic aircraft. The general performance requirements for manned-aircraft flight control systems are embodied in standard handling-qualities documents, for example MIL-F-8785C [1.20]. This particular document is employed to provide the performance objectives of the digital flight control system designs described in this dissertation. A design domain is defined and methodology developed which permits the direct transformation of handling qualities requirements into digital control-law specifications.

1.4 ORGANISATION OF THE DISSERTATION

The digital flight control design methodology is described in Chapters Two, Three and Four. Chapter Five presents the results of an application of the proposed methodology to the design of a Digital Flight Control (DFC) system. Although the scope of the design study is limited to a basic aircraft stabilisation and simple flight control law problem, the salient features of the methods given in this dissertation are exposed.

Chapter Two considers the basic aircraft modelling problems associated with the preliminary design of a flight control system. The development of the basic aircraft design model is approached from the perspective of the flight control design practitioner. Thus, the proposed design method accommodates an incremental assembly of the basic aircraft system and attempts to maintain a conspicuous representation of the physical dynamics. The proven concept of a linear time-invariant design model, coupled with a gain scheduling policy for global control over the total flight envelope, provides the basis for the proposed DFC design methods.

The rationale for DFC design in the discrete-data domain is considered in Section 2.3. The data domains incorporated in a DFC system are defined. The fundamental questions, concerning the domain in which a unified model of a mixed-data system can be established for the purpose of DFC design, are addressed.

The method of transforming a continuous-time, basic aircraft model

into an equivalent discrete-time model is considered in Section 2.4. To reflect normal DFC implementation practice, it is assumed that digital control data is applied to the continuous aircraft via a Zero-Order-Hold. This means that digital control data is available at the sampling instant as an impulse from a time sequence of impulses. The amplitude of each impulse is held and applied as a constant control action to the continuous aircraft over the following intersample period.

It is considered that the methods proposed in Chapter Two represent a contribution to the general practice of DFC design. Although the proposed methods are established techniques in control system design practice, it is believed that some novel applications have been identified, which overcome some of the common modelling problems associated with DFC design.

The classical interpretation of a discrete-time representation of a continuous-time model is a sampled-data system. The implicit assumption of a sampled-data system is that the sampled-data amplitude is continuous. The modern, practical implementation of a DFC system is a digital-data system; that is, the time sampled data undergoes a process of amplitude quantisation. In Chapter Three, it is reasoned that a DFC system must be implemented as a multirate sampled-data system. In this context, it is necessary to note that sampling refers to both the time sequence of impulses applied to control the basic continuous aircraft system and the sampled system's state-data, from which the control actions are generated.

The selection of a sampling policy is a critical factor in the design of a DFC system. Various methods of selecting a sampling-rate for a continuous-data system have been studied and reported [1.21]. For the design of a DFC system, it is observed that the selection of a sampling-rate, or sampling-policy must usually be made on the basis of very limited information. In fact, the available information is often restricted to the basic aircraft system dynamics. Other data, which would be relevant for the sampling rate selection procedure, only becomes known some time after the initial design decisions need to be made. Methods are given in Section 3.2 which establish quantitative measures for the selection of a sampling policy on the basis of limited system information.

A multirate sampled-data state-space model is developed in Section 3.4. The multirate model is developed because, in contrast to the currently available models [1.22], [1.23],and [1.24], the proposed assembly meets the objectives of the four maxims with greater facility. Although the multirate sampled-data model can be utilised in the direct design of a DFC system, its application challenges the requirements of the four maxims. Several case studies examined for the thesis have therefore been omitted from this dissertation and are given in a supplementary report [1.25]. The issue of a suitable multirate sampled-data DFC system design domain is addressed in Chapter Four.

Chapter Four considers the design, analysis and implementation issues associated with preliminary design of a DFC system. Section

4.2 reviews the w- and w'-planes as candidate domains for the design of multirate sampled-data DFC systems. The w- and w'-planes are identified by Whitbeck and Hofmann [1.26] to be particularly suitable for the design of DFC systems. Although the the w- and w'-planes design methods have advantages over z-plane design methods, there is no evidence of their widespread use in practical DFC design. A reason for this may lie in the fact that an innocuous z-plane transfer function can produce a confusing w- or w'-plane expression. As Tischler [1.27] states in a summary identifying the requirements for DFC design; "methods which allow easy transitions between the s-plane, the z-plane and the w-plane are needed". Methods which map the high order and multivariable system models from the time-domain state-space and s-plane, to the w-plane and w'-plane are developed for this thesis.

Section 4.3 presents methods for the analysis of the performance of DFC systems. The methods are developed from the well known s-plane graphical techniques, such as root-loci diagrams and Bode plots. A survey of the literature indicates that the z-plane root-locus is the most common method of sampled-data system performance analysis. The analysis methods sponsored by most reports are based on mapping the parameters of the s-plane criteria to the z-plane. The sampled-data and discrete system analysis criteria proposed in this dissertation are based on identifying the equivalence between the parameters of a continuous system and the parameters of a corresponding discrete system model.

The digital computer implementation of a DFC system casts the flight

control algorithms in a quantised-data discrete-time domain. This domain imposes additional constraints which must be considered during the preliminary stages of DFC system design. The adoption of a multirate sampled-data policy gives an implicit consideration of the implementation domain.

The results of a DFC design case study are presented in Chapter Five. The purpose of the design exercise is to explore the properties of the proposed methods that are not explicitly described by examples given in the preceding chapters and appendices. The w- and w'-planes are utilised to design the digital autopilot function of a manned aircraft. The DFC design target specifications are identified from the handling qualities document MIL-F-8785C and cast in terms of the discrete design domain.

The computational requirements of the proposed methods are serviced in a matrix manipulation environment, called MATLAB [1.28]. The influence of MATLAB on development of the multirate sampled-data DFC design methodology is significant. The facility which the package offers for realising high order numerical routines makes it an almost ideal environment for the proposed DFC system design methodology.

CHAPTER TWO

MODELLING AIRCRAFT DYNAMICS FOR DIGITAL FLIGHT CONTROL

2.1 INTRODUCTION

This chapter considers the development of a model for Digital Flight Control (DFC) design and analysis. The development addresses the specific requirements of design, analysis and implementation in the discrete-time domain. In the case of analogue flight control, the controller and aircraft are modelled by continuous-time differential equations, so the design, analysis and implementation processes are naturally carried out in one domain. However, when a digital computer is used to implement the flight control laws, the convenience of a single modelling domain is lost. This chapter address the issues of combining continuous and discrete processes for the purpose of DFC design.

2.1.1 A Generic Aircraft Model for DFC Design

The design model considered in this dissertation is based on a generic aircraft and DFC system. The total aircraft system is illustrated below in Fig.2.1. As a generic concept, the model encompasses all types of manned aircraft. The principal characteristics linking this generic model to a more general class of dynamical system are; high bandwidth, fast response and inherent

relaxed static-stability. Aircraft are dynamical systems which belong to the information-rich and energy-deficient system group. This classification is used for systems in which the plant dynamics can be readily identified but the available energy for their control is strictly limited. This classification contrasts with the notion of an information-deficient and energy-rich system which, for example, can be ascribed to a chemical processing plant. In this case relatively little is known about the plant dynamics but, as a fixed terrestrial system, high energy levels are available for control purposes.

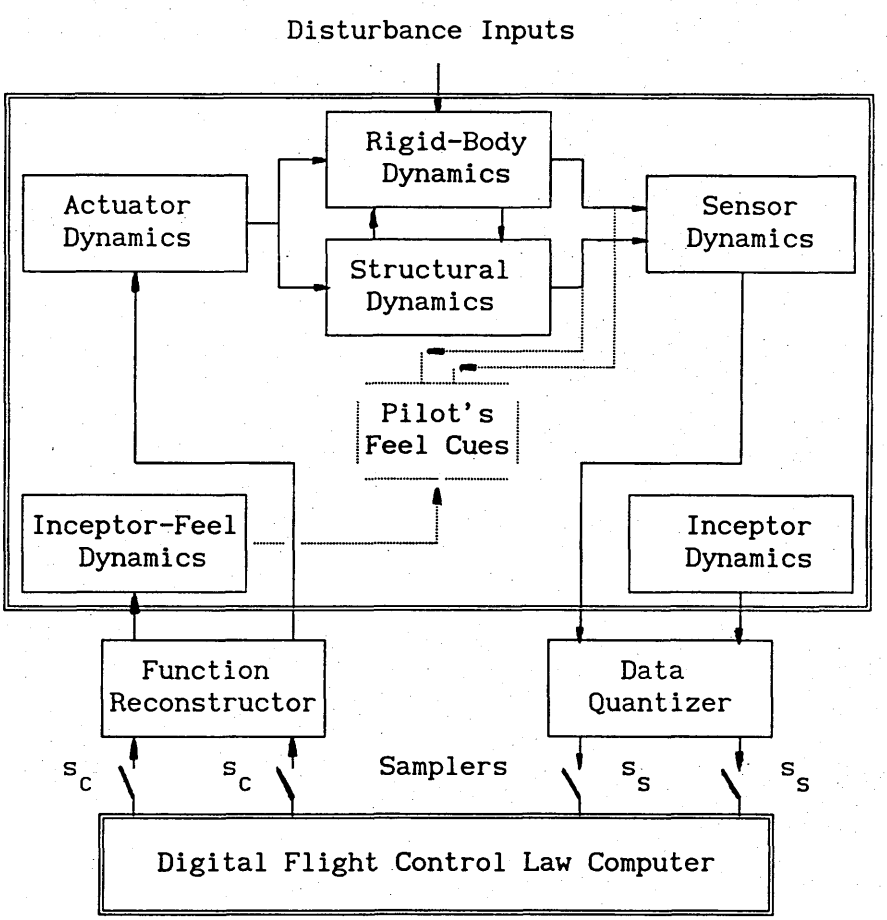

A generic aircraft design model controlled with a digital-flight-control computer

Fig.2.1

In practice, the design of a flight control system is initiated without a complete knowledge of the ultimate system specification, or even a complete set of data for the basic aircraft. A general flight control system design method must, therefore, accommodate an incremental approach to the assembly of a flight control system. The implicit consequence of this practical issue gives weight to the argument to base the design of an aircraft flight control system on the physical states and not to transform them to a mathematically more convenient set of state variables. The DFC design model, developed in this chapter, facilitates the requirements of the incremental assembly approach.

2.2 THE ANALOGUE-DATA MODEL OF THE BASIC AIRCRAFT

The most widely used method of modelling aircraft flight control systems is based on reducing the non-linear, time-varying dynamic equations of the basic aircraft to a set of linear, time-invariant equations [2.1]. The complex structure of the basic aircraft can be be generalised into two groups of first order equations, given as

$$\dot{\mathbf{x}}(t) = f(\dot{\mathbf{x}}(t),\mathbf{x}(t),\mathbf{u}(t),\mathbf{y}(t),t) \qquad (2.1a)$$

$$\mathbf{y}(t) = g(\dot{\mathbf{x}}(t),\mathbf{x}(t),\mathbf{u}(t),\mathbf{y}(t),t). \qquad (2.1b)$$

It is often convenient, particularly in large systems, to generate an auxiliary equation representing subsystem interconnections. The general form of the auxiliary equation is given by

$$\mathbf{a}(t) = h(\dot{\mathbf{x}}(t),\mathbf{x}(t),\mathbf{u}(t),\mathbf{y}(t),t). \qquad (2.1c)$$

For the three equations, $\mathbf{x}(t)$ is a vector of m time-dependent state functions, $\mathbf{u}(t)$ is a vector of q time-dependent input and $\mathbf{y}(t)$ is a vector of p time-dependent output functions. The functions f, g and h are non-linear.

Linearisation of f , g and h is achieved by considering perturbation models at strategic operating points in the aircraft's flight envelope [2.2]. The time-invariant requirement is achieved by assuming the time-varying parameters to be quasi-steady-state [2.3]. Linear flight control laws are defined on the basis of the aircraft's characteristics at these flight envelope design points. A scheme of parameter scheduling produces the necessary control law changes to account for the non-linear and time-varying dynamics of the aircraft as it transits from one design point to the next. This technique is a popular method for the design of analogue flight control systems. The equations produced by the linearisation process are given by

$$\dot{\mathbf{x}}(t) = \mathbf{F}_{\dot{x}}\,\dot{\mathbf{x}}(t) + \mathbf{F}_{x}\,\mathbf{x}(t) + \mathbf{F}_{y}\,\mathbf{y}(t) + \mathbf{F}_{u}\,\mathbf{u}(t) \qquad (2.2a)$$

$$\mathbf{y}(t) = \mathbf{G}_{\dot{x}}\,\dot{\mathbf{x}}(t) + \mathbf{G}_{x}\,\mathbf{x}(t) + \mathbf{G}_{y}\,\mathbf{y}(t) + \mathbf{G}_{u}\,\mathbf{u}(t) \qquad (2.2b)$$

$$\mathbf{a}(t) = \mathbf{H}_{\dot{x}}\,\dot{\mathbf{x}}(t) + \mathbf{H}_{x}\,\mathbf{x}(t) + \mathbf{H}_{y}\,\mathbf{y}(t) + \mathbf{H}_{u}\,\mathbf{u}(t). \qquad (2.2c)$$

The three members of (2.2) are rearranged to produce the standard, (**A**,**B**,**C**,**D**) quadruple form of the state and output equations, given as

$$\dot{\mathbf{x}}(t) = \mathbf{A}\,\mathbf{x}(t) + \mathbf{B}\,\mathbf{u}(t) \qquad (2.3a)$$

$$\mathbf{y}(t) = \mathbf{C}\,\mathbf{x}(t) + \mathbf{D}\,\mathbf{u}(t). \qquad (2.3b)$$

The state and output equations are the starting point for the digital flight control design, analysis and implementation methods proposed in this dissertation.

2.3 PRELIMINARY ISSUES

An approach to the DFC design is described which attempts to cast the popular analogue system techniques in the discrete-time domain. Although, in principle, this idea is not new, the use of multivariable w- and w'-plane models for the design of multirate sampled-data systems appear not to have been explored. The proposed method of designing a DFC system starts with the basic linear, time-invariant aircraft model, given by equations (2.3a) and (2.3b). The design objective is to determine a set of control law equations that, when implemented, cause the aircraft to have a defined performance policy.

2.3.1 Definitions of the Domains in a Mixed-Data DFC System

The design, analysis and implementation domains for digital flight control systems are defined in this section. These domains are explicitly considered for this thesis and represent an aspect of digital control system design that is often overlooked. Although the issues considered are framed in the context of aircraft flight control applications, the concepts are generic and apply to a wide range of control systems.

When defining the domain in which modern digital flight control systems operate, consideration must be given to the fact that control data is both time-sampled and amplitude-quantised. Classifying control systems by "data-type" defines four domains of operation. These domains are:

(a) Continuous-Amplitude, Continuous-Time....CACT,

(b) Continuous-Amplitude, Discrete-Time.....CADT,

(c) Discrete-Amplitude, Discrete-Time.....DADT,

(d) Discrete-Amplitude, Continuous-Time.....DACT.

The systems that correspond to each domain are:

(a) CACT.....Analogue-data system,

(b) CADT.....Sampled-data system,

(c) DADT.....Digital-data system,

(d) DACT.....Quantised-data system.

A digital flight control system, consisting of the aircraft, the digital-control processor and the aircraft-to-processor interfaces, involves all four data types. Comparing this situation with the classical analogue flight control system gives an indication of the added complexity generated by the introduction of digital control processes. This complexity is compounded by an expectation that enhanced control activity can be achieved with a digital computer.

2.3.2 The Mixed-Data Configuration of a DFC Aircraft

The data handling operation in digital flight control involves taking a measurement of an aircraft's analogue-data state vector and converting it to digital-data. The signals representing the aircraft state are processed as the parameters of the digital control laws. By definition, the digital control laws are implemented in the DADT domain and generate a digital-data control vector. To control the CACT aircraft system, the digital-data control vector is converted back to continuous-time. However, as no realisable scheme exists to convert the discrete amplitude aspects of the data into continuous, smooth control signals, the CACT aircraft is effectively controlled by a quantised-data control vector. In general terms, an aircraft employing digital flight control exemplifies a "mixed-data" system. The closed-loop configuration of a mixed-data system is shown in Fig.2.2.

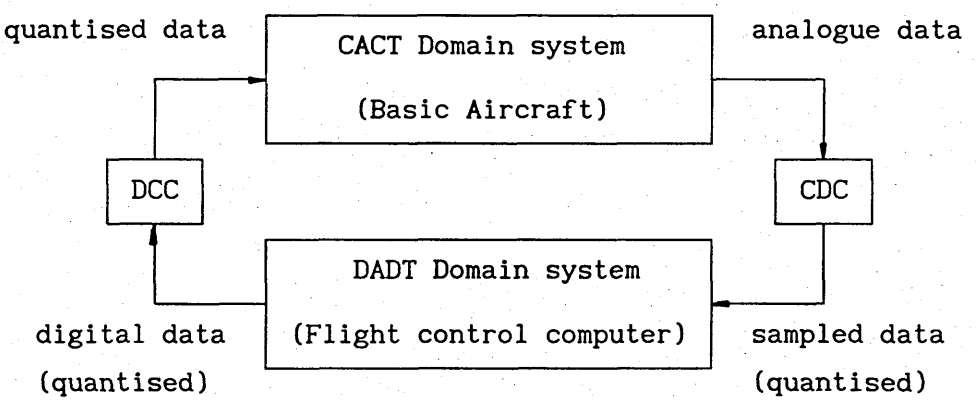

DCC is a Discrete to Continuous Converter
CDC is a Continuous to Discrete Converter.

The configuration of a mixed-data DFC system

Fig.2.2

2.3.3 Data Domain Conversion

The generation of a digital-data representation of the aircraft's analogue flight state vector is carried out by the Continuous-to-Discrete Converter, (CDC), shown Fig.2.2. In the case of digital flight control the CDC is usually implemented as an Analogue-to-Digital Converter (ADC) [2.4].

The generation of continuous-time flight control data from the DADT domain flight control computer is carried out by the Discrete-to-Continuous Converter, (DCC), shown in Fig.2.2. The generic name of the discrete-to-continuous process is function-reconstruction [2.5]. It is theoretically possible to define a perfect function reconstruction model [2.6]. In formal terms, if u(i) is a sampled-data version of an analogue-data signal, u(t), then a perfect function reconstructor will map the u(i) into u'(t) such that $\left(u(t)-u'(t)\right)$ is identically zero. In practice however, perfect function reconstruction cannot be achieved [2.7].

Function reconstruction is a dynamic process and therefore augments the basic aircraft dynamics. In the limit, as the order of the reconstructor dynamics tends to infinity, the reconstruction will become the perfect process, described above. The additional dynamics, introduced into a flight control system, by a function reconstructor, has a degrading effect on the closed-loop stability performance [2.8]. For this reason, the preferred implementation of the discrete-to-continuous process is a reconstructor with minimal order dynamics. In the case of digital flight control, the

discrete-to-continuous process is normally implemented with a Digital-to-Analogue Converter (DAC) [2.9]. In some related flight control cases [2.10], where the data reconstruction has the appearance of a high-order process the actual situation can be reduced to a DAC implementation with discrete-time dynamics that are modelled as augmentation states. For less fundamental but equally important reasons, the DAC is used because it is readily available as a proprietary device [2.11].

It is not uncommon for the ADC and DAC to be called a Sampler and Zero-Order-Hold (ZOH), respectively. Strictly, however, the notion of both a sampler and ZOH, referred to in classical sampled-data control system theory [2.12], does not include an amplitude quantisation effect, which is an implicit feature of the ADC and DAC data conversion processes.

2.3.4 The Proposed Route for DFC Design

As stated above, the modern implementation of a DFC system is a closed-loop arrangement of continuous and discrete functions that process all four data-types. The suggested method for the design and analysis of a DFC system follows an approach that maps the basic analogue-data aircraft model into an equivalent sampled-data model. The sampled-data model of the basic aircraft is then used for control law design and preliminary performance analysis. Although the stated objective of the proposed DFC design methodology is to take implicit account of the amplitude quantisation effects of the

DADT and DACT domains, the issues associated with the discrete amplitude domain represent a major activity in the total DFC design process. This observation identifies a significant extension to the DFC design methodology described in this dissertation and is therefore noted as a topic for future research.

2.3.5 The Case for DFC Design in the Discrete-Time Domain

The DFC design methodology is based on the proposition that DFC design should be carried out in the CADT domain. The proposed method is therefore associated with the direct digital design techniques [2.13]. The following observations make the case for using the CADT domain for the design of sampled-data systems.

To undertake a quantitative design on a mixed-data system, it is necessary to define a mathematical model of the system in a single data-type domain. To explore this issue, consider the discrete element subsystem shown in Fig.2.3.

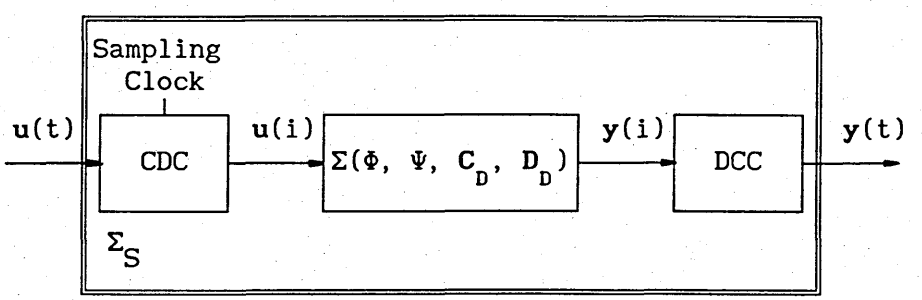

The arrangement to define a CACT system

in terms of the CADT system parameters

Fig.2.3

A possible method of producing a unified model of a mixed-data system is to recast the CADT subsystem of Fig.2.3 as an equivalent CACT system. This leads to the basic question; does a CACT S(A,B,C,D) exist which will map **u**(t) into **y**(t) in precisely the same way as the arrangement shown in Fig.2.3?. For the answer, it is observed that **y**(t) is produced by the discrete-to-continuous converter which, as stated above in Section 2.3.3, is implemented by a DAC. The signal constructed by a DAC is a staircase function for all inputs of **u**(t). As no continuous-time system S(A,B,C,D) has this characteristic the answer to the question is in the negative.

Another option of defining a unified data-domain model of a mixed-data system is based on the arrangement shown in Fig.2.4. The objective with this arrangement is to recast a CACT system as an equivalent discrete-time system. The question is therefore; does a discrete-time $\Sigma(\Phi,\Psi,C_D,D_D)$ system exist which will map **u**(i) into **y**(i) in precisely the same way the as continuous-time arrangement shown in Fig.2.4 suggests? The answer to the question is in the affirmative. This answer is examined below, in Section 2.4.

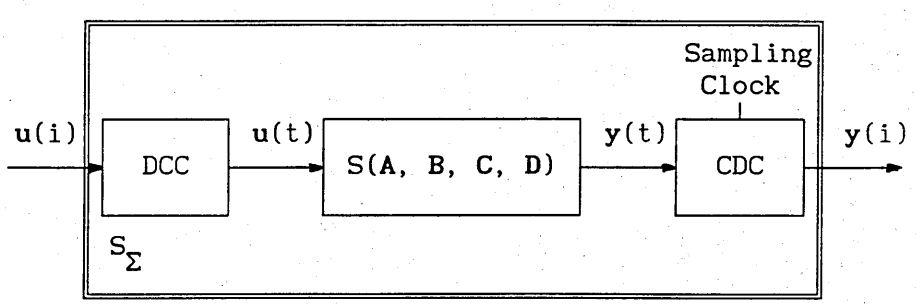

The arrangement to define a CADT system

in terms of the CACT system parameters

Fig.2.4

A further reason supporting the case of design in the CADT domain comes from the well known claim [2.14]; that a digital-control system, designed by a direct-digital method, can achieve a given performance with a minimum sampling-rate. This claim is usually asserted without proof. Appendix Two presents an analysis which demonstrates the validity of the claim through a simple example. An alternative demonstration of support for the direct-digital design approach is given in a recent report by Boucher *et al* [2.15]. The report compares two cases of controller designs for the same continuous-time process. In one case, the controller is designed by direct-digital methods while, in the other case, the controller is designed in the continuous-time domain and mapped to the z-plane for implementation. The result of the comparison confirms the validity of the claim, stated above.

2.4 DISCRETE-DATA MODELS OF CONTINUOUS-TIME SYSTEMS

The underlying principle of the direct-digital design method is that an equivalent discrete-time model can be defined for a continuous-time system. This section gives a review of the methods that are available to produce an equivalent discrete-time model of a continuous-time system. The basic assumptions upon which the methods in this section, and the remainder of this dissertation, are built have already been discussed and are reasserted as follows:

(i) The basic flight control system design model of an aircraft's non-linear, time-varying dynamics is represented as a set of

linear, time-invariant equations.

(ii) The non-linear, time-varying aspect is taken into account by adjusting or "scheduling" the parameters of the linear, time-invariant control equation as the aircraft manoeuvres over its flight envelope.

(iii) The continuous to discrete conversion processes are instrumented by analogue to digital converters and the discrete to continuous conversion processes are instrumented by digital to analogue converters. The combined effect of these converters is an impulse sampler followed by a zero order hold.

The linear time-invariant equations, for a basic CACT domain aircraft system with deterministic control inputs, can be cast in state-space form. This is discussed in Section.2.2 and is given by the equations (2.2a) and (2.2b),

$$\dot{\mathbf{x}}(t) = \mathbf{A}\,\mathbf{x}(t) + \mathbf{B}\,\mathbf{u}(t) \qquad (2.3a)$$

$$\mathbf{y}(t) = \mathbf{C}\,\mathbf{x}(t) + \mathbf{D}\,\mathbf{u}(t) \quad . \qquad (2.3b)$$

Under the assumptions, given above the system state at time t_1 is given by the solution of the differential equation (2.3a). From a zero initial condition, $\mathbf{x}(0)$, the solution of (2.3a) is given by

$$\mathbf{x}(t) = \exp(\mathbf{A}t)\,\mathbf{x}(0) + \int_0^t \exp\left[\mathbf{A}(t-\tau)\right]\mathbf{B}\,\mathbf{u}(\tau)\,d\tau \quad . \qquad (2.4)$$

This equation is the basis of the time-domain continuous to discrete state-space mapping that is central to the DFC system design method described in this dissertation. The proposed method is generally referred to as a direct digital design technique and is in direct contrast with the widely used emulation method. The emulation method starts by solving the differential equation (2.3a) via Laplace transforms to determine the s-plane state

$$sX(s) = A\,X(s) + B\,U(s). \qquad (2.5)$$

When (2.5) is substituted into 2.3b with an initial condition $x(0)=0$, the resulting system model is the s-plane transfer function matrix description and is given by

$$Y(s) = \left(C\,[sI - A\,]^{-1}B + D\right) U(s) \quad . \qquad (2.6)$$

The single input single output transfer-functions, that are derived from (2.6), are models of the basic aircraft system. In the emulation design approach, a continuous-time flight controller is designed, using an s-plane model of the basic aircraft. The resulting continuous-time control equations are transformed into an set of discrete-time equations for implementation in a DFC computer.

2.4.1 Transfer-Function Methods

Although the transfer-function model is mainly used in the emulation design method, a transfer-function model can be employed for a direct digital design approach. The method proposed in this dissertation requires a CADT domain model of the basic aircraft

equations. When these CACT aircraft equations are generated as s-plane transfer-functions, mapping them directly from the CACT domain into a CADT domain produces a z-plane transfer-function model of the basic aircraft. Flight control law design is then carried out using classical sampled-data control system techniques.

The classical approach [2.16], usually associated with sampled-data servomechanisms, uses the a z-transform substitution, $z = \exp(sh)$. This substitution maps the CACT domain transfer-function to a "pulse transfer-function", $F_p(z)$ [2.17], where

$$F_p(z) = \sum_{i=1}^{m} \left(\text{residue of } \frac{F(s)}{1-\exp(sh)\, z^{-1}} \text{ at the pole i of } F(s) \right) \quad . \quad (2.7)$$

There is a temptation to regard $F_p(z)$ as a realisable CADT domain representation of the CACT domain transfer-function. This assertion is incorrect. The pulse transfer-function, $F_p(z)$, is interpreted in terms of the concept of a perfect switch, producing a chain of delta-functions spaced by a time interval h. Each delta-function assumes the strength of the sampled analogue signal at the sampling instant. As no physical system can realise a delta-function, the switch concept is replaced by a function reconstructor, described in Section 2.3.3.

As noted in Section 2.3.3, the usual implementation of a function reconstructor in DFC systems is the DAC. The classical ZOH model, that the DAC conforms to, has a transfer-function given by

$$F_H(s) = \frac{1 - \exp(-sh)}{s} \quad . \quad (2.8)$$

Assuming the continuous-to-discrete conversion interface is implemented by a ZOH, then the CADT domain model is obtained by transforming the product of CACT and ZOH transfer functions to an equivalent z-plane model.

$$F_D(z) = Z\Big[F_H(s)\, F(s) \Big] \quad . \tag{2.9}$$

The direct transfer-function mapping technique is cumbersome; this is particularly so in the cases of high order and/or multivariable systems. An alternative transfer-function mapping technique makes use of the Tustin bilinear transform [2.18]. The Tustin bilinear transform is a substitution for the s variable of transfer-functions and is given by

$$s = \frac{2}{h} \frac{z - 1}{z + 1} \quad . \tag{2.10}$$

The Tustin bilinear transform is usually used in the emulation method of DFC design. Its application is to map control laws, designed in the CACT domain and expressed as s-plane transfer-functions, to an "equivalent" set of CADT domain z-plane transfer-functions. From the z-plane transfer-functions, a set of corresponding difference equations can be deduced. These difference equations represent an algorithm of the DFC laws. For complex transfer-functions, the Tustin transform mapping technique produces unwieldy algebraic equations.

The discussion of this section has been included for completeness. The emulation method is not relevant to the objectives of the DFC design method proposed for this dissertation. A comprehensive

account of the emulation method and its application to DFC system design is available [2.19].

2.4.2 State Space Mapping Methods

A state-space representation of a mixed-data system can be derived by integrating, with respect to time, equations (2.3). To illustrate this approach, consider the closed-loop system shown in Fig.2.2. Assume the CACT aircraft state is propagated from an initial state $\mathbf{x}(t_0)$ and an impulse sample of the state is taken at time t_h, where $t_h - t_0 = h$. This measured state will be identical to the solution of continuous-time state equation, (2.4), defined with an initial condition $\mathbf{x}(t_0)$ and an integration interval h. This observation assumes an error free measurement and a continuous-to-discrete conversion that does not incur an amplitude quantisation process. When the sampling process is generalised into a continuous sequence of samples, separated in time with a period h, the mixed-data system represents a sampled-data system [2.20]. This well known method of producing an equivalent CADT model of a mixed-data system forms the basis of the DFC design methodology described in this dissertation. As shown below, various forms of the basic mapping functions are produced from equation (2.4).

From an initial state given at time $t_0 = nh$, the state at time $t_h = nh+h$ is calculated by substituting these time values into (2.4). Therefore, the solution to the CACT state equation (2.3a), at time (n+1)h is given by

$$\mathbf{x}((n+1))h = \exp(\mathbf{A}h)\ \mathbf{x}(nh) + \int_{nh}^{(n+1)h} \exp\Big(\mathbf{A}(nh+h-\tau)\Big)\mathbf{B}\ \mathbf{u}_n\ d\tau \quad , \quad (2.11)$$

where n is the sample number, h is the sampling period and τ is an integration variable.

The usual flight control system implementation of the discrete-to-continuous converter is the DAC. The DAC maintains a constant value of **u**(nh) at the input of the system S_Σ (see Fig.2.4) during the time period $nh \leq \tau < (n+1)h$. If, in addition to this, λ is substituted for $(nh+h-\tau)$ in equation (2.11) then the solution to the state equation at the sample point is given by

$$\mathbf{x}((n+1))h = \exp(\mathbf{A}h)\ \mathbf{x}(nh) + \int_0^h \exp(\mathbf{A}\lambda)\ d\lambda\ \mathbf{B}\ \mathbf{u}(nh) \quad . \quad (2.12)$$

Consider the situation for the general case, in which a new member of the number sequence **u**(i) arrives at the discrete-to-continuous converter every h units of time. If the continuous-to-discrete converter is clocked after a delay of Δ seconds, following presentation of data number to the discrete-to-continuous converter then, for the input **u**, occurring at time nh, there is a corresponding output **y**, occurring at time $n(h + \Delta)$. This type of sampling policy is called "non-synchronous" sampling. With the ZOH implementing the discrete-to-continuous interface, the system has the solution given by

$$\mathbf{x}((n+1))h = \exp(\mathbf{A}h)\ \mathbf{x}(nh) + \int_0^h \exp(\mathbf{A}\lambda)\ d\lambda\ \mathbf{B}\ \mathbf{u}(nh) \quad , \qquad (2.13a)$$

$$\mathbf{y}((n+\Delta)h) = \mathbf{C}\ \exp(\mathbf{A}\Delta)\ \mathbf{x}(nh) + \left[\mathbf{C}\int_0^{\Delta} \exp(\mathbf{A}\lambda)d\lambda\ \mathbf{B} + \mathbf{D}\right]\mathbf{u}(nh) \quad . (2.13b)$$

The CADT domain quadruple, in terms of the CACT quadruple, is deduced from equations (2.13a) and (2.13b), and is given by four equations;

$$\Phi = \exp(\mathbf{A}h) \quad , \qquad (2.14)$$

$$\Psi = \int_0^{\lambda} \exp(\mathbf{A}\lambda)\ d\lambda\ \mathbf{B} \quad , \qquad (2.15)$$

$$\mathbf{C}_D = \mathbf{C}\ \exp(\mathbf{A}\Delta) \quad , \qquad (2.16)$$

$$\mathbf{D}_D = \mathbf{D}\int_0^{\Delta} \exp(\mathbf{A}\lambda)\ d\lambda\ \mathbf{B} + \mathbf{D} \quad . \qquad (2.17)$$

For synchronous sampling the delay parameter Δ is zero, so the coefficient matrices $\mathbf{C}_D$ and $\mathbf{D}_D$ of the output equation become $\mathbf{C}_D = \mathbf{C}$ and $\mathbf{D}_D = \mathbf{D}$.

Substituting the terms from the left-hand-side of equation (2.14) to (2.17) into equations (2.13a) and (2.13b) produces the standard form of state and output difference equation that represent the basic aircraft as an equivalent discrete-time system, given as

$$\mathbf{x}(n+1)h = \Phi\ \mathbf{x}(nh) + \Psi\ \mathbf{u}(nh) \qquad (2.18a)$$

$$\mathbf{y}(n+\Delta)h = \mathbf{C}_D\ \mathbf{x}(nh) + \mathbf{D}_D\ \mathbf{u}(nh) \quad . \qquad (2.18b)$$

In the case of sampled-data system with synchronous input and sampling, the delay time $\Delta = 0$ and hence $\mathbf{y}(n+\Delta)h$ reduces to $\mathbf{y}(nh)$. The state-space diagram for this system is given in Fig.2.5.

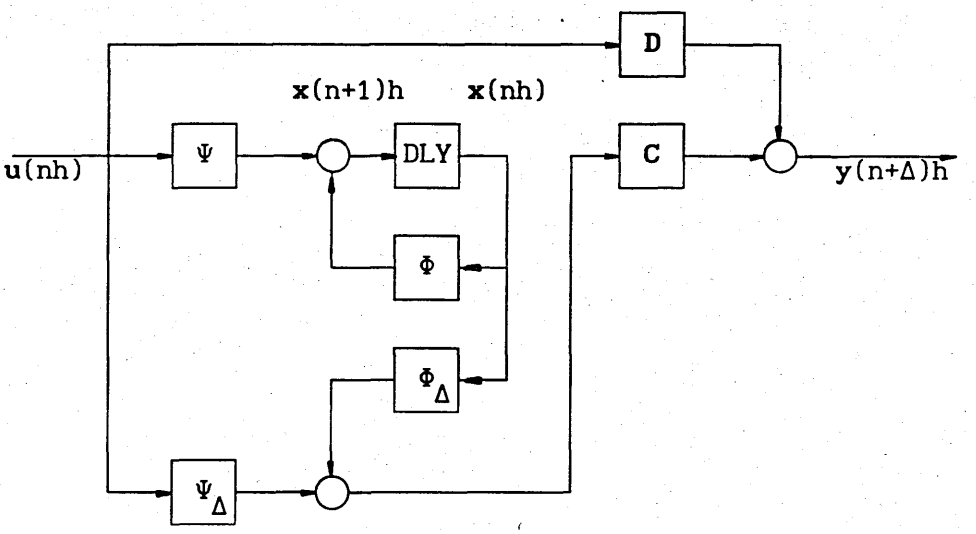

$$\Phi_\Delta = \exp(\mathbf{A}\Delta) \ ,$$

$$\Psi_\Delta = \int_0^\Delta \exp(\mathbf{A}\lambda)\, d\lambda\ \mathbf{B} \ ,$$

DLY symbolises a single sample delay.

The general discrete system diagram deduced from the CACT to CADT mapping functions

Fig.2.5

Equations (2.18a) and (2.18b) are the basic aircraft model employed in the digital flight control law design methodology. The key issue in deriving these equations is the selection of a sampling period, h. In the most basic form, the CADT sampled-data model is defined for a unirate (single-rate) sampling policy. However, for the thesis developed in Chapter One, it is recognised that, in general, a DFC system will require a multirate sampling policy. Further

consideration of this central issue is given in Chapter Three. The purpose of this chapter is served by assuming a unirate sampling policy.

2.4.3 Mapping a CACT Model into the CADT Domain

The key technique in producing an equivalent CADT domain state-space model from the CACT state-space is evaluation of the matrix function exp(**A**h). A large amount of published material is available that discusses various ways of evaluating this matrix function [2.21]. The requirement to numerically compute the exponential matrix exp(**A**h) efficiently and without error is obvious. The problems of computing an exponential matrix function are widely discussed in the literature. An extensive review of these problems is given by Moler and Van-Loan [2.22]. This section presents methods of checking the correctness of the computation of exp(**A**h).

Surprisingly, many textbooks that include a discussion on the matrix exponential imply a straight forward exponential series solution. Informed sources [2.23] consider the weakness in the series method and offer a more robust and efficient solution. However, the problems in computing, for example, exp(**A**h), are such that results must be checked for correctness. Methods to check the correctness of the computation of exp(**A**h) are developed below.

The basis of the method used to check the correctness of a mapping from **A** to Φ, by the exponential matrix function exp(**A**h), arises from

the observation that, at the sampling instants, the continuous-time states are equal to the equivalent sampled-data states. Formally, this is expressed as $\mathbf{x}(t) = \mathbf{x}(nh)$ where, at the sampling instants, $t = nh$. Under steady-state conditions where $\dot{\mathbf{x}}(t) = \mathbf{0}$, the continuous-time state and output equations are given by

$$\mathbf{0} = \mathbf{A}\,\mathbf{x}_{ss}(t) + \mathbf{B}\,\mathbf{u}_{ss}(t) \quad , \tag{2.19a}$$

$$\mathbf{y}_{ss}(t) = \mathbf{C}\,\mathbf{x}_{ss}(t) + \mathbf{D}\,\mathbf{u}_{ss}(t) \quad . \tag{2.19b}$$

The state equation (2.19a) can be rearranged to give

$$\mathbf{x}_{ss}(t) = -\,\mathbf{A}^{-1}\mathbf{B}\,\mathbf{u}_{ss}(t) \quad . \tag{2.20}$$

In the case of steady-state sampled-data where $\mathbf{x}(nh+h) = \mathbf{x}(nh)$, the state and output equations are given by

$$\mathbf{x}_{ss}(nh) = \Phi\,\mathbf{x}_{ss}(nh) + \Psi\,\mathbf{u}_{ss}(nh) \quad , \tag{2.21a}$$

$$\mathbf{y}_{ss}(nh) = \mathbf{C}\,\mathbf{x}_{ss}(nh) + \mathbf{D}\,\mathbf{u}_{ss}(nh) \quad . \tag{2.21b}$$

The state equation can be rearranged to give

$$\mathbf{x}_{ss}(nh) = [\mathbf{I} - \Phi]^{-1}\Psi\,\mathbf{u}_{ss}(nh) \quad . \tag{2.22}$$

Assuming that the sampled-data amplitude is not quantised, then, at the sampling instants where $t = nh$, equations (2.19a) and (2.21a)

$$-\,\mathbf{A}^{-1}\mathbf{B}\,\mathbf{u}_{ss}(t) = [\mathbf{I} - \Phi]^{-1}\Psi\,\mathbf{u}_{ss}(nh) \quad . \tag{2.23}$$

A check for the correctness of the mapping from **A** to Φ is provided by equation 2.23. If

$$- \mathbf{A}^{-1}\mathbf{B} = [\mathbf{I} - \Phi]^{-1}\Psi \qquad (2.24)$$

then the sampled-data system given by the quadruple $(\Phi,\Psi,\mathbf{C}_D,\mathbf{D}_D)$, is an accurate equivalent of the continuous-time system quadruple, given by **(A,B,C,D)**. If **A** is rank deficient its inverse cannot be determined; however, a check on the CACT to CADT mapping can be performed by rearranging (2.24) to give

$$-\mathbf{A}\,\Psi = [\mathbf{I} - \Phi]\,\mathbf{B} \quad . \qquad (2.25)$$

Another method of checking the equivalence of **A** and Φ is to use the following procedure:

(1) Compute the eigenvalues of the continuous-time state matrix **A** using

$$\det[\lambda\mathbf{I} - \mathbf{A}] = \mathbf{0} \quad . \qquad (2.26)$$

(2) Map each eigenvalue λ_i to the z-plane using the scalar function $\exp(\lambda_i h)$ to give z_i.

(3) Compute the eigenvalues of the sampled-data state matrix Φ using

$$\det[\zeta\mathbf{I} - \Phi] = \mathbf{0} \quad . \qquad (2.27)$$

(4) Compare the mapped continuous-time system eigenvalues λ_i with the directly computed sampled-data eigenvalues ζ_i and establish a sampling period h to give $z_i = \zeta_i$.

A further check on the correctness of the mapping function can be made by the inverse of the above procedure. The inverse correctness check is as follows:

(1) Using equations (2.26) and (2.27) compute the eigenvalues, λ and ζ, of the continuous-time and sampled-data systems, respectively.

(2) Map the sampled-data eigenvalues to the s-plane using the function

$$s_i = \frac{1}{h} \ln(z_i) \qquad (2.28)$$

where $z_i = \sigma_z + j\omega_z$.

(3) Compare the eigenvalues, s, of the mapped z to s domain sampled-data model, with the directly computed with the continuous-time eigenvalues, λ, and establish and confirm the sampling period value h that gives $s_i = \lambda_i$.

There is an ambiguity in the inverse correctness check that must be considered. The inverse mapping from the z-plane to the s-plane is not unique. However, with a sampling-rate, $\frac{1}{h}$, that complies with the requirements of the Nyquist-rate, the mapping defined by (2.28) is one-to-one.

The solution of the integral terms depend on the way in which the exponential matrix, exp(**A**h), is evaluated, so the evaluation checking techniques, developed above also apply to the integral

terms. The integral always exists; its evaluation can be simplified, if the CACT state matrix **A** is of full rank and hence has an inverse $\mathbf{A}^{-1}$. For these cases, the integrals (2.15) and (2.17) can be evaluated by

$$\int_0^h \exp(\mathbf{A}\lambda)\, d\lambda = \mathbf{A}^{-1}\left[\exp(\mathbf{A}h) - \mathbf{I}\right] \qquad (2.29)$$

and

$$\int_0^\Delta \exp(\mathbf{A}\lambda)\, d\lambda = \mathbf{A}^{-1}\left[\exp(\mathbf{A}\Delta) - \mathbf{I}\right] \quad . \qquad (2.30)$$

The two right-hand-side terms of equations, (2.29) and (2.30), give an algebraically convenient solution to integrals (2.15) and (2.17). However, the occurrence of rank-deficient state matrices in the basic aircraft model is not uncommon. In spite of this, some commercially available computer-aided-design programs offer the simplified expressions as the only means of mapping a model from the CACT domain to the CADT domain [2.24].

A solution to the rank-deficient state matrix problem, that avoids the need to explicitly solve the integrals (2.15) and (2.17), even when the matrix, **A**, is singular, is outlined below and described in more detail in Appendix One. Surprisingly, this technique cannot be attributed to any of the published literature reviewed for this thesis.

When the CACT system has a rank-deficient state matrix, **A**, caused by the presence of open-loop integrations, an equivalent discrete-time

system quadruple $(\Phi,\Psi,\mathbf{C}_D,\mathbf{D}_D)$ can be computed as follows:

$$\exp\begin{bmatrix} \mathbf{A}h & \mathbf{B}h \\ \mathbf{0} & \mathbf{0} \end{bmatrix} = \begin{bmatrix} \Phi & \Psi \\ \mathbf{0} & \mathbf{I} \end{bmatrix} \tag{2.31}$$

$$\exp\begin{bmatrix} \mathbf{A}\Delta & \mathbf{B}\Delta \\ \mathbf{0} & \mathbf{0} \end{bmatrix} = \begin{bmatrix} \Phi_\Delta & \Psi_\Delta \\ \mathbf{0} & \mathbf{I} \end{bmatrix} . \tag{2.32}$$

The discrete-time equivalent state equation terms are sub-matrices with dimensions that correspond to the their continuous-time counterparts in (2.31). The output equation terms, $\mathbf{C}_D$ and $\mathbf{D}_D$, are evaluated by

$$\mathbf{C}_D = \mathbf{C}\,\Phi_\Delta \tag{2.33}$$

$$\mathbf{D}_D = \mathbf{C}\,\Psi_\Delta + \mathbf{D} \quad . \tag{2.34}$$

The CACT to CADT mapping techniques given in this section are only applicable to sampled-data systems, where the sampled-data has infinite amplitude resolution. In the case of DFC systems or, indeed, any mixed-data digital control process, in which the control is provided by a digital computer, the added complications of data amplitude quantisation must be considered. Amplitude quantisation of the sampled-data is a stochastic process which is more readily included as part of a simulation exercise. However, it is appropriate to consider some features of amplitude quantisation during the initial design stage. These features are described in Chapter Four.

2.5 SUMMARY

This chapter presents a view of the data-domains associated with modern computer based DFC systems. Classifying the functions of a DFC system in terms of the CACT, CADT, DADT and DACT data-domain operations represents a novel view of digital computer control systems. While this view may be regarded as obvious, explicit attention to the quantisation issue is omitted from much of the literature covering general design aspects of computer-based control. Having set the route for DFC design and implementation, a review of methods of recasting an analogue-data model into an equivalent sampled-data model was presented. Support for this chapter is provided by the appendices. In particular, Appendix Two describes an experiment, the results of which support the case for direct-digital-design. Appendix One gives details of the development of the CACT to CADT mapping techniques presented in this chapter. The work of this chapter contributes to DFC design practice by exposing some useful techniques seldom, if at all, found in standard tutorial reference texts.

CHAPTER THREE

A SAMPLED-DATA AIRCRAFT MODEL FOR DFC DESIGN

3.1 INTRODUCTION

The case to transform the Continuous-Amplitude, Continuous-Time, state-space model of a basic aircraft into an equivalent Continuous-Amplitude, Discrete-Time domain, for the purpose of DFC system design, was presented in Chapter Two. The key parameter of the CACT to CADT mapping procedure is the sampling-period, h. This chapter addresses the issues concerned with the selection of the sampling-period and the production of a CADT state-space for the purpose of DFC design.

A general feature of a modern DFC system is a multirate sampling policy, which is employed in the implementation of the control functions. The principal aspect of the DFC design model, that is developed in this chapter, is the accommodation of a multirate sampling policy. Multirate sampling is necessary for the practical implementation of a DFC system; this assertion is based on two unrelated observations. The first observation focuses on the integrated-systems concept associated with modern DFC. In contrast to a classical analogue flight control system, a DFC system integrates information from a wide range of aircraft sensors and subsystems for the purpose of automatic flight control. As autonomous entities, these sensors and subsystems produce

information over a wide spectrum of bandwidths and data-rates. These bandwidths and data-rates are naturally selected to suit the primary function of the sensor or subsystem. The application of the information in flight control is a secondary function, therefore the data-rates may not be harmonised for a unirate sampled-data DFC process. For example, a terrain-following flight control function employs information from an inertial navigation system, a forward looking sensor (radar), a downward looking sensor (radio-altimeter) and a data-base of terrain contours. Each of these subsystems will, in general, have a frequency or data-rate at which information is made available for the secondary purpose of the terrain-following control system. A terrain-following flight controller which accommodates a spectrum of data-rates is, by definition, a multirate sampled-data system.

A second observation, which leads to the adoption of a multirate sampling policy for a DFC system, is concerned with the fundamental property of data amplitude quantisation. Amplitude quantisation is an implicit feature of a digital computer implementation of a control system. A classical view of the sampling-rate selection problem is that the ultimate, ideal sampling-period is zero. This view does not apply to sampled-data systems implemented in the Discrete-Amplitude, Discrete-Time domain of a digital computer. For a given characteristic frequency, in addition to the classical lower-bound limit on the sampling-rate, (maximum h), there is also an upper-bound limit, (minimum h); a demonstration of this fact is given in Section 3.2. A dynamical system consisting of several characteristic frequencies will not, in general, be encompassed

within the boundaries of a single sampling rate. Consequently, for the digital control of large-scale systems such as aircraft, a multirate sampling policy will be selected.

Although methods of assembling models of multirate sampled-data systems have been reported, [3.1], [3.2], their complexity, even in the state-space form, [3.3], [3.4], is considered to violate the four design methodology maxims that were prescribed in Section 1. of Chapter One. A state-space multirate sampled-data model format is developed which is considered to be more compatible with the design methodology objectives of the thesis.

3.2 THE SAMPLING RATE SELECTION PROBLEM

Given a CACT domain model of a basic aircraft, the primary design task is to transform it to an equivalent CADT domain (sampled-data) model. The method by which this can be achieved was described in Chapter Two. The cardinal issue of the CACT to CADT mapping problem is the selection of a sampling period, h. As with any rational approach to an engineering problem, a sampling period must be selected from known facts. In the case of a typical digital flight control system problem, the design is usually initiated with only a partial model of the basic aircraft available. It is, however, necessary to know, with reasonable certainty, the CACT dynamics of the system which includes the basic aircraft, the control actuators and the response sensors, plus any amplification, signal-processing and signal-filtering.

3.2.1 Sampling Rate and Digital Processing Wordlength

Before the methodology of selecting a sampling-rate or sampling-policy is considered, some results are presented to demonstrate the intimate relationship between sampling-rate and digital-data wordlength. These results are obtained in Appendix Three and serve to reinforce the arguments of this chapter.

Consider the modal form, discrete-data model of a sampled-data CACT system,

$$\mathbf{x}(n+1) = \Lambda_D \, \mathbf{x}(n) + \mathbf{w}_Q \quad , \tag{3.1}$$

where Λ_D is a discrete, m×m, diagonal state-matrix, produced by mapping a CACT domain m×m diagonal matrix, Λ, to the CADT domain. The input function, $\mathbf{w}_Q$, from a digital computer, is an m×1 vector of white-noise quantities, representing the quantisation noise produced by the finite wordlength digital-data. The analysis given in Appendix Three produces the following equations which relate the sampling-rate to the digital-data wordlength, in terms of a noise amplification parameter.

The noise amplification factor is defined as

$$\eta = \frac{\sigma_x}{\sigma_w} \quad , \tag{3.2}$$

where σ_x is the standard deviation of the noise component associated

with a single state x, and σ_W is the standard deviation of the quantisation noise of a single control input. As shown in Appendix Three, each diagonal element of the matrix Λ_D produces one eigenvalue. Defining the eigenvalue of x as λ then, as shown in Appendix Three the sampling period, h, is given in terms of this eigenvalue and the quantisation noise amplification, η, by

$$h = \frac{1}{\lambda}\left(-1 \pm \sqrt{1 - \frac{1}{\eta^2}} \right) \quad . \qquad (3.3)$$

Since λ is a pole of the system, it is clear that if the noise amplification term is constant then, as the pole moves towards zero, h tends to infinity. Equation (3.3) shows that, to achieve a given constant noise amplification, the sampling-period, h, must be increased as the pole location is reduced. Assuming the quantisation noise variance in terms of the digital computer wordlength, W, is given as $\sigma_W^2 = \frac{(2^{-W})^2}{12}$, [3.5] then, as shown in Appendix Three, W is given by

$$W = \frac{1}{\log(2)} \log\left\{ \frac{1}{\sqrt{12}\ \sigma_x \sqrt{(\lambda h)^2 + 2\lambda h}} \right\} \quad . \qquad (3.4)$$

This expression indicates that, for a given standard deviation of output noise, σ_x ,a reduction in the sampling period will require an increase in the data-conversion process wordlength, W. It is also clear that, for both a constant standard deviation of output noise and constant sampling period, a decrease in the pole location must

be accompanied by an increase in the wordlength of the data conversion devices.

3.3 SELECTING A SAMPLING POLICY

It is assumed, that a sampling policy for a digital flight control system must be identified on the basis of a subset of the CACT, open-loop state-space model of the basic aircraft. The implicit information available in this subset model, are the natural frequency components of the system's characteristic frequency response. It is common practice to select a single sampling-rate on the basis of the some multiple of the highest natural frequency component [3.6]. As illustrated in the previous section, a sampling-rate can be too high as well as too low. For a system with both high and low frequency modes, an appropriate sampling-rate for the high frequency mode may be too fast for the low frequency mode.

The sampling-rate selection problem receives surprisingly little attention in the digital control systems literature. However, a noted exception to this paucity is the widely quoted work of Powell and Katz, [3.7]. However, their technique is not suitable for the approach to DFC system design that is proposed for this thesis. The sampling-rate, or -policy, must be established in order to transform the basic CACT aircraft system into an equivalent CADT model, on which the DFC design tasks are undertaken. Therefore, the sampling-policy selection procedure starts with an open-loop, CACT, state-space model of the basic aircraft. The procedure is based on

the intersample divergence characteristics of the basic aircraft state, which occurs in response to a random disturbance signal applied to the control input. The procedure explicitly addresses each state and input and therefore has the facility to identify a multirate sampling-policy. To ensure that the selected sampling-policy meets the minimum sampling rate requirements of Shannon's Sampling Theorem (or the Nyquist Sampling Criteria), [3.8], a z-plane diagram of the zeros of the system's characteristic equation is produced. Details of this and the selection procedure are described in the following paragraphs.

In this section, guidelines and techniques are given that can be used to select a sampling policy for a DFC system. The fundamental principle upon which these techniques are based is summarised as follows: At each sampling instant, the sampling switch is closed and an unbroken path effectively exist between the control signal source and the control inputs of the basic aircraft. At this instant the basic aircraft system is under control and the state error is assumed to be zero. Between sampling instants, the sampling switch is open, thus breaking the connection between the control signal source and the basic aircraft. For this period the basic aircraft system is free-running and diverging from the required, controlled state. When the magnitude of the error of a free-running, physical-state of the system reaches a predefined level, another sample of control activity must be applied to zero the state error, which is built up during the intersample period.

3.3.1 Sampling Policy Selection Procedure

This section describes another technique, which has a practical application in the methodology of selecting a sampling policy for a DFC system. The technique focuses on a time history analysis of the open-loop system state uncertainties, when the control inputs are exercised with stochastic functions. The technique compliments the method described in the last section by effectively addressing the lowest control signal regimes. It is assumed that the control inputs are exercised with signals which are produced by a numerical round-off quantisation process within the DAC interface device. Although this is a slight misinterpretation of the real process taking place in the combined ADC/Digital-Computer/DAC subsystem, it does not matter for the purpose of this analysis. The assumptions permit the stochastic control inputs to be defined in terms of the the variance of the quantisation noise, $\sigma_w = \frac{(2^{-W})^2}{12}$. The state equation with a stochastic signal applied to the control inputs is defined as

$$\dot{\mathbf{x}}(t) = \mathbf{A}\,\mathbf{x}(t) + \mathbf{B}\,\mathbf{w}(t) \quad . \tag{3.5}$$

The terms **A**, **B**, and **x**(t) have their usual meaning in the sense of the CACT state equation (2.3a). The term **w**(t) is a vector of white noise functions that couple into the system through control matrix, **B**. The interpretation of the noise term is given in Appendix Four. Further comments on the questionable validity of this equation are also given Appendix Four. The covariances of the stochastic inputs and output states are defined as

$$Q_c(t) = \mathcal{E}\left[w(t)w^T(t)\right] \quad , \tag{3.6}$$

and

$$G_c(t) = \mathcal{E}\left[x(t)x^T(t)\right] \quad , \tag{3.7}$$

respectively, where $\mathcal{E}$ is the expectation operator. The state covariance is propagated in time by the differential equation

$$\dot{G}_c(t) = A\,G_c(t) + G_c(t)\,A^T + B\,Q_c B^T \quad . \tag{3.8}$$

Equation (3.8) is recast in terms of first order discrete-time approximations to **A** and **B**, in order to obtain a numerical solution. The approximate form of (3.8) is

$$G_{K+1} = \left[I + A\,\delta t\right]G_K\left[I + A\,\delta t\right]^T + B\,Q_c B^T\delta t \quad , \tag{3.9}$$

where δt is a time step, chosen by the rule, [3.9]

$$\delta t = \frac{1}{2\,\|A\|\,10^4} \quad , \tag{3.10}$$

and $\|A\|$ denotes a norm of the m×m matrix **A**, which is defined as $\|A\| = \left(\sum_{i=1}^{m}\sum_{j=1}^{m}(a_{ij})^2\right)^{\frac{1}{2}}$ with a_{ij} representing the elements of **A**. From an assumed initial state covariance of $G_K = 0$ ($G_c(t_0) = 0$), equation (3.9) is propagated in steps of δt to a final state covariance $G_c(t_1)$. The resulting record of the state covariance time-history provides a quantitative measure in the process of selecting a sampling policy. From the DFC system design example,

considered in detail in Chapter Six, the resulting covariance time-history for two of the four state elements is shown in Fig.3.1.

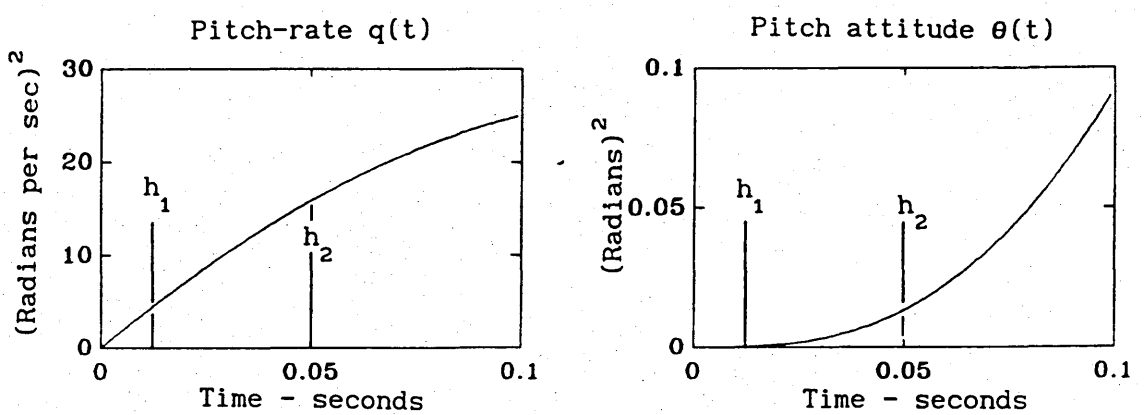

The covariance time-history for two state elements from the DFC system design example described in Chapter Five

Fig.3.1

The application of the state covariance time-history for the determination of a sampling rate for each state element and each control input proceeds as follows: Consider, for example, a state element, x, its covariance plotted according to the procedure described above. From zero uncertainty at time t=0 (assumed as a sampling instant), the uncertainty increases as time progresses (assumed as the intersample period). The time at which the value of the uncertainty reaches an unacceptable level represents the maximum sampling period of the state x. For the two state elements considered above in Fig.3.1a and Fig.3.1b, the sampling-periods are selected (as described in Chapter Five) as h_1 and h_2, respectively.

What constitutes a value of acceptable uncertainty for any given state element is a matter of engineering judgment which is based on an interpretation of the physical significance and scaling of each state element. This is one reason why emphasis is placed on retaining the physical states of the basic system dynamics. In the case of an aircraft, guidelines on the uncertainty are provided by the standard flight control and aircraft handling qualities specifications, such as MIL-F-8785C.

The lower sampling-rate boundary is set by the requirements of Shannon's Sampling Theorem and the derived Nyquist-rate, which gives the theoretical lower limit of the sampling-rate. The above procedure produces a sampling-policy on the basis of an open-loop, uncontrolled system model. However the application of a feedback controller will modify the dynamics of the basic system and hence the related distribution z-plane poles and zeros. The problem is that these closed-loop characteristics are are also function of the sampling policy. This is easily seen by inspecting the closed-loop, sampled-data, z-plane transfer-function,

$$\mathbf{x}(z) = \left[zI - \exp(Ah)\ [I+A^{-1}]B\ H + A^{-1}B\ H\right]^{-1} A^{-1}\left[\exp(Ah) - I\right]B\ \mathbf{v}(z). \tag{3.11}$$

where the closed-loop input $\mathbf{v}(z) = \mathbf{u}(z) - H\ \mathbf{x}(z)$. The matrix, H, is the negative state feedback function which, in the case of DFC systems, represents the digital flight computer.

The problem of selecting a closed-loop sampling policy, on the basis of an open-loop model, suggests that the direct digital design method must proceed from an *a priori* knowledge of the required closed-loop characteristics. For flight control systems, particularly in the case of the inner-control-loops which are associated with aircraft stability, the *a priori* knowledge of the required closed-loop characteristics can be deduced from the appropriate flight control or aircraft handling qualities documents. When only the basic open-loop aircraft model data is available, a sampling-policy which maps the CACT domain dynamics to a sector of a right-half z-plane usually gives adequate results. Using this method, the minimum sampling rate of a multirate sampling policy is determined from the sampling period h that casts the highest frequency eigenvalues inside the envelope indicated in Fig.3.2.

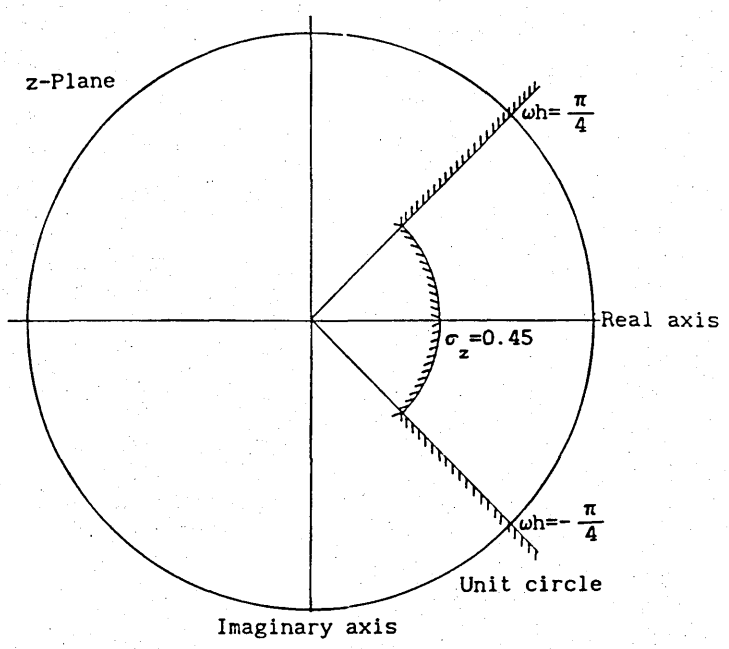

Mapping boundary for the highest frequency eigenvalue

Fig.3.2

The basis of the boundary is the establishment of a design margin between the highest frequency mode and the Nyquist sampling frequency limit, which is represented as the negative-real axis of the z-plane. The design margin must be sufficient to accommodate the pole-shifts produced by the design of closed-loop controllers. The margin must also accommodate the increasing z-plane sensitivity of a system's dynamic characteristics as they map towards the negative real axis. In the case of the inner-loop control of aircraft including stability augmentation and autopilot systems, the boundary defined in Fig.3.2 has been shown to be adequate [3.10].

A formal statement of the z-plane boundary is defined as follows:

Given a CACT system pole $\lambda_s=\sigma\pm j\omega$, the equivalent z-plane pole under a sample period mapping h is given by

$$\lambda_z = \exp(\lambda_s h) = \exp(\sigma h)\Big(\cos(\omega h) \pm j\sin(\omega h)\Big) \quad . \qquad (3.12)$$

The value of h is selected to map λ_z on a z-plane such that

$$\exp(\sigma h) \geq 0.45 \quad \text{and} \quad \omega h \leq \frac{\pi}{4} \quad .$$

The significance of the values assigned to these quantities is described in detail in Appendix Seven.

The criterion imposed by the z-plane boundary, described above, is interpreted as a property of the CADT domain. To assess the DACT domain properties of the system's dynamics, as they apply to this application of the z-plane, interest focuses on the separation of

the individual z-plane poles and zeros. Distinct CACT poles and zeros can be, by virtue of the selected sampling-rate, collocated in the z-plane and give rise to a number of design and implementation problems. In general, these problems are identified as a loss of controllability and observability caused by time-sampling and amplitude-quantisation of the CACT data. This observation has been studied in detail [3.11], [3.12].

As applied in this current research, the sampling-policy selection procedure, described in this section, is a pseudo-analytic approach. However, the potential of the procedure to determine a multirate sampling policy for a DFC system hinges on the ease with which an aircraft's handling qualities can be directly related to its physical state elements. This issue is a topic that is identified for further study.

3.3.2 The Presentation of a Multirate Sampling Policy

The result of the sampling-rate selection exercise is, in general, a multirate sampling policy. To keep a practical perspective of a complex multirate sampled-data model requires a systematic approach to the multirate data structure. In principle, a separate sampling-rate could be defined for each control input and each state output of the multiple-input, multiple-output basic aircraft system. In practice, there is usually sufficient flexibility in the assignment of a sampling rate to allow more than one control input and/or one state output to be grouped under a single sampling rate.

In the case of flight control applications both the modelling and implementation tasks become more tractable if the sampling periods are synchronised and scheduled as integer multiples of the shortest sampling period; for an example refer to Fig.3.3. The form of the multirate state measurement sampling vector is

$$\mathbf{x}^T(t) = \left[\mathbf{x}_1^T(t) \;\middle|\; \mathbf{x}_2^T(t) \;\middle|\; .... \;\middle|\; \mathbf{x}_f^T(t) \right] , \qquad (3.13)$$

where $\left(\mathbf{x}_i^T(t) \;, i = 1, 2, \ldots f\right)$ defines a transposed column subvector of states that are assigned to the i-th state measurement sampling rate and f is the number of sampling-rates assigned to the state measurement process. The multirate sampling control inputs are the elements of the vector

$$\mathbf{u}^T(t) = \left[\mathbf{u}_1^T(t) \;\middle|\; \mathbf{u}_2^T(t) \;\middle|\; .... \;\middle|\; \mathbf{u}_k^T(t) \right] , \qquad (3.14)$$

where $\left(\mathbf{u}_i^T(t) \;, i = 1, 2, \ldots k\right)$ defines a transposed column subvector of control inputs that are applied to the CACT system at the i-th sampling rate and k is the number of sampling-rates assigned to the control input process.

3.4 A MULTIRATE SAMPLED-DATA MODEL FOR DFC DESIGN

As indicated in the introduction to this chapter, a consequence of the proper recognition of the four domains associated with a DFC system results in a controller with a multirate sampling policy. A general method is therefore required by which the basic aircraft and

subsequent control structures can be modelled and analysed. The concept of multirate sampling is not new. However, it was concluded from a survey of the various available methods of modelling multirate sampled-data system that an alternative method was required to meet the DFC design maxims of this thesis. This section describes a multirate sampled-data system model that has been developed to meet the objectives of the thesis. Before this model is described, a summary of the methods reviewed for the thesis is given.

3.4.1 A Review of Multirate Sampled-data Modelling Methods

The original methods of modelling multirate sampled-data system were established as part of the classical transfer-function approaches to sampling [3.13], [3.14]. State-space methods of modelling multirate sampled-data systems have been developed [3.15], [3.16], [3.17]. Most notable among these state-space methods is the work of Kalman and Bertram. Although Kalman and Bertram's method satisfies the generality objectives, their model is considered to be unsuitable for this thesis for the following reasons. First, the combined configuration of the CACT and CADT subsystems must be defined before a model can be developed. This means that the reduction of the state-space model to a transfer-function will be a closed-loop system equation. Second, the state-space model is not automatically cast in the form of the **(A,B,C,D)** quadruple. Third, the growth in complexity, as a specific symbolic model is assembled, is considered to compromise the design maxims of the thesis.

Techniques that overcome the first two deficiencies have been developed, and are described in an ancillary report of this thesis [3.18]. This report also demonstrates the growth in complexity that is considered to undermine the utility of the Kalman and Bertram model.

3.4.2 A Development of a Multirate Sampled-Data System Model

A method of assembling a multirate sampled-data system model is described in this section. The proposed assembly method has been developed to meet the design maxims and systematic modelling objectives of the thesis. The technique builds on an open-loop, state-space quadruple model of a basic aircraft. The control input to this model is the partitioned vector, $\mathbf{u}(t)$, that was defined in Section 3 as the multirate sampled control data. Substituting the multirate sampled control data vector into the state-space quadruple (A,B,C,D) gives

$$\dot{\mathbf{x}}(t) = \mathbf{A}\,\mathbf{x}(t) + \sum_{\ell=1}^{k} \mathbf{B}_\ell \mathbf{u}_\ell(t) \qquad (3.15a)$$

$$\mathbf{y}(t) = \mathbf{C}\,\mathbf{x}(t) + \sum_{\ell=1}^{k} \mathbf{D}_1 \mathbf{u}_1(t) \quad . \qquad (3.15b)$$

The controls, $\left(\mathbf{B}_\ell \ , \ell=1\ldots k\right)$ and direct matrix terms, $\left(\mathbf{D}_\ell \ , \ell=1\ldots k\right)$ are submatrices of B and D, respectively. The row dimensions of the $\mathbf{B}_\ell$ and $\mathbf{D}_\ell$ terms are given by the number of states and number of outputs, respectively. The column dimensions of both the $\mathbf{B}_\ell$ and $\mathbf{D}_\ell$ terms are determined by the number of inputs assigned to each partition.

3.4.3 A Proposed Model of a Multirate Sampled-Data System

The process of assembling a multirate sampled-data model of an open-loop CACT state-space system is described for the case of a three rate sampling schedule. Limiting the development to a specific sampling schedule serves two purposes. First, the specific case facilitates the description of the assembly procedure without compromising the generality of the methodology. Second, the ease by which the principles of the specific case are extended to other sampling schedules demonstrates the compatibility of the method with the prescribed design maxims.

Consider a CACT domain system, with its control inputs partitioned for the application of three different sampling rates. The CACT state-equation, deduced from (3.15a), is given by

$$\dot{\mathbf{x}}(t) = \mathbf{A}\,\mathbf{x}(t) + \mathbf{B}_1\mathbf{u}_1(t) + \mathbf{B}_2\mathbf{u}_2(t) + \mathbf{B}_3\mathbf{u}_3(t). \qquad (3.16)$$

For the purpose of the description, it is assumed that the system has been assigned the multirate sampling policy which is defined by the schedule shown in Fig.3.3.

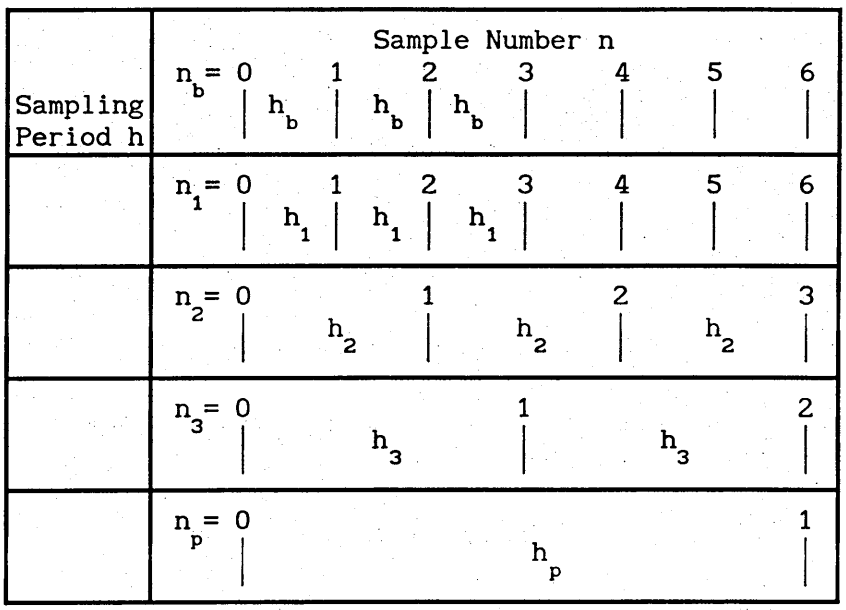

The demonstration three rate sampling policy schedule

Fig.3.3

From the sampling policy schedule it can be seen that the base sampling period $h_b = h_1$ and the program period $h_p = 6h_b$. The program period is formally defined as the lowest common multiple (LCM) of the sampling-rates, in this case given by

$$LCM(s_1, s_2, s_3) = LCM(1,2,3) = 6 = h_p \qquad (3.17)$$

For the notation used in the development of this example, it is convenient to define $h_p = \rho$. The sampling policy schedule also shows that all the samplers are asserted at the initial increment of the program sample sequence.

The process of defining a CADT domain model for the system, given by equation (3.16), starts by finding the solution to the state equation at the initial program increment. The initial solution is propagated over the base-rate time interval because a ZOH keeps the sampled input constant between base-rate samples. At time increment n, shown as the initial sample on the schedule of Fig.3.3, the CADT domain state equation for the period $((n_1)t \leq \tau_n < (n_1+1)t)$ is given by

$$\mathbf{x}\Big((n+1)h_1\Big) = \Phi\, \mathbf{x}(nh_1) + \Psi_1\, \mathbf{u}_1(nh_1) + \Psi_2\, \mathbf{u}_2(nh_1) + \Psi_3\, \mathbf{u}_3(nh_1), \quad (3.18)$$

where n is the initial sample number of the program period.

There is no loss of generality by considering the initial program sample as the increment $n_p = 0$. Under this condition, equation (3.18) is recast as

$$\mathbf{x}(1) = \Phi\, \mathbf{x}(0) + \Psi_1\, \mathbf{u}_1(0) + \Psi_2\, \mathbf{u}_2(0) + \Psi_3\, \mathbf{u}_3(0). \quad (3.19)$$

Repeating the solution for each new member of the input set for one cycle of the program produces the CADT domain multirate sampled-data state equation, given by

$$\mathbf{x}(6) = \Phi^6\,\mathbf{x}(0) + \Phi^5\Psi_1 u_1(0) + \Phi^5\Psi_2 u_2(0) + \Phi^5\Psi_3 u_3(0)$$
$$+ \Phi^4\Psi_1 u_1(1) + \Phi^4\Psi_2 u_2(0) + \Phi^4\Psi_3 u_3(0)$$
$$+ \Phi^3\Psi_1 u_1(2) + \Phi^3\Psi_2 u_2(1) + \Phi^3\Psi_3 u_3(0)$$
$$+ \Phi^2\Psi_1 u_1(3) + \Phi^2\Psi_2 u_2(1) + \Phi^2\Psi_3 u_3(1)$$
$$+ \Phi\,\Psi_1 u_1(4) + \Phi\,\Psi_2 u_2(2) + \Phi\,\Psi_3 u_3(1)$$
$$+ \Psi_1 u_1(5) + \Psi_2 u_2(2) + \Psi_3 u_3(1). \qquad (3.20)$$

The coefficient matrices of (3.20) are given in terms of the CACT state-equation (3.16) coefficients by

$$\Phi = \exp(\mathbf{A}\,h_b) \qquad (3.21)$$

$$[\Psi_1] = \left[\int_0^{h_b} \exp(\mathbf{A}\,\lambda)\,d\lambda\right]\mathbf{B}_1 \qquad (3.22)$$

$$[\Psi_2] = \left[\int_0^{h_b} \exp(\mathbf{A}\,\lambda)\,d\lambda\right]\mathbf{B}_2 \qquad (3.23)$$

$$[\Psi_3] = \left[\int_0^{h_b} \exp(\mathbf{A}\,\lambda)\,d\lambda\right]\mathbf{B}_3. \qquad (3.24)$$

The next task is to rearrange equation (3.20) into the standard state-equation form. This is achieved by separating the input coefficient matrices from the input vectors to give

$$\mathbf{x}(\rho) = [\Phi\,]^{\rho}\,\mathbf{x}(0) + \Gamma\left[{}^{\rho}\,\Phi\right]\mathbf{B}_{\rho}\,\mathbf{u}_{\rho}(k_{0,5}, k_{0,3}, k_{0,2}). \qquad (3.25)$$

From equations (3.16) and (3.17) $\rho = 6$. The notation of k parameters, associated with the three inputs, is interpreted as follows; $k_{0,5}$ defines u_1 over five base sampling periods, $k_{0,3}$

defines u_2 over three base sampling periods, and $k_{0,2}$ defines u_3 over two base sampling periods. The matrices associated with the inputs are defined as

$$\Gamma = \int_0^{h_b} \exp(A\,\lambda)\, d\lambda \quad , \tag{3.26}$$

$$\begin{bmatrix} \rho & \Phi \end{bmatrix} = \begin{bmatrix} \Phi^5 & \Phi^4 & \Phi^3 & \Phi^2 & \Phi & I \end{bmatrix} \tag{3.27}$$

$$\text{for } \rho = 6 \quad ,$$

$$B_\rho = \begin{bmatrix} B_1 & 0 & 0 & 0 & 0 & 0 & B_2 & 0 & 0 & B_3 & 0 \\ 0 & B_1 & 0 & 0 & 0 & 0 & B_2 & 0 & 0 & B_3 & 0 \\ 0 & 0 & B_1 & 0 & 0 & 0 & 0 & B_2 & 0 & B_3 & 0 \\ 0 & 0 & 0 & B_1 & 0 & 0 & 0 & B_2 & 0 & 0 & B_3 \\ 0 & 0 & 0 & 0 & B_1 & 0 & 0 & 0 & B_2 & 0 & B_3 \\ 0 & 0 & 0 & 0 & 0 & B_1 & 0 & 0 & B_2 & 0 & B_3 \end{bmatrix} \quad , \tag{3.28}$$

$$u_\rho(k) = \begin{bmatrix} u_1(0) \\ u_1(1) \\ u_1(2) \\ u_1(3) \\ u_1(4) \\ u_1(5) \\ u_2(0) \\ u_2(1) \\ u_2(2) \\ u_3(0) \\ u_3(1) \end{bmatrix} \quad . \tag{3.29}$$

The CACT output equation for this is deduced from equation (3.15b) and is given by

$$y(t) = C\,x(t) + D_1\,u_1(t) + D_2\,u_2(t) + D_3\,u_3(t). \tag{3.30}$$

Mapping equation (3.30) to the CADT domain with the multirate sampling policy defined in Fig.3.3 produces the multirate sampled-data output equation given by

$$\mathbf{y}(\rho-1)=\mathbf{C}\ [\Phi]^{\rho-1}\mathbf{x}(0)+\mathbf{C}\ \Gamma\left[\Phi^{\rho-1}\ \middle|\ \mathbf{0}\right]\mathbf{B}_{\rho}\mathbf{u}_{\rho}(k)+\mathbf{D}_{\rho}\mathbf{u}_{\rho}(k_{0,5},k_{0,3},k_{0,2}) \quad . \tag{3.31}$$

The matrix, **C**, is identical to the **C** matrix of the CACT domain output equation. The matrix terms Φ , Γ , and $\mathbf{B}_{\rho}$ are given above by equations (3.27), (3.26) and (3.28), respectively. The multirate input vector $\mathbf{u}_{\rho}$ is defined as equation (3.29) and $\mathbf{x}(0)$ is the system state at the beginning of each multirate program period. The remaining terms, for ρ=6, are given by

$$\left[\ \Phi^{\rho-1}\ \middle|\ \mathbf{0}\ \right] = \left[\ \Phi^4\ \ \Phi^3\ \ \Phi^2\ \ \Phi\ \ \mathbf{I}\ \middle|\ \mathbf{0}\ \right] \tag{3.32}$$

$$\mathbf{D}_{\rho} = \left[\ 0\ 0\ 0\ 0\ 0\ \mathbf{D}_1\ \middle|\ 0\ 0\ \mathbf{D}_2\ \middle|\ 0\ \mathbf{D}_3\right]. \tag{3.33}$$

The dimensions of the coefficient matrices are deduced from the dimensions of the state vector, $\mathbf{x}(t)$, the input vector, $\mathbf{u}(t)$, the output vector, $\mathbf{y}(t)$, and the parameters of the sampling policy. Consider, for example, the three rate system described above, assuming the model has m states, q inputs and r outputs. These quantities produce the following information for the CADT model.

$\mathbf{x}(nh)$	-	m state vector
$\mathbf{y}(nh)$	-	r output vector
Φ	-	m×m matrix
Γ	-	m×m matrix
$\mathbf{C}$	-	r×m matrix.

To determine the dimensions of the remainder of the terms, in both the state and output equations, requires analysis of the multirate sampling policy. Using the results of the above example, some general observations can be made to support this analysis. Consider the q element input vector $\mathbf{u}(t)$; this is partitioned for three sampling rates $\mathbf{u}_1$, $\mathbf{u}_2$, and $\mathbf{u}_3$. Assume that $\mathbf{u}_1$ is a vector with α elements, $\mathbf{u}_2$ is a vector with β elements and $\mathbf{u}_3$ is a vector with γ elements.

First observation	$q = \alpha + \beta + \gamma$.
Second observation	$\mathbf{B}_1$ is an m×α matrix .
	$\mathbf{B}_2$ is an m×β matrix .
	$\mathbf{B}_3$ is an m×γ matrix .

The null sub-matrices have dimensions that are given by the **B** matrix of the column in which they occur. In the case of the example, the dimension of the matrix $\mathbf{B}_\rho$ is given by

$$(m\ \rho) \times \left(\alpha \frac{\rho}{h_1} + \beta \frac{\rho}{h_2} + \gamma \frac{\rho}{h_3} \right) .$$

The general form of the notation employed in equation (3.32) is

$$\left[{}^{y}X \right] = \left[X^{y} \quad X^{y-1} \ldots\ldots\ldots X^{2} \quad X \quad I \right]. \qquad (3.34)$$

The dimensions of $\left[{}^{\rho}\Phi \right]$ and $\left[{}^{\rho-1}\Phi \;\middle|\; 0 \right]$ are $m \times m(\rho+1)$

The matrix, $\mathbf{D}_{\rho}$, is partitioned, where the number of partitions is given by ρ. Each partition has one **D** sub-matrix; all the other sub-matrices in the associated partition are assigned as null matrices. The dimensions of the null matrices assume the dimensions of their associated **D** sub-matrix. In the case of the example, the dimensions of the three **D** sub-matrices are

$$\mathbf{D}_1 = r \times \alpha \;, \; \mathbf{D}_2 = r \times \beta \;\text{ and }\; \mathbf{D}_3 = r \times \gamma.$$

The number of null sub-matrices in each partition is given by $\frac{\rho}{h_1}-1$, $\frac{\rho}{h_2}-1$, and $\frac{\rho}{h_3}-1$ for the terms associated with $\mathbf{D}_1$, $\mathbf{D}_2$, and $\mathbf{D}_3$, respectively.

The overall dimension of the matrix $\mathbf{D}_{\rho}$ is given by

$$r \times \left(\alpha \frac{\rho}{h_1} + \beta \frac{\rho}{h_2} + \gamma \frac{\rho}{h_3} \right).$$

The CADT domain multirate sampled-data state and output equations are put into the standard, generalised quadruple form by defining

the following relationships,

$$\Phi_P = [\ \Phi\ ]^{\rho} \tag{3.35}$$

$$\Lambda_P = \Gamma \left[{}^{\rho}\Phi \right] B_{\rho} \tag{3.36}$$

$$X_P = C\ [\ \Phi\ ]^{\rho-1} \tag{3.37}$$

$$\Theta_P = \left[C\ \Gamma \left[{}^{\rho-1}\Phi \;\middle|\; 0 \right] B_{\rho} + D_{\rho} \right]. \tag{3.38}$$

From these expressions the state and output equation are given as

$$\mathbf{x}\Big((n_P+1)h_P\Big) = \Phi_P\ \mathbf{x}(n_P h_P) + \Lambda_P\ \mathbf{u}(n_P h_P) \tag{3.39a}$$

$$\mathbf{y}(n_P h_P) = X_P\ \mathbf{x}(n_P h_P) + \Theta_P\ \mathbf{u}(n_P h_P)\ , \tag{3.39b}$$

where the subscript p denotes the program period.

3.4.4 Multirate Sampling with State-Feedback

Consideration is now given to the organisation of a state-feedback model for systems with their control input partitioned for multirate sampling. The utility of the resulting closed-loop equations and the importance of keeping a physical insight of the system these equations represent are significant features of the formulation. A specific example is used to illustrate the method of organising a state-feedback model for a multirate sampled-data system. The proposed organisation of a state-feedback model starts by

considering a closed-loop arrangement of the form illustrated in Fig.3.4.

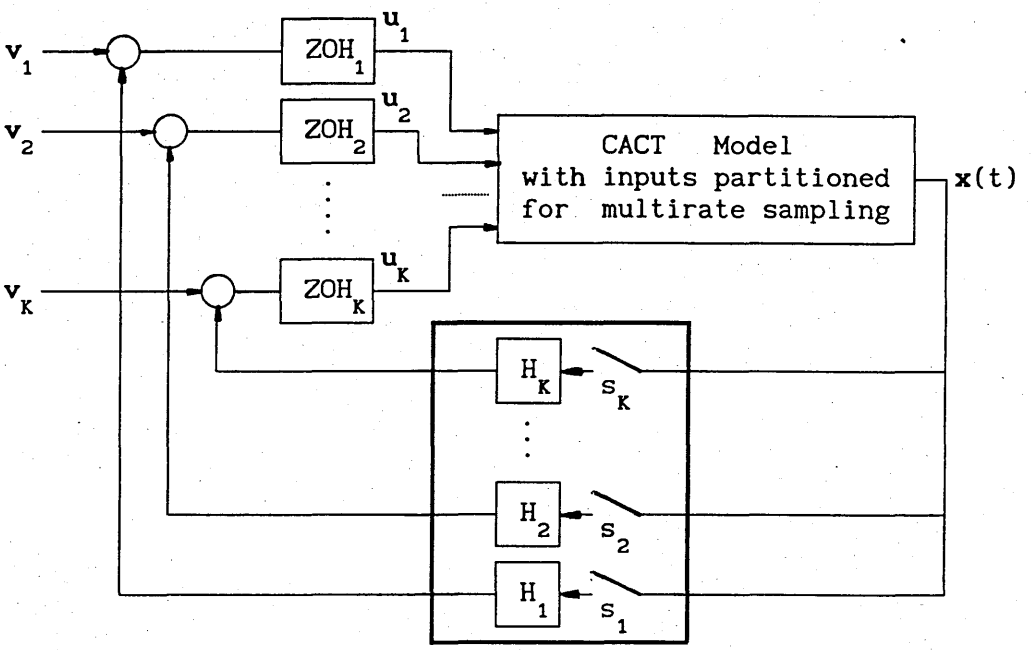

The general arrangement of a multirate sampled-data system model employing state feedback control

Fig.3.4

Consider the system, described in Section 3.4.2,which employs a three-rate sampling-policy. The structure of the overall state feedback element, **H**, is a key feature of a closed-loop multirate sampled-data system. With the multirate sampling defined in Fig.3.3, the input equations for the state-feedback system are defined over one program period, h_p, by

$$
\begin{aligned}
u_1(0) &= H_1 x(0) + v_1(0) \\
u_1(1) &= H_1 x(1) + v_1(1) \\
u_1(2) &= H_1 x(2) + v_1(2) \\
u_1(3) &= H_1 x(3) + v_1(3) \\
u_1(4) &= H_1 x(4) + v_1(4) \\
u_1(5) &= H_1 x(5) + v_1(5) \\
\\
u_2(0) &= H_2 x(0) + v_2(0) \\
u_2(1) &= H_2 x(2) + v_2(1) \\
u_2(2) &= H_2 x(4) + v_2(2) \\
\\
u_3(0) &= H_3 x(0) + v_3(0) \\
u_3(1) &= H_3 x(3) + v_3(1) \quad .
\end{aligned}
$$

In matrix form this set of multirate input equations is recast as

$$
\begin{bmatrix} u_1(0) \\ u_1(1) \\ u_1(2) \\ u_1(3) \\ u_1(4) \\ u_1(5) \\ u_2(0) \\ u_2(1) \\ u_2(2) \\ u_3(0) \\ u_3(1) \end{bmatrix}
=
\begin{bmatrix}
H_1 & 0 & 0 & 0 & 0 & 0 \\
0 & H_1 & 0 & 0 & 0 & 0 \\
0 & 0 & H_1 & 0 & 0 & 0 \\
0 & 0 & 0 & H_1 & 0 & 0 \\
0 & 0 & 0 & 0 & H_1 & 0 \\
0 & 0 & 0 & 0 & 0 & H_1 \\
H_2 & 0 & 0 & 0 & 0 & 0 \\
0 & 0 & H_2 & 0 & 0 & 0 \\
0 & 0 & 0 & 0 & H_2 & 0 \\
H_3 & 0 & 0 & 0 & 0 & 0 \\
0 & 0 & 0 & H_3 & 0 & 0
\end{bmatrix}
\begin{bmatrix} x(0) \\ x(1) \\ x(2) \\ x(3) \\ x(4) \\ x(5) \end{bmatrix}
+
\begin{bmatrix} v_1(0) \\ v_1(1) \\ v_1(2) \\ v_1(3) \\ v_1(4) \\ v_1(5) \\ v_2(0) \\ v_2(1) \\ v_2(2) \\ v_3(0) \\ v_3(1) \end{bmatrix}
\quad . \qquad (3.40)
$$

Writing (3.40) in a succinct form

$$
u_\rho(k) = H_\rho \; x_\rho(n_1) \; + \; v_\rho(k) \quad . \qquad (3.41)
$$

Substituting this equation into equations (3.39a) and (3.39b), respectively, gives

$$\mathbf{x}(\rho) = [\Phi\ ]^{\rho}\ \mathbf{x}(0) + \Gamma\left[{}^{\rho}\ \Phi\ \right]\mathbf{B}_{\rho}\mathbf{H}_{\rho}\ \mathbf{x}_{\rho}(n_1) + \Gamma\left[{}^{\rho}\ \Phi\ \right]\mathbf{B}_{\rho}\ \mathbf{v}_{\rho}(k) \qquad (3.42)$$

and

$$\begin{aligned}\mathbf{y}(\rho-1) \;=\;& \mathbf{C}\ [\Phi\ ]^{\rho-1}\ \mathbf{x}(0) \\ &+ \mathbf{C}\ \Gamma\left[{}^{\rho-1}\ \Phi \;\middle|\; 0\ \right]\mathbf{B}_{\rho}\mathbf{H}_{\rho}\mathbf{x}_{\rho}(n_1) + \mathbf{D}_{\rho}\mathbf{H}_{\rho}\ \mathbf{x}_{\rho}(n_1) \\ &+ \mathbf{C}\ \Gamma\left[{}^{\rho-1}\ \Phi \;\middle|\; 0\ \right]\mathbf{B}_{\rho}\ \mathbf{v}_{\rho}(k) \;+ \mathbf{D}_{\rho}\ \mathbf{v}_{\rho}(k) \quad . \qquad (3.43)\end{aligned}$$

These two equations are further refined by eliminating all but the initial program state, $\mathbf{x}(0)$, from the incrementing state vector, $\mathbf{x}_{\rho}(n_1)$. The substitution term is developed by propagating the state equation over one program period and collecting the expressions for each state increment as elements in a matrix equation. This process produces the following equation:

$$\begin{bmatrix} x(0) \\ x(1) \\ x(2) \\ x(3) \\ x(4) \\ x(5) \end{bmatrix} = \begin{bmatrix} I & 0 & 0 & 0 & 0 \\ \Pi_{123} & 0 & 0 & 0 & 0 \\ 0 & \Pi_1 & 0 & 0 & 0 \\ 0 & 0 & \Pi_{12} & 0 & 0 \\ 0 & 0 & 0 & \Pi_{13} & 0 \\ 0 & 0 & 0 & 0 & \Pi_1 \end{bmatrix} \begin{bmatrix} x(0) \\ x(1) \\ x(2) \\ x(3) \\ x(4) \end{bmatrix}$$

$$+ \begin{bmatrix} 0 & 0 & 0 & 0 & 0 & 0 & 0 & 0 & 0 & 0 & 0 \\ \Psi_1 & 0 & 0 & 0 & 0 & 0 & \Psi_2 & 0 & 0 & \Psi_3 & 0 \\ 0 & \Psi_1 & 0 & 0 & 0 & 0 & 0 & 0 & 0 & 0 & 0 \\ 0 & 0 & \Psi_1 & 0 & 0 & 0 & 0 & \Psi_2 & 0 & 0 & 0 \\ 0 & 0 & 0 & \Psi_1 & 0 & 0 & 0 & 0 & 0 & 0 & \Psi_3 \\ 0 & 0 & 0 & 0 & \Psi_1 & 0 & 0 & 0 & 0 & 0 & 0 \end{bmatrix} \begin{bmatrix} v_1(0) \\ v_1(1) \\ v_1(2) \\ v_1(3) \\ v_1(4) \\ v_1(5) \\ v_2(0) \\ v_2(1) \\ v_2(2) \\ v_3(0) \\ v_3(1) \end{bmatrix} , \quad (3.44)$$

where the sub-matrix terms of the state coefficient matrix are defined as

$$\Pi_{123} = [\Phi + \Psi_1 H_1 + \Psi_2 H_2 + \Psi_3 H_3] , \quad (3.45)$$

$$\Pi_1 = [\Phi + \Psi_1 H_1] , \quad (3.46)$$

$$\Pi_{12} = [\Phi + \Psi_1 H_1 + \Psi_2 H_2] , \quad (3.47)$$

$$\Pi_{13} = [\Phi + \Psi_1 H_2 + \Psi_3 H_3] . \quad (3.48)$$

The reduction of the right-hand-side state vector continues by reapplying the substitution process, as shown below.

$$\begin{bmatrix} \mathbf{x}(0) \\ \mathbf{x}(1) \\ \mathbf{x}(2) \\ \mathbf{x}(3) \\ \mathbf{x}(4) \end{bmatrix} = \begin{bmatrix} \mathbf{I} & 0 & 0 & 0 & 0 \\ \Pi_{123} & 0 & 0 & 0 & 0 \\ 0 & \Pi_{1} & 0 & 0 & 0 \\ 0 & 0 & \Pi_{12} & 0 & 0 \\ 0 & 0 & 0 & \Pi_{13} & 0 \end{bmatrix} \begin{bmatrix} \mathbf{x}(0) \\ \mathbf{x}(1) \\ \mathbf{x}(2) \\ \mathbf{x}(3) \end{bmatrix}$$

$$+ \begin{bmatrix} 0 & 0 & 0 & 0 & 0 & 0 & 0 & 0 & 0 & 0 & 0 \\ \Psi_1 & 0 & 0 & 0 & 0 & 0 & \Psi_2 & 0 & 0 & \Psi_3 & 0 \\ 0 & \Psi_1 & 0 & 0 & 0 & 0 & 0 & 0 & 0 & 0 & 0 \\ 0 & 0 & \Psi_1 & 0 & 0 & 0 & 0 & \Psi_2 & 0 & 0 & 0 \\ 0 & 0 & 0 & \Psi_1 & 0 & 0 & 0 & 0 & 0 & 0 & \Psi_3 \end{bmatrix} \begin{bmatrix} \mathbf{v}_1(0) \\ \mathbf{v}_1(1) \\ \mathbf{v}_1(2) \\ \mathbf{v}_1(3) \\ \mathbf{v}_1(4) \\ \mathbf{v}_2(5) \\ \mathbf{v}_2(0) \\ \mathbf{v}_2(1) \\ \mathbf{v}_2(2) \\ \mathbf{v}_3(0) \\ \mathbf{v}_3(1) \end{bmatrix} \quad . (3.49)$$

The following notation provides a convenient mechanism to illustrate the completion of the reduction process. The notation defines

the state vector with n elements as ..... $\mathbf{x}_{0n}$
the coefficient matrix of $\mathbf{x}_{0n}$ as ..... Π_{0n}
the matrix Π_{00} as ..... $\mathbf{I}$
the coefficient matrix of $\mathbf{x}_{0m}$, for (m =n+1) as ..... Ψ_{0n} .

Using this notation for the six element state vector under consideration gives

$$\mathbf{x}_{05} = [\Pi_{04}\ \Pi_{03}\ \Pi_{02}\ \Pi_{01}\ \mathbf{I}]\mathbf{x}(0) + [\Psi_{04}\ \Psi_{03}\ \Psi_{02}\ \Psi_{01}\ \Psi_{00}]\mathbf{v}_{\rho}(k) \quad . \quad (3.50)$$

Substituting $\mathbf{x}_{05}$ for the state vector $\mathbf{x}(n_1)$ in both the state and output equations, respectively, casts the multirate sampled-data state quadruple into the desired form. In this form, the state,

when propagated over one program period h_p is determined by considering only the value of the state at the start of the program.

3.4.5 An Alternative Form of the Multirate Sampling Model

The multirate sampled-data system model, described above, represents the multirate properties through an augmented control vector, **u**, in the open-loop case and the control vector, **v**, in the closed-loop case. This model can be recast to a form in which the multirate features are represented by an augmented state vector. The basis of the transformation method is a formal definition of the zero-order-hold (ZOH) elements. This formal definition of a multirate sampling and ZOH operation is given by

$$\begin{bmatrix} \mathbf{u}_1 \\ \mathbf{u}_2 \\ \vdots \\ \mathbf{u}_k \end{bmatrix} = \begin{bmatrix} \mathbf{0} & \mathbf{0} & \cdots & \mathbf{0} \\ \mathbf{0} & \mathbf{0} & \cdots & \mathbf{0} \\ \vdots & \vdots & & \vdots \\ \mathbf{0} & \mathbf{0} & \cdots & \mathbf{0} \end{bmatrix} \begin{bmatrix} \mathbf{u}_1 \\ \mathbf{u}_2 \\ \vdots \\ \mathbf{u}_k \end{bmatrix} + \begin{bmatrix} \mathbf{s}_1 & \mathbf{0} & \cdots & \mathbf{0} \\ \mathbf{0} & \mathbf{s}_2 & \cdots & \mathbf{0} \\ \vdots & \vdots & & \vdots \\ \mathbf{0} & \mathbf{0} & \cdots & \mathbf{s}_k \end{bmatrix} \begin{bmatrix} \mathbf{v}_1 \\ \mathbf{v}_2 \\ \vdots \\ \mathbf{v}_k \end{bmatrix}, \quad (3.51)$$

where $\mathbf{s}_i$, for i=1,...,k, is a diagonal matrix that couples the sampler inputs, $\mathbf{v}_i$, to the hold state at an assigned sampling instant. This notation presents an explicit expression of the multirate sampling switch function. Consider the CACT state and output equation (3.15), with the control inputs partitioned for

multirate sampling. Using equation (3.51) with the highest sampling rate inputs grouped in the vector, $\mathbf{u}_1$, equation (3.15a) is reformed in terms of a sampling policy for the highest sampling rate. This form is given by

$$\begin{bmatrix} \mathbf{x}(t) \\ \mathbf{u}_k(t) \\ \vdots \\ \mathbf{u}_j(t) \\ \mathbf{u}_i(t) \end{bmatrix} = \begin{bmatrix} \mathbf{A} & \mathbf{B}_k & \cdots & \mathbf{B}_j & \mathbf{B}_i \\ \mathbf{0} & \mathbf{0} & \cdots & \mathbf{0} & \mathbf{0} \\ \vdots & \vdots & & \vdots & \vdots \\ \mathbf{0} & \mathbf{0} & \cdots & \mathbf{0} & \mathbf{0} \\ \mathbf{0} & \mathbf{0} & \cdots & \mathbf{0} & \mathbf{0} \end{bmatrix} \begin{bmatrix} \mathbf{x}(t) \\ \mathbf{u}_k(t) \\ \vdots \\ \mathbf{u}_j(t) \\ \mathbf{u}_i(t) \end{bmatrix} + \begin{bmatrix} \mathbf{B}_1 & \mathbf{0} & \cdots & \mathbf{0} & \mathbf{0} \\ \mathbf{0} & \mathbf{s}_k & \cdots & \mathbf{0} & \mathbf{0} \\ \vdots & \vdots & & \vdots & \vdots \\ \mathbf{0} & \mathbf{0} & \cdots & \mathbf{s}_j & \mathbf{0} \\ \mathbf{0} & \mathbf{0} & \cdots & \mathbf{0} & \mathbf{s}_i \end{bmatrix} \begin{bmatrix} \mathbf{u}_1(t) \\ \mathbf{v}_k(t) \\ \vdots \\ \mathbf{v}_j(t) \\ \mathbf{v}_i(t) \end{bmatrix}. \tag{3.52}$$

The open-loop CACT model of the multi-rate sampled-data system, defined by equation (3.52), is mapped to an equivalent CADT open-loop model using the methods described in section 2.4 of Chapter Two and Section A1.4 of Appendix One. The time interval for the mapping is given by the highest sampling rate in the multi-rate schedule. The equivalent CADT model of equation (3.52) is therefore given by

$$\begin{bmatrix} \mathbf{x}((n_1+1)h_1) \\ \mathbf{u}_k((n_1+1)h_1) \\ \vdots \\ \mathbf{u}_j((n_1+1)h_1) \\ \mathbf{u}_i((n_1+1)h_1) \end{bmatrix} = \begin{bmatrix} \Phi & \Psi_k & \cdots & \Psi_j & \Psi_i \\ 0 & I & \cdots & 0 & 0 \\ \vdots & \vdots & & \vdots & \vdots \\ 0 & 0 & \cdots & I & 0 \\ 0 & 0 & \cdots & 0 & I \end{bmatrix} \begin{bmatrix} \mathbf{x}(n_1h_1) \\ \mathbf{u}_k(n_1h_1) \\ \vdots \\ \mathbf{u}_j(n_1h_1) \\ \mathbf{u}_i(n_1h_1) \end{bmatrix}$$

$$+ \begin{bmatrix} \Psi_1 & \Psi_k\mathbf{s}_k & \cdots & \Psi_j\mathbf{s}_j & \Psi_i\mathbf{s}_i \\ 0 & \mathbf{s}_k & \cdots & 0 & 0 \\ \vdots & \vdots & & \vdots & \vdots \\ 0 & 0 & \cdots & \mathbf{s}_j & 0 \\ 0 & 0 & \cdots & 0 & \mathbf{s}_i \end{bmatrix} \begin{bmatrix} \mathbf{u}_1(n_1h_1) \\ \mathbf{v}_k(n_kh_k) \\ \vdots \\ \mathbf{v}_j(n_jh_j) \\ \mathbf{v}_i(n_ih_i) \end{bmatrix}, \tag{3.53}$$

where n_1, n_i, n_j and n_k are increment numbers for the samplers $\mathbf{s}_1$, $\mathbf{s}_i$, $\mathbf{s}_j$, and $\mathbf{s}_k$, respectively. The sub-matrix elements of the controls matrix, that are functions of $\mathbf{s}$, only appear at their appropriate sampling instant; at other times, these sub-matrix elements are set to zero.

The augmented state, multirate sampled-data model represents the state-space link between the augmented control vector assembly and the open-loop form of the Kalman and Bertram model. It is considered that the augmented control vector form offers a greater facility for the time-domain and transfer-function analysis methods of the current research.

3.5 ACCOUNTING FOR COMPUTATIONAL DELAY IN THE DFC CONTROLLER

The control requirements of the basic aircraft can usually be achieved with a state-feedback controller. In the case of an analogue controller, the computational processes are confined to simple state scaling operations. As such, the order of the total feedback control system dynamics is no greater than the order of the dynamics of the basic open-loop aircraft model.

In the ideal case of a digital state feedback controller, the digital process is once again a non-dynamic scaling operation. However, with a practical realisation of a state feedback controlled DFC system, the controller may require a dynamic element to account for computational delay. It is appropriate to consider this requirement as part of the initial stages of a DFC design exercise and to model the delay dynamics as augmentation states attached to the basic CADT aircraft system. In general, a model can be defined to accommodate a computational delay of any length. From a practical point of view, it is desirable to avoid delays that exceed more than one sampling period. This can be done by either increasing the processing speed of the digital controller or reducing the sampling-rate of the system.

A unirate sampled-data model of a single-input, single-output system, which includes the dynamics of a computational delay, is developed in [3.19]. In this section, this computational delay model is extended to the multirate sampled-data system.

Consider the CADT domain multirate sampled-data state equation given by equation (3.18). This equation is partitioned for the application of a three rate sampling policy. If the multirate control inputs are delayed by one sampling period then, equation (3.18) is modified to give

$$\mathbf{x}(n+1)h = \Phi\,\mathbf{x}(nh) + \Psi_1\mathbf{u}_1(n-1)h + \Psi_2\mathbf{u}_2(n-1)h + \Psi_3\mathbf{u}_3(n-1)h \quad . \qquad (3.54)$$

The diagram which reveals the structure of the system modelled by (3.67) is given in Fig.3.5; the functions DLY_1, DLY_2 and DLY_3 represent a time delay of h_1,h_2 and h_3, respectively.

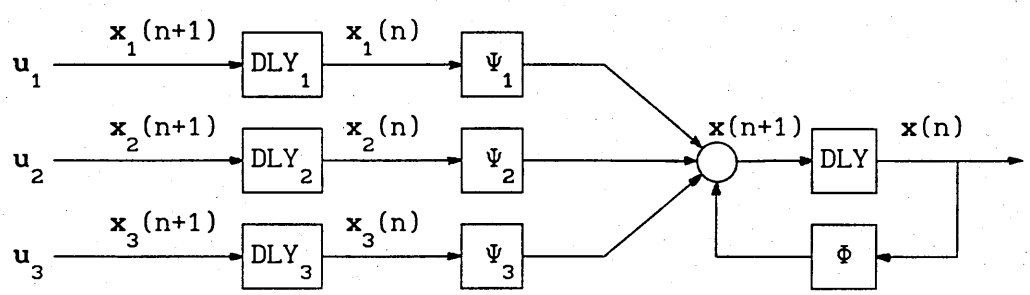

A multirate (three) sampled-data model including delay dynamics

Fig.3.5

The normal state space form is directly produced from Fig.3.5 to give

$$\begin{bmatrix} \mathbf{x}(n+1)h \\ \mathbf{x}_1(n+1)h \\ \mathbf{x}_2(n+1)h \\ \mathbf{x}_3(n+1)h \end{bmatrix} = \begin{bmatrix} \Phi & \Psi_1 & \Psi_2 & \Psi_3 \\ 0 & 0 & 0 & 0 \\ 0 & 0 & 0 & 0 \\ 0 & 0 & 0 & 0 \end{bmatrix} \begin{bmatrix} \mathbf{x}(nh) \\ \mathbf{x}_1(nh) \\ \mathbf{x}_2(nh) \\ \mathbf{x}_3(nh) \end{bmatrix} + \begin{bmatrix} 0 & 0 & 0 \\ I & 0 & 0 \\ 0 & I & 0 \\ 0 & 0 & I \end{bmatrix} \begin{bmatrix} \mathbf{u}_1 \\ \mathbf{u}_2 \\ \mathbf{u}_3 \end{bmatrix} \quad . \qquad (3.55)$$

The general form of the output state-space equation is similarly deduced and is given by

$$\mathbf{y}(n) = \begin{bmatrix} \mathbf{C} & \mathbf{D}_1 & \mathbf{D}_2 & \mathbf{D}_3 \end{bmatrix} \begin{bmatrix} \mathbf{x}(nh) \\ \mathbf{x}_1(nh) \\ \mathbf{x}_2(nh) \\ \mathbf{x}_3(nh) \end{bmatrix} . \qquad (3.56)$$

The delayed inputs are recast as the augmentation state elements, $\mathbf{x}_1$, $\mathbf{x}_2$ and $\mathbf{x}_3$, these state elements can also be included as inputs to a state-feedback controller.

3.6 SUMMARY

In this chapter, a method of constructing a multirate sampled-data system model, in a state-space format, is developed. Two new techniques are presented for this development; first, the identification of the multirate sampling policy through the covariance time-history of the state elements, and second, the open-loop assembly of the multirate sampled-data model. Alternative methods are considered and rejected because it is not possible to cast them in a form which meets the requirements of the design maxims of the thesis. The most promising of the reviewed methods is the approach developed by Kalman and Bertram. Although the techniques reported in [3.20] overcome the deficiencies of the Kalman-Bertram method, the complexity of the model assembly

mitigated against its utility for this thesis. The example used to describe the assembly of a multirate sampled-data model demonstrates equivalence proposed method to other multirate modelling techniques.

The multirate, sampled-data, time-domain state-space model, developed in this chapter, can be directly applied to the problem of DFC design. However, as with a unirate sampled-data digital flight control design, the main difficulty arises from the interpretation of the standard flight control specification which as previously mentioned, gives no regard to the possibility of a digital system implementation.

In Chapter Four, two data domains are reviewed which are identified as suitable instruments for design and analysis of DFC systems. These data domains are commonly referred to as the w- and w'-planes. The usual application of these two planes is for the direct digital design of DFC systems that employ unirate sampled-data controllers. The multirate sampled-data state-space model, developed in this chapter, is readily transformed to either a w- or w'-plane description by employing a multivariable system mapping algorithm. This algorithm, together with performance and analysis measures, is developed in Chapter Four.

CHAPTER FOUR

DESIGN AND ANALYSIS OF DFC SYSTEMS

4.1 INTRODUCTION

The handling characteristics of manned aircraft provide the fundamental criteria on which the performance of flight control systems are assessed. The general specifications of aircraft handling qualities, embodied in documents such as MIL-F-8785C [4.1], are cast in terms of both time-domain and frequency-domain criteria. Although the multirate, sampled-data CADT model, developed in Chapter Three, is suitable for time-domain analysis, it is convenient to have a CADT design and analysis domain which is equivalent to the CACT s-plane. The most familiar CADT domain that fills this role is the z-plane. A sampled-data, time-domain, aircraft model is defined as a z-plane model by taking the z-transform of the CADT state-space quadruple to produce a set of z-plane transfer-functions. When the CADT domain state-space model has a multirate sampled-data structure, the z-plane transfer-function matrix is defined in terms of the program sampling period h_p. This procedure is demonstrated in Appendix Five and results in equation (A5.13).

The z-plane design of a digital control system can incur numerical problems, [4.2]. These problems are, in general, associated with systems that have widely separated natural frequencies. It is, of

course, this type of characteristic that generates the need for the multirate sampled-data system model that is developed in Chapter Three. The numerical problems associated with z-plane design methods are eliminated if the CADT design is undertaken in either the w-plane or w′-plane.

Both the w- and w′-planes have, on several occasions, been identified as suitable domains for the design of sampled-data flight control systems [4.3], [4.4], [4.5]. This chapter includes a brief review of the both the w- and w′-planes and discusses their application in the design of DFC systems. The major difficulty in applying both the w- and w′-plane in the design of sampled-data control systems, is the awkward method of mapping equivalent w domain[1] CADT models from the z-plane. The traditional mapping technique starts with a z-plane transfer-function. The z-plane to w- or w′-plane bilinear transformation is then substituted for z to produce an equivalent w domain transfer-function. Not only is this procedure unsuitable for high-order systems, it also results in a cluttered expression of the w plane transfer-function. This chapter introduces a method to directly map a CADT domain state-space model to an equivalent w-plane or w′-plane model. The familiar transfer-function matrix technique can be applied to the resulting model to obtain the w′-plane transfer-functions.

---

[1] To avoid confusion, when discussing the w- and w′-planes, the following convention has been adopted: (w-) refers to the w-plane, (w′-) refers to the w′-plane and (w domain) implies a simultaneous reference to both the w- and w′-planes.

To assess the behaviour of proposed DFC systems, this chapter includes descriptions of z-, w- and w'-plane stability and performance measures. Stability and performance measures for sampled-data systems are usually defined in terms of the z-plane. It is a common practice to define these z-plane measures by mapping the equivalent CACT s-plane criteria to the z-plane, [4.6]. The stability and performance criteria, described in this chapter, departs from the conventional s- to z-plane mapping and directly defines the measures in terms of the CADT domain state-space parameters. These alternative definitions are considered to be a natural consequence of the direct digital design methodology. The w- and w'-plane stability and performance measures are derived from their corresponding z-plane definitions and are therefore mapped from the z-plane to w-plane or w'-plane by the appropriate z to w domain transformation.

4.2 w-PLANE AND w'-PLANE ANALYSIS METHODS

This section gives a detailed commentary on the characteristics of w-plane and w'-plane. Familiar s-plane CACT performance measures are extended to the w- and w'-planes for use in the design of digital control systems. During the last three decades, numerous reports have proposed both the w-plane and w'-planes as suitable domains for the design and analysis of digital flight control systems. However, there is a paucity of reported applications in which the w- and w'-plane methods have been used. A possible reason for the rarity of w domain designed digital control systems is the

practical inconvenience of generating w- and w'-plane models [4.7]. A contribution of this chapter is the development of a method to directly transform the CADT state-space equation to an equivalent w- or w'-plane model.

4.2.1 Properties of the w-Plane

The advantage of the w plane is that the design is carried out in a complex Cartesian frame rather than the complex polar frame of the z-plane. This means that the well known s-plane methods used in CACT systems work can be directly applied in the design and analysis of CADT domain systems.

The w-plane is related to the z-plane through the bilinear transform. Cast as the z-plane to w-plane parameter-mapping function, the bilinear transform has the form

$$z = \frac{1 + w}{1 - w} \quad . \tag{4.1}$$

The inverse of equation (4.1), which maps the w-plane to the z-plane, is given as

$$w = \frac{z - 1}{z + 1} \quad . \tag{4.2}$$

The corresponding cardinal points on the z and w complex-planes are identified in Fig.4.1.

z-plane point	$-\infty$	-1	$-\frac{1}{2}$	0	$+\frac{1}{2}$	$+1$	$+\infty$	$-j$	$+j$
w-plane point	$+1$	$-\infty$	-3	-1	$-\frac{1}{3}$	0	$+1$	$-j$	$+j$

Cardinal point mappings between the z-plane and the w-plane

Fig.4.1

4.2.2 The w-Plane Analogue of Frequency

In Section A7.3.2 of Appendix Seven, it is shown that the imaginary axis of the s-plane maps to the unit circle of the z-plane. Points on the unit circle are defined by $\exp(j\phi)$, indicating that the z-plane analogue of the the s-plane frequency variable is ϕ. In this section, a relationship is developed that gives the w-plane imaginary axis in terms of the z-plane unit circle.

Defining the complex w-plane as $w = \sigma_w \mp j\omega_w$ and comparing it with the z-plane unit circle, $z = \exp(j\phi)$, gives $\sigma_w = 0$ and

$$j\omega_w = \frac{\exp(j\phi) - 1}{\exp(j\phi) + 1} \quad . \tag{4.3}$$

Converting equation (4.3) to the form in which the variable ϕ is cast in terms of the half angle $\frac{\phi}{2}$ gives

$$\omega_w = \tan\left(\frac{\phi}{2}\right) \quad . \tag{4.4}$$

Equation (4.4) shows that the z-plane parameter, ϕ, given in the range $(-\pi,\pi)$, produces a value of ω_w in the range $(-\infty,\infty)$. Defining a sampling period, h, which in terms of the envelope-cycle shown in Fig.A7.3 of Appendix Seven, is given by $h = \frac{T}{\mu}$, the analysis of Section A7.3 produces the relationships $\mu = \frac{2\pi}{\omega h}$, with $\omega = \frac{2\pi}{T}$, and $\phi = \omega h$. Substituting $\phi = \omega h$ into equation (4.4) defines the w-plane variable, ω_w, in terms of the CACT frequency, ω, and thus ω_w is given by

$$\omega_w = \tan(\frac{\omega h}{2}) \quad . \tag{4.5}$$

4.2.3 Properties of the w'-Plane

An equivalent w'-plane model is obtained by multiplying equation (4.5) by the factor $\frac{2}{h}$ to give

$$w' = \frac{h}{2} w \quad , \tag{4.6}$$

or, in terms of the z-plane,

$$w' = \frac{h}{2}\left[\frac{z - 1}{z + 1}\right] \quad . \tag{4.7}$$

The following analysis describes the profound effect of this simple modification in regard to the interpretation of the w domains.

The corresponding cardinal points on the z and w' complex-planes are identified in Fig.4.1.

z-plane point	$-\infty$	-1	$-\frac{1}{2}$	0	$+\frac{1}{2}$	$+1$	$+\infty$	$-j$	$+j$
w'-plane point	$+\frac{h}{2}$	$-\infty$	$\frac{-3h}{2}$	$-\frac{h}{2}$	$-\frac{h}{6}$	0	$+\frac{h}{2}$	$-j\frac{h}{2}$	$+j\frac{h}{2}$

Cardinal point maps between the z-plane and the w'-plane

Fig.4.2

An additional facility of the w'-plane is revealed by considering the effect of a sampling interval, h, that tends to zero. Consider first, the w-plane given by equation (4.2), when it is cast in terms of a z-transform, where z is defined as

$$z = \exp(sh) = \sum_{n=o}^{\infty} \frac{(sh)^n}{n!} \quad . \tag{4.8}$$

Substituting the summation term of (4.8) into equation (4.2) gives

$$w = \frac{\sum_{n=1}^{\infty} \frac{(sh)^n}{n!}}{2 + \sum_{n=1}^{\infty} \frac{(sh)^n}{n!}} \quad . \tag{4.9}$$

Equation (4.9) shows that, in the limit, as h tends to zero, w tends to zero. Consider the w'-plane as defined by equation (4.7). Substituting the summation term of equation (4.5) for z gives

$$w' = \frac{2}{h} \; \frac{\sum_{n=1}^{\infty} \frac{(sh)^n}{n!}}{2 + \sum_{n=1}^{\infty} \frac{(sh)^n}{n!}} \quad . \qquad (4.10)$$

Consequently, $\lim_{h \to 0} w' = s$. This means, at high sampling rates, a sampled-data w'-plane model has dynamics which are numerically similar to the dynamics of its equivalent, CACT domain, s-plane model. In summary, the intuitive expectation, that, with an infinite sampling rate, a CADT system becomes a CACT system, is a feature of the w'-plane where, for h=0, w'=s. In contrast to this, the w-plane limit for h=0 is w=0. The main purpose of both the w-plane and w'-plane is to emulate the geometry of the s-plane and thereby bring to the design and analysis of digital control systems the well established and widely understood CACT control system performance measures. The analysis for h=0 indicates that, for high sampling rates at least, the w'-plane is better than the w-plane for emulating the s-plane.

The diagram, given in Fig.4.3, represents the distortion which exists between the s-plane and the w planes. The diagram is produced by taking the difference between given points on the s-plane and their equivalent counterparts on the w'-plane. The w-plane distortion is identical to the distortion of the w'-plane; the difference measure produced by the s- and w'-planes directly quantifies the absolute distortion.

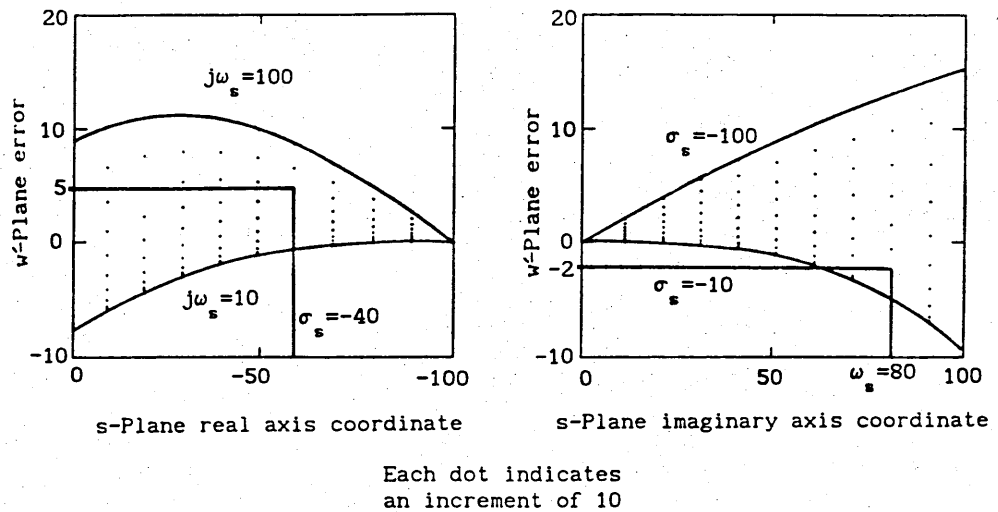

Distortion measure between the s-plane and w'-plane

Fig.4.3

The identified points on Figs.4.3a and 4.3b indicate that a complex location in the s-plane, given as s = -40 + j80, maps to the w-plane location, w = (-40 + 5) + j(80 - 2), when the sampling period is h=0.01.

4.2.4 Frequency Response Plots in the w- and w'-Planes

Frequency response is an important device for the design, analysis and appraisal of CACT systems. Even in sophisticated Computer Aided Control System Design environments, based on the techniques of

modern control theory, the insight gained from graphical presentations of a CACT frequency response is widely accepted. The classical graphical presentations of frequency response are:

Bode gain and phase plots,

Nyquist gain-phase polar plots,

Nichols gain-phase plots,

Root-locus plots.

These classical graphical methods are widely recognised as suitable instruments for the design and analysis of CACT control systems. In particular the s-plane root-locus is usually preferred for design of aircraft analogue-flight control systems. Although z-plane frequency domain diagrams can be produced for CADT systems, they present unfamiliar data visualisation patterns. The contribution of w- and w'-planes, for the design and analysis of CADT control systems, is in casting the sampled-data system frequency response graphs in the same form as their analogue-data counterparts.

An example, illustrating the utility of both the w- and w'-plane gain and phase frequency response characteristics, is discussed in this section. The example illustrates the transformation of a second order CACT domain model into equivalent w- and w'-plane models. The respective gain and phase frequency responses are plotted and comparisons are made between the characteristics produced by the CACT system and those produced by the equivalent w- and w'-plane models.

Consider the single-input, single-output CACT state-space model, given as

$$\begin{bmatrix} \dot{x}_1(t) \\ \dot{x}_2(t) \end{bmatrix} = \begin{bmatrix} 0 & 1 \\ -25 & -7 \end{bmatrix} \begin{bmatrix} x_1(t) \\ x_2(t) \end{bmatrix} + \begin{bmatrix} 0 \\ 1 \end{bmatrix} u(t) \quad , \qquad (4.11a)$$

$$y(t) = \begin{bmatrix} 1 & 0 \end{bmatrix} \begin{bmatrix} x_1(t) \\ x_2(t) \end{bmatrix} \quad . \qquad (4.11b)$$

With a sampling period h = 0.05, the equivalent w-plane system is[2]

$$\begin{bmatrix} wX_1(w) \\ wX_2(w) \end{bmatrix} = \begin{bmatrix} -0.009 & 0.025 \\ -0.622 & -0.175 \end{bmatrix} \begin{bmatrix} X_1(w) \\ X_2(w) \end{bmatrix} + \begin{bmatrix} -0.0006 \\ 0.0293 \end{bmatrix} U(w) \quad , \qquad (4.12a)$$

$$Y(w) = \begin{bmatrix} 1 & 0 \end{bmatrix} \begin{bmatrix} X_1(w) \\ X_2(w) \end{bmatrix} + \begin{bmatrix} -0.079 \end{bmatrix} U(w) \quad . \qquad (4.12b)$$

Under the same sampling period, the w′-plane model is given by

$$\begin{bmatrix} w'X_1(w') \\ w'X_2(w') \end{bmatrix} = \begin{bmatrix} -0.036 & 0.995 \\ -24.87 & -7 \end{bmatrix} \begin{bmatrix} X_1(w') \\ X_2(w') \end{bmatrix} + \begin{bmatrix} -0.023 \\ 1.17 \end{bmatrix} U(w') \quad , \qquad (4.13a)$$

$$y(w') = \begin{bmatrix} 1 & 0 \end{bmatrix} \begin{bmatrix} x_1(w') \\ x_2(w') \end{bmatrix} + \begin{bmatrix} -0.079 \end{bmatrix} u(w') \quad . \qquad (4.13b)$$

---

[2] The strict notation is $X\left(\frac{1+w}{1-w}\right)$ in the case of the w-plane and $X\left(\frac{1+w'}{1-w'}\right)$ in the case of the w′-plane. In the interest of simplicity the notation X(w) and X(w′), respectively is adopted.

The gain and phase frequency response diagrams, for each of the three systems are given in Fig.4.4. The CACT system's gain and phase response is, shown in Fig.4.4a provides a benchmark for the purpose of comparison. The w-plane gain and phase characteristics are shown in Fig.4.4b. The point at which the conditions of the sampling theorem are violated is indicated by a rapid transition of both the gain and phase. The frequency axis scaling in terms of ω is produced from the analysis of Section 4.2.2 and is given by

$$\omega = \frac{2}{h}\arctan(\omega_w) \quad . \tag{4.14}$$

The w'-plane gain and phase plots, shown in Fig.4.4c, circumvents the need to calculate ω from $\omega_{w'}$. The frequency axis scaling is deduced from the approximation

$$\frac{2}{h}\arctan(\omega_w) \cong \frac{2}{h}\omega_w = \omega_{w'} \quad . \tag{4.15}$$

The w'-plane plot behaves quite differently to the w-plane plot. At high frequencies, both the gain and phase plots continue to $\omega_{w'} = \infty$. Unlike the w-plane diagram, the w'-plane plot gives no indication of the problems which exist at the sampling limit, π/h.

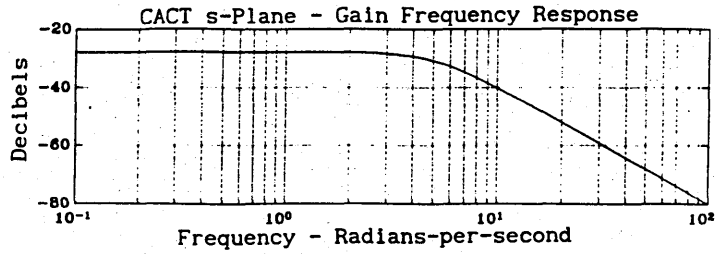

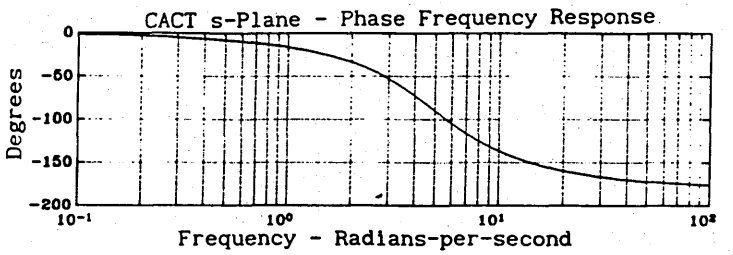

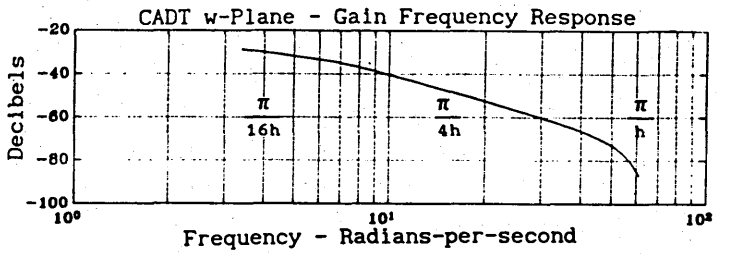

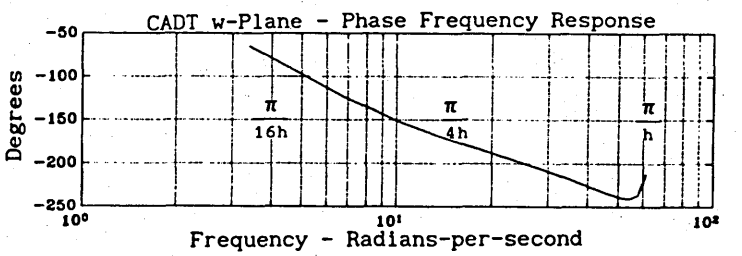

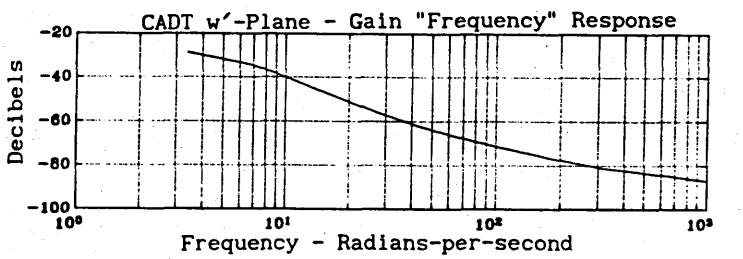

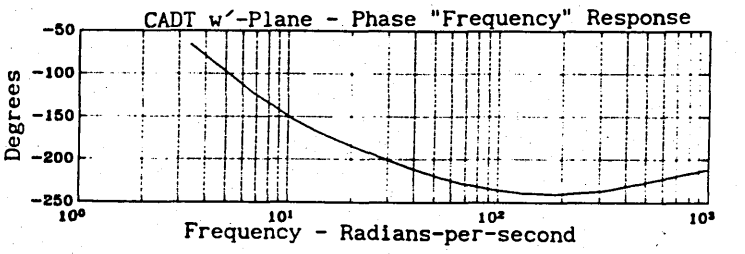

Corresponding s, w- and w′- gain and phase frequency response plots

Fig.4.4

4.2.5 Mapping the State Equations to the w- and w'-Planes

As mentioned in Section 4.1, the usual method of producing both the w- and w'-plane system models from the CACT state-space domain progresses via z-plane transfer-functions and in some cases via both s-plane and z-plane transfer-functions. In this section, direct methods of mapping a CACT state-space model to an equivalent w or w' state-space are described. The methods are numerically more sound than the transfer-function approaches and accommodate multiple-input, multiple-output systems with more facility.

The standard methods of mapping a time domain model of a CACT system into the w-plane or w'-plane are identified in Fig.4.5. The diagram indicates that the z-plane transfer function description is required for the mapping procedure.

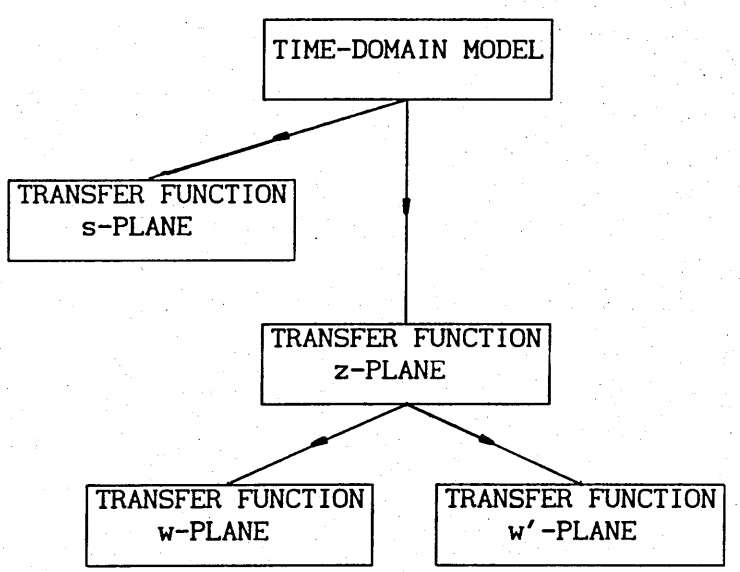

Conventional approaches for mapping a CACT domain state-space model into the w-plane or w'-plane

Fig.4.5

It is thought that a possible reason which inhibits the application of the w-plane and w'-planes for the design and analysis of sampled-data control systems is the inconvenience of the transfer-function mapping processes, outlined in Fig.4.5. Even when efficient computer aided design facilities [4.8] are available, the process of mapping between s-plane, z-plane and w planes involves numerical algorithms that have recognised weaknesses [4.9], and which inevitably cast doubt on the validity of solutions.

In this section, methods of mapping a CADT state-variable model directly from the time-domain to the w- and w'-planes, are presented. The two CADT domain to w domain algorithms, together with the basis of their derivations, is given below. A comprehensive derivation the two algorithms is given in Appendix Six.

Consider the z-plane state-space model of the standard CADT state-space quadruple, $(\Phi,\Psi,\mathbf{C}_D,\mathbf{D}_D)$, given as

$$z\,\mathbf{X}(z) = \Phi\ \mathbf{X}(z) + \Psi\,\mathbf{U}(z) \qquad (4.16a)$$

$$\mathbf{Y}(z) = \mathbf{C}_D\,\mathbf{X}(z) + \mathbf{D}_D\mathbf{U}(z) \quad . \qquad (4.16b)$$

Equations (4.16) are mapped to the w-plane by applying the z-plane to w-plane bilinear transform (4.1). The z-plane state and output equations, (4.16a) and (4.16b), are thereby recast as

$$\left(\frac{1+w}{1-w}\right)\mathbf{X}(w) = \Phi\,\mathbf{X}(w) + \Psi\,\mathbf{U}(w) \qquad (4.17a)$$

$$\mathbf{Y}(w) = \mathbf{C}_D\mathbf{X}(w) + \mathbf{D}_D\mathbf{U}(w) \quad . \qquad (4.17b)$$

The w-plane state and output equations derived from equation (4.17) are defined as

$$wX(w) = A_w X(w) + B_w U(w) \qquad (4.18a)$$

$$Y(w) = C_w X(w) + D_w U(w) \quad . \qquad (4.18b)$$

where, as shown in Appendix Six, the w-plane quadruple, (A_w, B_w, C_w, D_w), when cast in terms of the CADT quadruple, is given by

$$A_w = -(I + \Phi)^{-1}(I - \Phi) \quad , \qquad (4.19)$$

$$B_w = 2(I + \Phi)^{-2}\Psi \quad , \qquad (4.20)$$

$$C_w = C_D \quad , \qquad (4.21)$$

$$D_w = -C_D(I + \Phi)^{-1}\Psi + D_D \quad . \qquad (4.22)$$

Mapping a CADT domain model to an equivalent w-plane state-space model, by applying equations (4.19) through (4.22), circumvents the need to calculate s- and z-domain transfer-functions. In computer aided design and analysis, this is a convenient feature because the computational robustness of the matrix computations associated with this algorithm are superior to computations using the alternative transfer-function approach.

An interpretation of the w-plane system model is shown in Fig.4.6. The model illustrates the relationship between the w-plane system states, $X(w)$, and the CADT system states, $X_D(w)$, in the w-domain, where X_D is given by

$$X_D(w) = X(w) - [I + \Phi]^{-1}\Psi\, U(w) \quad . \qquad (4.23)$$

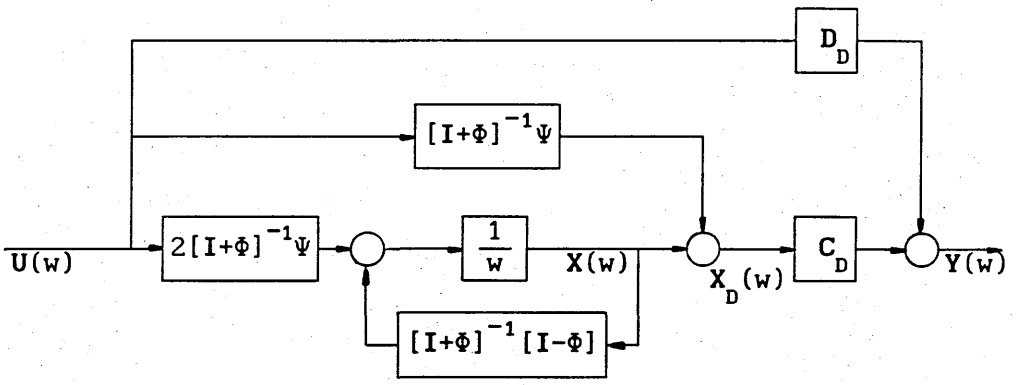

The w-plane system diagram

Fig.4.6

The inverse transformation equations, that map a w-plane model to a CADT domain state-space model, are derived by recasting equations (4.19) through (4.22) to give

$$\Phi = [I + A_w][I + A_w]^{-1} \quad , \tag{4.24}$$

$$\Psi = 2[I - A_w]^{-2}B_w \quad , \tag{4.25}$$

$$C_D = C_w \quad , \tag{4.26}$$

$$D_D = C_w[I - A_w]^{-1}B_w + D_w \quad . \tag{4.27}$$

The w'-plane state-space model can be derived directly from a CADT state space model using the approach developed in Section A6.2 of Appendix Six. However, substituting $w = \frac{h}{2}w'$ in the w- state-space equation (4.18) and the CADT to w- state-space algorithm, equations (4.19) through (4.22), gives the w'- state and output equation as

$$w'X(w') = A_{w'}X(w') + B_{w'}U(w') \qquad (4.28a)$$

$$Y(w') = C_{w'}X(w') + D_{w'}U(w') \quad . \qquad (4.28b)$$

and the CADT to w' state space mapping algorithm as

$$A_{w'} = -\frac{2}{h}[I + \Phi]^{-1}[I - \Phi] \quad , \qquad (4.29)$$

$$B_{w'} = \frac{4}{h}[I + \Phi]^{-2}\Psi \quad , \qquad (4.30)$$

$$C_{w'} = C_D \quad , \qquad (4.31)$$

$$D_{w'} = -C_D[I + \Phi]^{-1}\Psi + D_D \quad . \qquad (4.32)$$

As in the case of the w-plane, the utility and robustness with which these quadruple mapping equations can be computed makes this method of mapping a CADT system in the w'-plane superior to the alternative transfer-function methods. The w'-plane state-space model can be interpreted in the form illustrated in Fig.4.7.

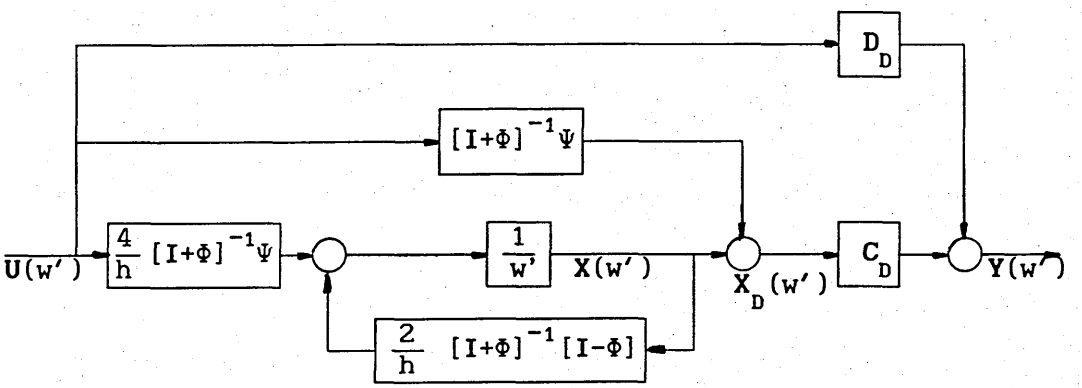

The w'-plane system diagram

Fig.4.7

The inverse, w'-plane to CADT domain state-space coefficient matrices are derived by recasting equations (4.29) through (4.32) to give

$$\Phi = [I + \frac{h}{2}A_{w'}][I - \frac{h}{2}A_{w'}]^{-1} \quad , \qquad (4.33)$$

$$\Psi = 2[I - \frac{h}{2}A_{w'}]^{-2}\frac{h}{2}B_{w'} \quad , \qquad (4.34)$$

$$C_D = C_{w'} \quad , \qquad (4.35)$$

$$D_D = C_{w'}[I - \frac{h}{2}A_{w'}]^{-1}\frac{h}{2}B_{w'} + D_{w'} \quad . \qquad (4.36)$$

4.3 ANALYSIS PARAMETERS FOR CADT DIRECT DIGITAL DESIGN

The practical processes of a control system design are usually augmented by a graphical presentation of the system's dynamical performance. The frequency domain presentations are particularly useful during the preliminary design phase. In the case of CACT control systems, the facility of the graphical data presentations is enhanced by a set of general system parameters, against which the results of the design processes can be assessed. These parameters are particularly relevant in the design of flight control systems because they convey the general specifications embodied in aircraft design standards, such as MIL-F-8785C, into the control system design process. For sampled-data control system design, a similar set of general system parameters can also be defined. One, widely reported method of defining these sampled-data parameters is to map the CACT parameters from the s-plane to the z-plane [4.10]. This section defines an alternative set of parameters which can be

applied to assess the performance of sampled-data systems. These alternative parameters are considered to be more appropriate for direct digital design methods.

Six analysis parameters are derived in Appendix Seven; the first three are produced by comparing the geometries of the s-plane and z-plane and are defined as follows:

Envelope-frequency	ϕ ,
Samples-per-envelope-cycle	μ ,
Decrement-per-unit-cycle	γ .

The remaining three parameters are derived by comparing the s-plane and z-plane geometries associated with complex conjugate pole-pair and are defined as follows:

Natural-frequency	ϕ_n ,
Resonance-frequency	ϕ_m ,
Resonance-magnification	m_z .

4.3.1 Envelope-Frequency and Samples-per-Envelope-Cycle

The envelope-frequency, ϕ, is a notional CACT periodic function which intersects all the values, u(n), in the discrete time sequence, n. The number of samples and hence control-law iterations, within each period of the envelope frequency, is referred to as the samples-per-envelope-cycle parameter, μ. For

example, if a sequence of μ iterations occurs within the envelope period of a sinusoidal function and produces a set of values, u(n), then

$$u(n) = \sin\left(\frac{2\pi}{\mu} n\right) \quad . \tag{4.32}$$

The envelope-frequency, ϕ, is defined as $\frac{2\pi}{\mu}$. Comparing equation (4.32) with its CACT counterpart, u(t) = sin(ωt), indicates that ϕ and n correspond to the frequency, ω, and time, t, respectively. For the case of ϕ in the range $(-\pi,+\pi)$, then $\mu > 2$ in order to satisfy the minimum requirements of the Sampling Theorem [4.11]. This observation can be interpreted as a graphical overlay of the z-plane, as illustrated in Fig.4.8.

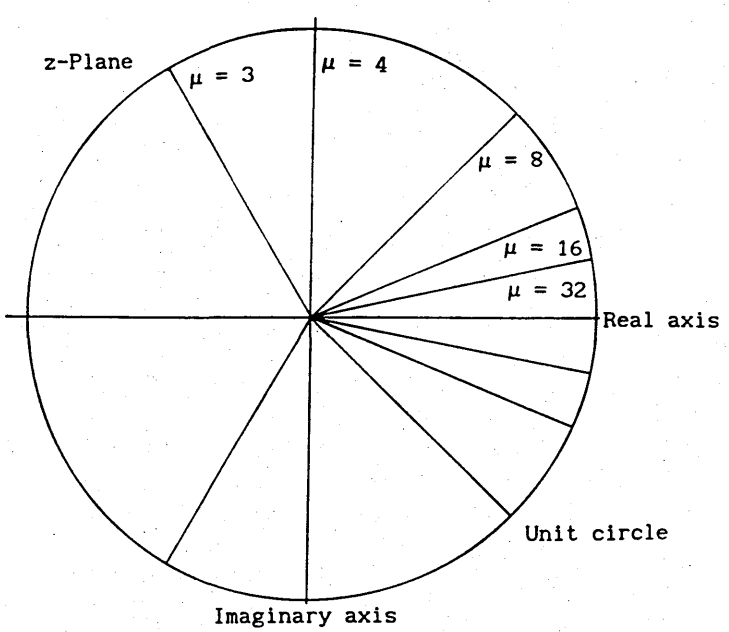

Lines of Samples-per-envelope-cycle ($\mu = \frac{2\pi}{\phi}$)

Fig.4.8

4.3.2 Decrement-per-Envelope-Cycle

The decrement-per-envelope-cycle, γ, as derived in Appendix Seven, corresponds to the CACT domain concept of damping-factor. The decrement-per-envelope-cycle z-plane contour is given by

$$\gamma = \left(r \right)^{\frac{1}{\phi}} , \qquad (4.33)$$

where r is a radius measure from the origin of the z-plane. A point on the z-plane unit circle is defined by r = 1; thus, r < 1 implies stability and r > 1 implies instability.

The z-plane contours of decrement-per-envelope cycle are also the sampling-rate root-loci of complex pole-pairs. This is a useful feature in the exercise of selecting sampling rates. It should be noted that the decrement-per-envelope-cycle contour, given by (4.33), is inversely related to the s-plane constant damping radial when it is mapped to the z-plane. A family of decrement-per-envelope-cycle contours is illustrated in Fig.4.9.

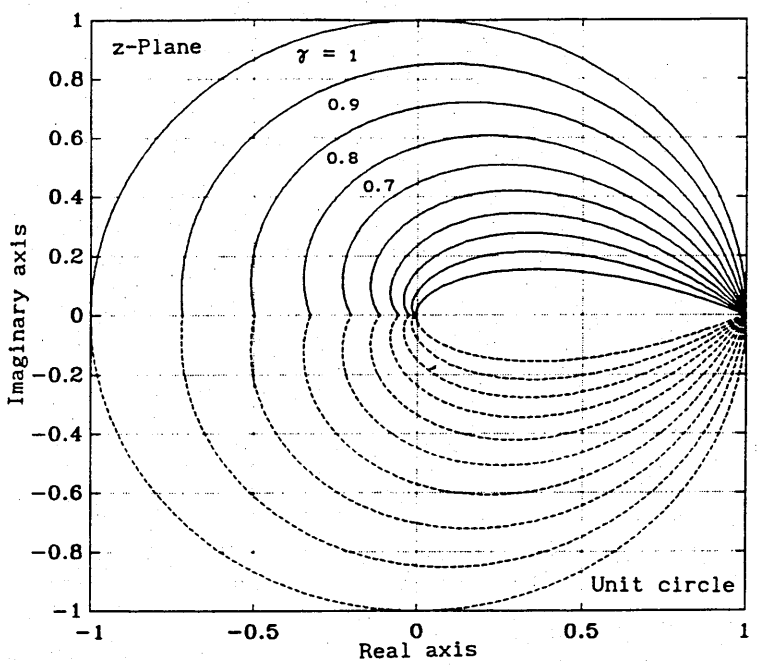

Contours of constant decrement-per-cycle $\left[\gamma = \left(r \right)^{\frac{1}{\phi}}\right]$

Fig.4.9

4.3.3 Natural Frequency and Resonance Magnification

The three CACT domain parameters of natural-frequency, ω_{ns}, resonance-frequency, ω_{ms}, and resonance-magnification, m_s, are important measures in the specification and assessment of control systems. As in the case of the damping factor described above, the natural-frequency and resonance parameters can be mapped from the s-plane to a z-plane. Details of the s-plane to z-plane mapping method are well documented [4.12]. The concepts of natural-frequency and resonance, based on the direct CADT domain definition, are developed in Appendix Seven.

The z-plane contours of natural frequency, ϕ_n, and resonance magnification, m_z, are shown in Fig.4.10 and Fig.4.11, respectively. These two sets of contours are defined in terms of the z-plane but are derived from the w-plane and mapped to the z-plane. In terms of the z-plane geometry, the contours for these two parameters, together with the z-plane definition of resonance frequency, ϕ_m, are given by

$$\phi_n = \arccos\left(\frac{2r_0}{1 + r_0^2} \cos(\phi_0) \right) , \qquad (4.34)$$

$$m_z = \frac{(1 + r_0^2) - 2r_0 \cos(\phi_0)}{(1 - r_0^2) \sin(\phi_0)} , \qquad (4.35)$$

$$\phi_m = \arccos\left(\frac{1 + r_0^2}{2r_0} \cos(\phi_0) \right) , \qquad (4.36)$$

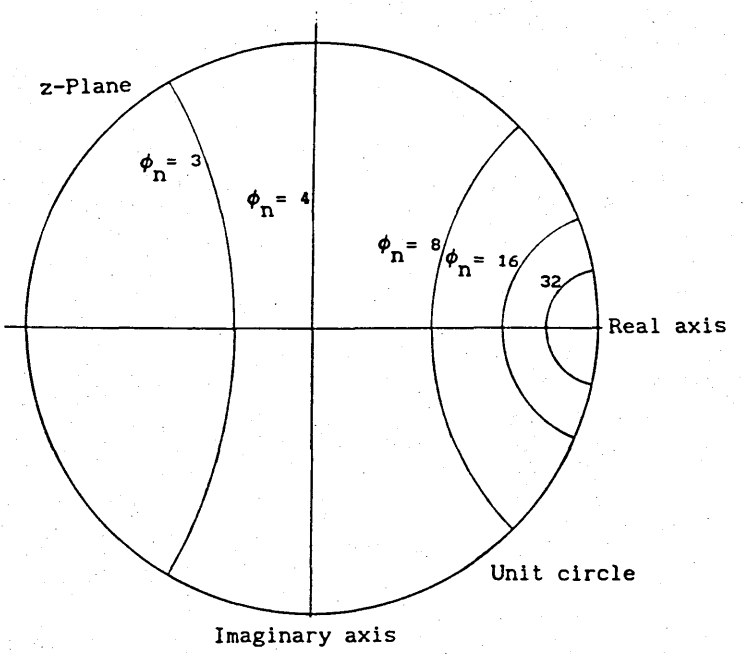

CADT domain natural frequency contours ϕ_n

Fig.4.10

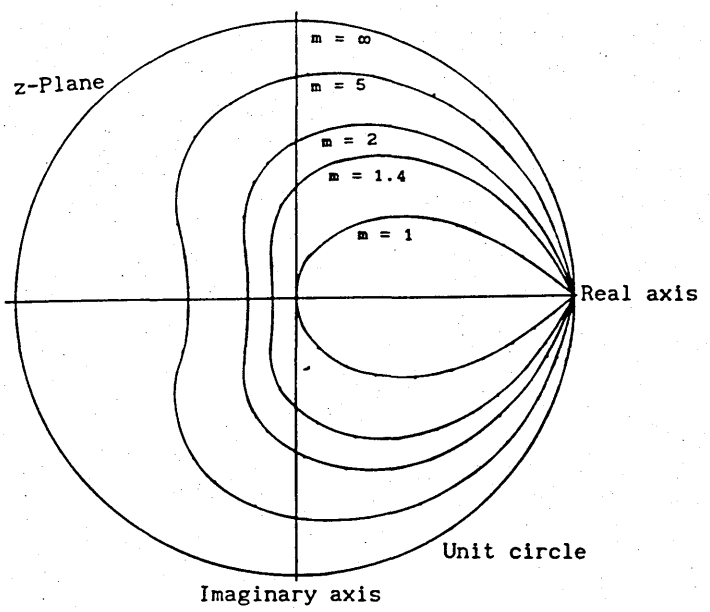

CADT domain resonance magnification contours

Fig.4.11

4.3.4 The Two Parameter Root-Locus

The concept of the two parameter root-locus is introduced in this section. A root-locus plot can be developed for a transfer-function model which is cast in any of the three CADT domains described in this chapter. A conventional root-locus, which is defined in terms of a transfer-function gain parameter, can be plotted on the z-plane, the w-plane or the w'-plane to assess the stability characteristics of a unirate sampled-data system. A two parameter root-locus, defined in terms of gain and sampling period, can be used to estimate the behaviour of multirate sampled-data systems.

The idea of the two parameter root-locus is straight forward; a surface grid is produced by computing the gain root-locus of a given CADT domain transfer-function at different sampling periods. In formal terms, the two parameter z-plane root-locus is defined as follows:

The general single-input single-output z-plane transfer-function is given by

$$\frac{C(z(h))}{R(z(h))} = \frac{G(z(h))}{1 + GH(z(h))} \quad , \tag{4.37}$$

where C is the controlled output variable, R is the control reference variable, G is the forward path z-plane transfer-function and H is the feedback path z-plane transfer function. The sampled data transfer-functions are defined for the sampling period, h. The open-loop transfer-function can be represented by

$$GH(z(h)) = K \frac{N(z(h))}{D(z(h))} \quad , \tag{4.38}$$

where N and D are the z domain numerator and denominator polynomials, respectively, and K is the gain parameter. Equation (4.38) can therefore be recast as

$$\frac{C(z(h))}{R(z(h))} = \frac{N(z(h))}{D(z(h)) + KN(z(h))} \quad . \tag{4.39}$$

The closed-loop poles of (4.39) are the roots of

$$D(z(h)) + KN(z(h)) = 0 \quad . \tag{4.40}$$

The solutions of (4.40) are produced at values of K from zero to infinity and values of h from zero to $1/\mu_{min}$, where μ_{min}=2 samples-per-envelope-cycle of the highest frequency component in GH(s). These solutions can be mapped onto the z-plane to give the

two parameter root-locus or, more correctly, a root location surface. An example, to illustrate the utility of the two parameter root-locus in the analysis of a multirate sampled-data system, is given below.

Consider the CACT s-plane transfer function

$$\frac{C(s)}{R(s)} = \frac{K(s + 10)}{s(s + 2 \pm j4.58)} \quad . \tag{4.41}$$

The root-locus plot of this system, with $0 \leq K \leq 25$, is shown in Fig.4.12. Mapping the transfer function to the CADT z-domain at sampling periods, h = 0.1, 0.2, 0.3 and 0.4, produces a z-plane transfer-function of the form

$$\frac{C(z(h))}{R(z(h))} = K \frac{(z + n_1)(z + n_2)}{(z + d_1)(z + d_3 \pm jd_4)} \quad . \tag{4.42}$$

The components of the transfer function, for different values of h, are summarised in Table 4.1. The corresponding two parameter z-plane root-locus, for $0 \leq K \leq 25$ and $0.1 \leq h \leq 0.4$, is shown in Fig.4.13.

	n_1	n_2	d_1	d_3	d_4
h = 0.1	-1.1963	0.3364	-1	-0.7343	0.3622
h = 0.2	-1.3093	0.12	-1	-0.4079	0.5319
h = 0.3	-1.2974	0.0073	-1	-0.1069	0.5383
h = 0.4	-1.1763	-0.0563	-1	0.1165	0.434

The components of the z-plane transfer-function (4.42)

Table 4.1

The equivalent CADT w-plane transfer function has the form

$$\frac{C(w(h))}{R(w(h))} = K\frac{(w + n_1)(w + n_2)(w + n_3)}{w(w + d_1 \pm jd_2)} \quad . \qquad (4.43)$$

The component values of (4.43) are summarised in Table 4.2.

	n_1	n_2	n_3	d_1	d_2
h = 0.1	-11.1889	-1	0.4647	0.105	0.2308
h = 0.2	-7.4663	-1	0.7858	0.2431	0.4696
h = 0.3	-7.7257	-1	0.9855	0.4613	0.7106
h = 0.4	-12.3437	-1	1.1192	0.8237	0.8958

The components of the w-plane transfer-function (4.43)

Table 4.2

Finally, the CADT w'-plane equivalent model of (4.41) is given by

$$\frac{C(w'(h))}{R(w'(h))} = K\frac{(w' + n_1)(w' + n_2)(w' + n_3)}{w'(w' + d_1 \pm jd_2)} \quad . \qquad (4.44)$$

The components of the w'-plane transfer-function are summarised in Table 4.3.

	n_1	n_2	n_3	d_1	d_2
h = 0.1	-223.778	-20	9.2734	2.1007	4.6157
h = 0.2	-74.6635	-10	7.8577	2.4311	4.6961
h = 0.3	-51.5046	-6.6667	6.5701	3.0751	4.7376
h = 0.4	-61.7187	-5	5.5962	4.1185	4.4788

The components of the w'-plane transfer-function (4.44)

Table 4.3

The two parameter root-locus plots with $0 \leq K \leq 25$ and $0.1 \leq h \leq 0.4$, for the equivalent CADT domain w and w'-plane transfer-functions, are shown in Figures 4.14 and 4.15, respectively.

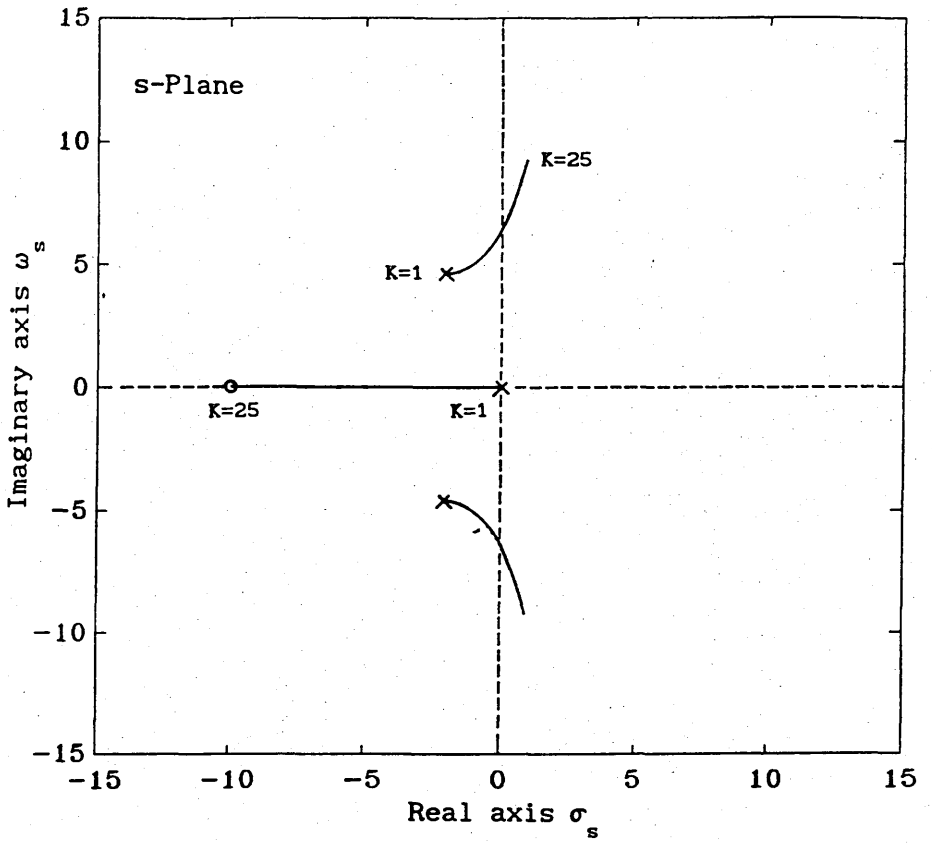

The s-plane root-locus plot for the transfer-function (4.41)

Fig.4.12

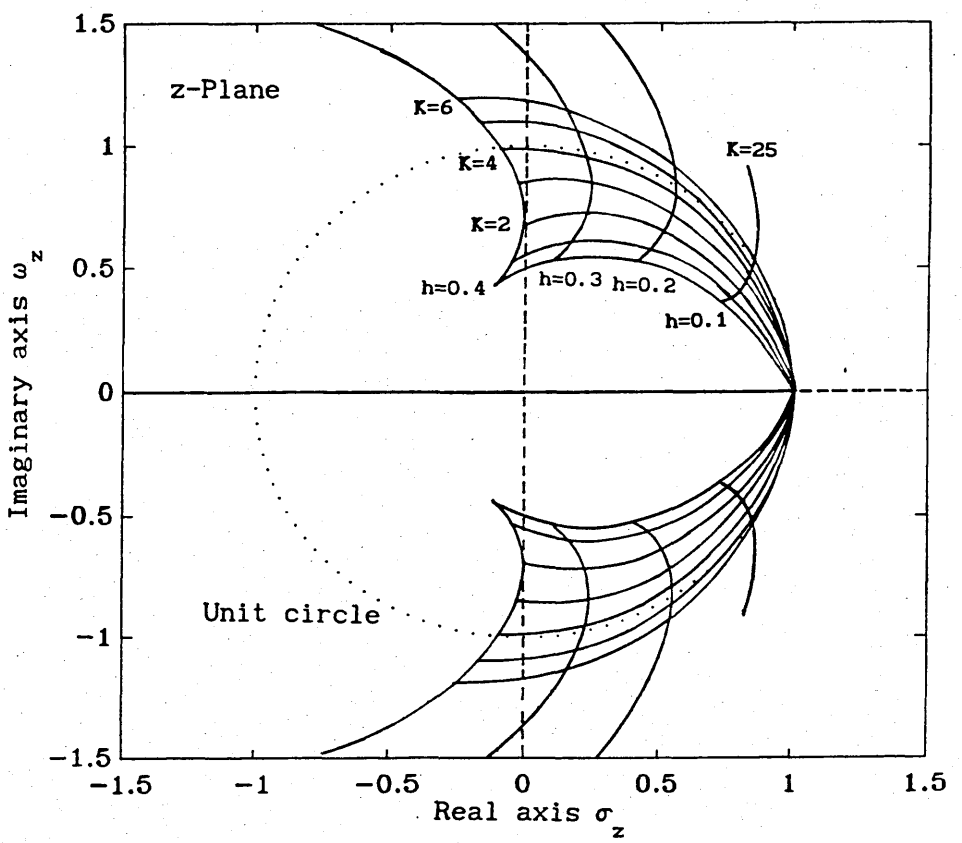

The two parameter z-plane root-locus plot corresponding to Fig.4.12

Fig.4.13

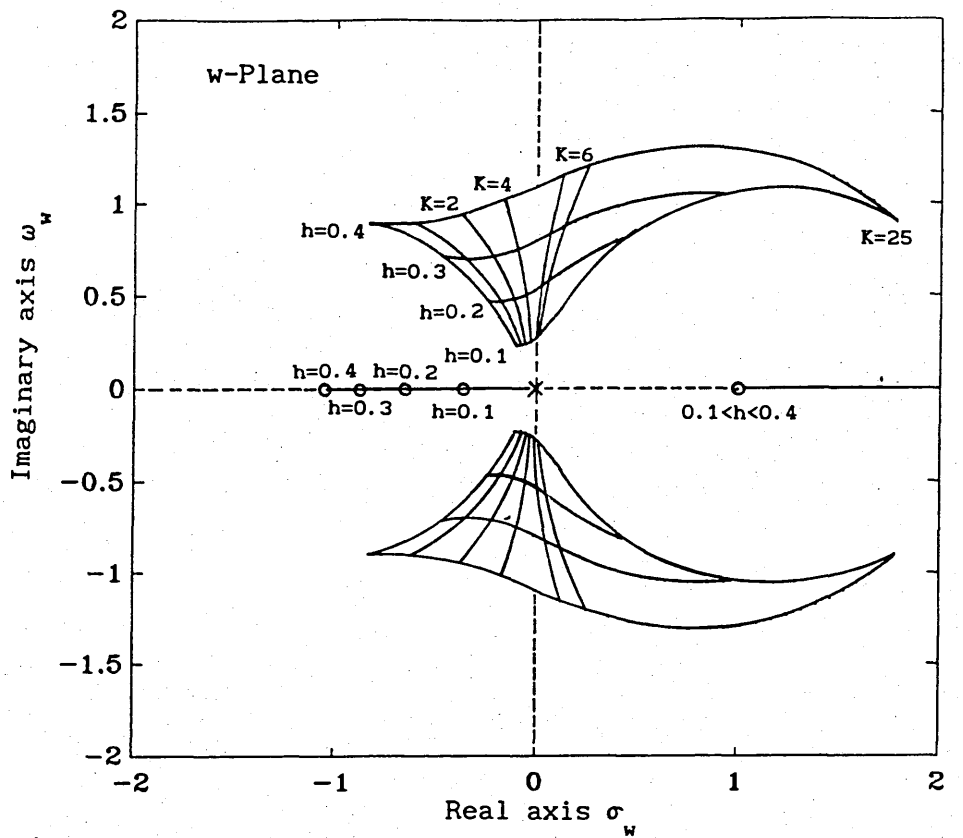

The two parameter w-plane root-locus plot corresponding to Fig.4.13

Fig.4.14

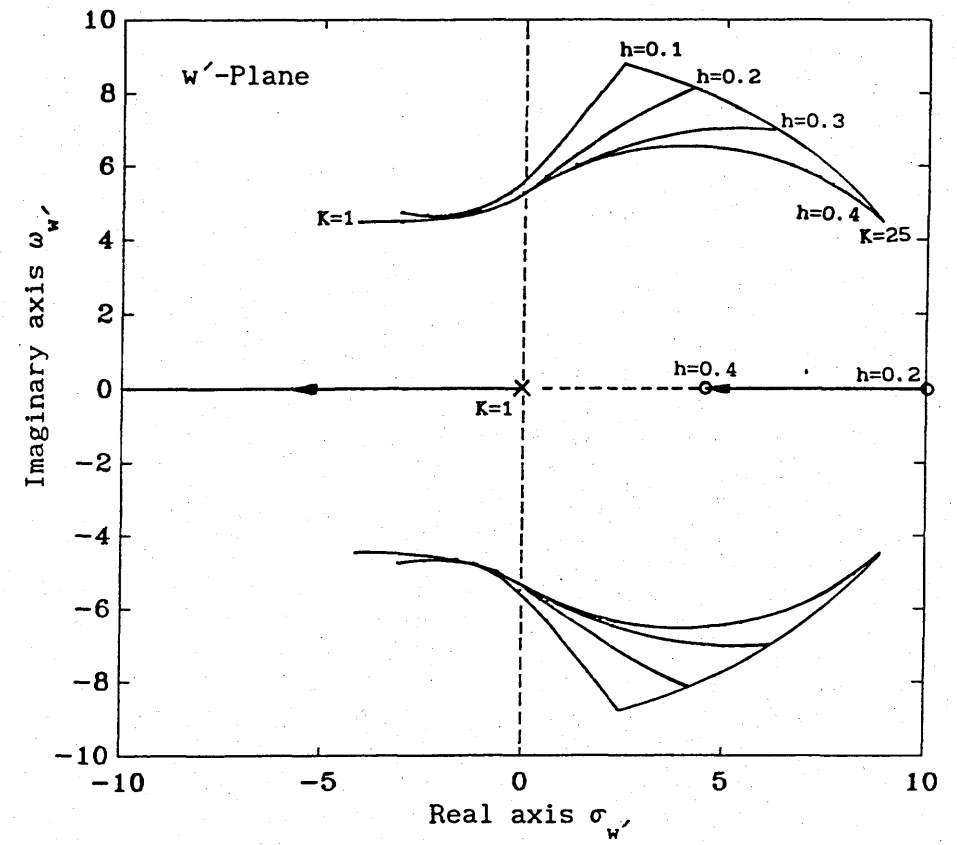

The two parameter w′-plane root-locus plot corresponding to Fig.4.13

Fig.4.15

4.4 SUMMARY

Consideration has been given to the CADT domain methods of design and analysis. The w- and w'-plane techniques have been exposed to the extensive range of CACT state-space methods through the two CADT domain to w domain algorithms. The w domain model of a multirate system is simply defined in terms of the program period h_p. An alternative approach to the w domain design of a multirate sampled-data control system is to consider a separate control strategy for each rate in the multirate sampling policy. This technique is considered in detail for the design case study, described in Chapter Five.

The quantitative performance parameters, described in Section 4.3, are presented as appropriate measures for the analysis of mixed-data control systems. Although the final appearance of the geometry produced by the parameters has the form of the directly mapped s-plane to z-plane geometry, the basis of the two sets measures are fundamentally different.

CHAPTER FIVE

A DIGITAL FLIGHT CONTROL DESIGN CASE STUDY

5.1 INTRODUCTION

This chapter presents the application of the proposed digital flight control design methods, in the context of a manned-aircraft flight control problem. The intermediate and final results of a DFC design exercise are discussed. The DFC design problem focuses on the requirements to stabilise and control the basic dynamics of an F4-E combat aircraft. The control specifications are defined by the relevant clauses of the handling qualities standard, MIL-F-8785C. These specifications are cast into the CADT domain for the purpose of DFC design.

The first part of the DFC design case study is concerned with the stability augmentation of the longitudinal dynamics of a basic F4-E aircraft. The second part of the design is an attempt to define a control law that decouples the longitudinal speed and attitude dynamics. The digital control is designed with a multirate (dual-rate) sampling policy. The stability augmentation control is applied at the faster of the two sampling-rates and the decoupling control-law is applied at the slower sampling rate. This separation of the two functions, in terms of the sampling policy, illustrates the point that the flight instrumentation, from which the control-law data is derived, will, in general, produce data at

different rates.

The stability augmentation control is achieved through a suboptimal state-feedback control-law. The primary, optimal control-law, from which the suboptimal controller is deduced, is designed through a standard state-space optimal pole placement algorithm, [5.1]. The speed/attitude decoupling control-law is derived through a state-space system decoupling algorithm, [5.2]. Although these two algorithms are defined in terms of the CACT state-space their application to CADT domain design is facilitated through the w- and w'-planes

5.2 A STATEMENT OF THE FLIGHT CONTROL DESIGN PROBLEM

The four-state, linear, perturbation model of the basic F4-E combat aircraft, which represents the kernel of the longitudinal axis dynamics, is given in terms of the following state variables:

u	forward-speed	metres-per-second,
w	normal-speed	metres-per-second,
q	pitch-rate	radians-per-second,
θ	pitch-angle	radians.

The basic longitudinal axis model is exercised by two flight control inputs, these are;

η	elevator-angle	radians,
ε	engine-thrust	newtons.

The CACT state matrix, **A**, and control input matrix, **B**, of the aircraft, when it is flying at Mach 1.1 at sea level, are given as

$$\mathbf{A} = \begin{bmatrix} -0.068 & -0.011 & 0 & -9.81 \\ 0.023 & -2.1 & 375 & 0 \\ 0.011 & -0.16 & -2.2 & 0 \\ 0 & 0 & 1 & 0 \end{bmatrix} \tag{5.1}$$

$$\mathbf{B} = \begin{bmatrix} -0.41 & 1 \\ -77 & -0.09 \\ -61 & -0.11 \\ 0 & 0 \end{bmatrix} \tag{5.2}$$

The output equation consists of a 4x4 identity state output matrix, **C**, and a null direct matrix, **D**, and therefore does not require an explicit representation in this exercise.

The stability characteristics of this system, defined by the roots of the characteristic equation, $\rho(s) = \det[sI-A]$, are;

(i) The short-period mode roots are, $s_{SP}=-2.15\pm j7.75$. The associated damping factor and natural frequency are $\zeta_{SP}=0.27$ and $\omega_{SP}=8$, respectively.

(ii) The phugoid mode roots are, $s_{PH}=-0.035\pm j0.041$. The associated damping factor and natural frequency are $\zeta_{PH}=0.64$ and $\omega_{PH}=0.055$, respectively.

Table 5.1 summarises the characteristics of the required longitudinal dynamics, as defined by MIL-F-8785C. The comparison of the specified and actual characteristics, together with the compliance status, is noted.

Characteristic Mode		MIL-F-8785C	Basic F4-E	Status
Short period damping	ζ_{SP} min	0.35	0.27	not compliant
	ζ_{SP} max	1.3		
Phugoid mode Damping ζ_{PH} (Stable)		> 0.04 (level 1)	0.64	compliant
Natural frequency ω_{PH}(rad/sec) (Unstable)		> 0.114 (level 2)	--	

A comparison of the required and actual

F4-E longitudinal stability parameters

Table 5.1

The stability characteristics of the basic aircraft are clearly revealed by the state time-history diagrams, shown in Fig.5.1. The time-history diagrams illustrate the state response of the basic aircraft, following a ±0.1 radian doublet movement of the aircraft's elevator. The control problem is to design a DFC system that will stabilise the basic aircraft to the level specified by MIL-F-8785C. This control function is know as stability augmentation.

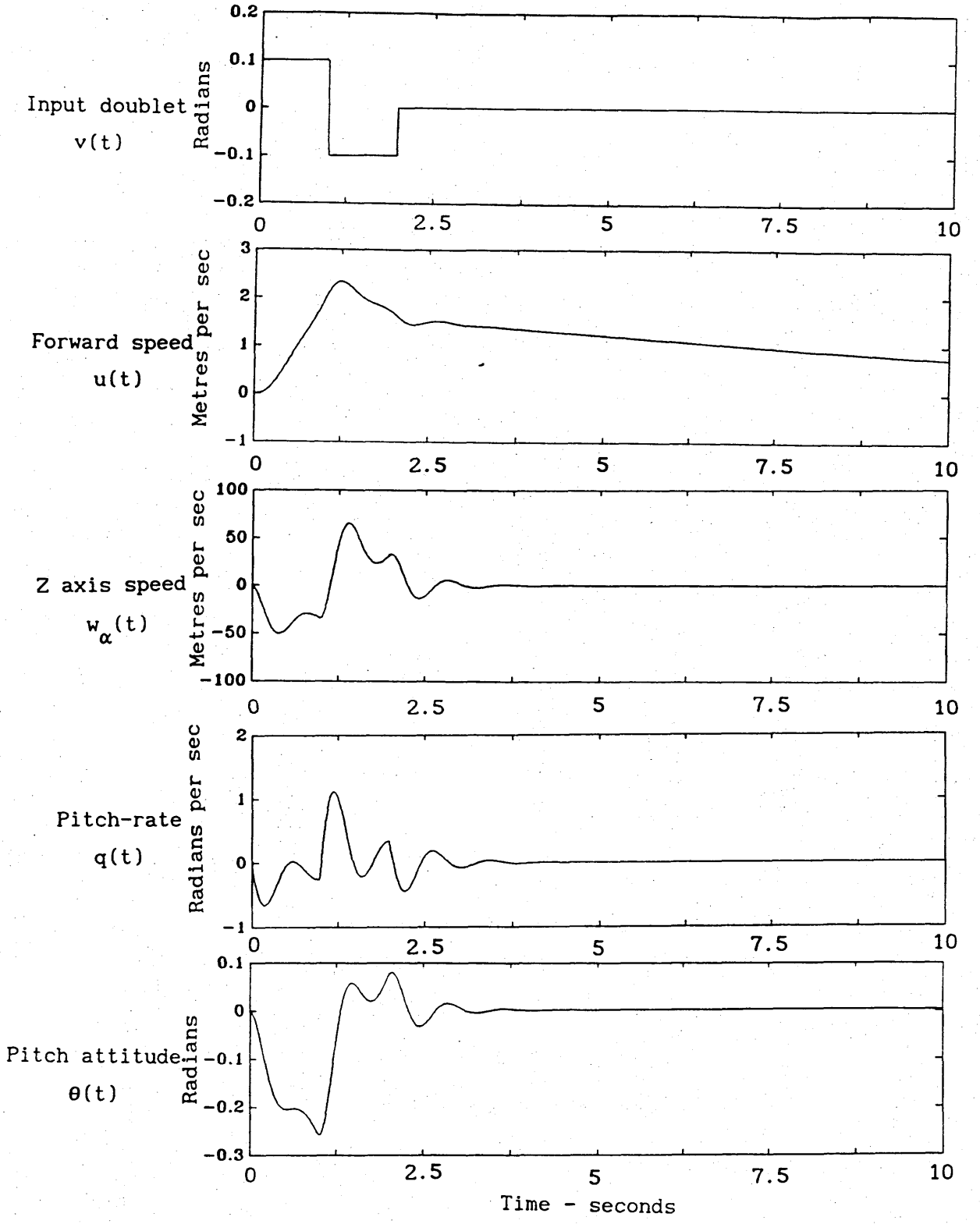

A ten second time-history of the basic aircraft's state elements, produced by applying a scaled (±0.1 radian) unit doublet to the elevator.

Fig.5.1

5.3 THE SAMPLING POLICY

The first task in the design process is to identify a multirate (two-rate) sampling policy for the stability augmentation control function. The sampling rates selection procedure, described in Section 3.2, is applied to this task. In addition to the basic aircraft model, the procedure requires an estimate of the disturbance energy that impinges on the aircraft and which the DFC system is design to reject. In terms of the selection procedure defined by equation (3.9), this means estimating the element values Q_c. These values must be chosen to make the resulting matrix symmetric, positive-definite. In practice, disturbance information, such as, for example, a stochastic model of the air turbulence in which an aircraft operates, may be available to relate the elements of Q_c to the specific requirements of a handling qualities specification. For the demonstration purpose of this case study, it is assumed that the disturbances are applied through the elevator and thrust controls. The matrix Q_c, chosen for this case study is

$$Q_c = \begin{bmatrix} 0.1 & 0 \\ 0 & 0.1 \end{bmatrix} , \qquad (5.3)$$

the element values are heuristic estimates. With G_c assigned an initial value of 0, equation (3.9) is propagated in time for 0.01 seconds to produce the time-history estimate of the uncertainty associated with the value of the state elements. These measures of state element uncertainties are plotted in Fig.5.2.

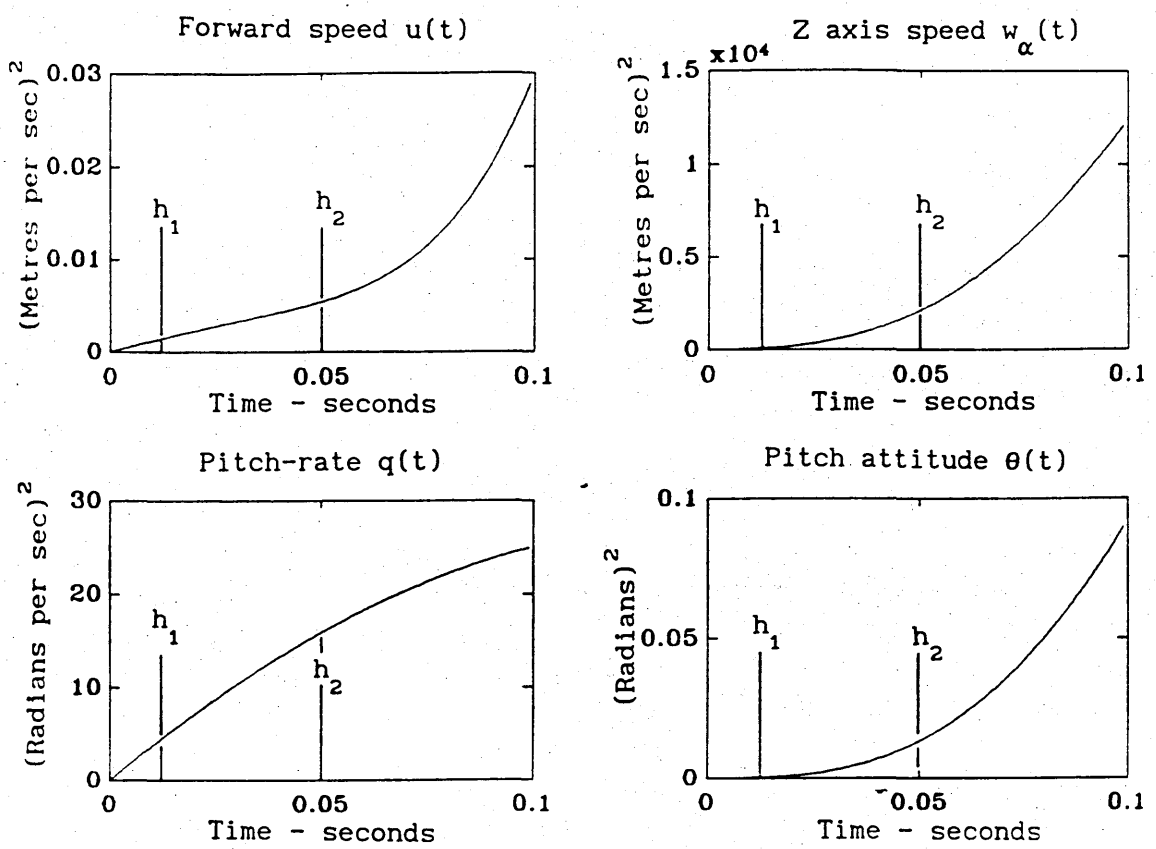

The covariance time-history of each state element of the basic CACT aircraft model

Fig.5.2

A qualitative inspection of covariance time-history diagrams indicates that pitch-rate, q, is the most sensitive state element. A similar analysis with each input exercised separately, reveals that the elevator has greater control authority than the thrust input over a short time period. The sampling policy which this analysis produces is given by the schedule shown in Fig.5.3. In the case of this example, the levels at which the state element covariances are deemed unacceptable is somewhat arbitrary. The procedure is only intended to illustrate the sampling period selection technique. However, it seems reasonable to suggest that a firm link between this method and the general aircraft handling qualities could be established.

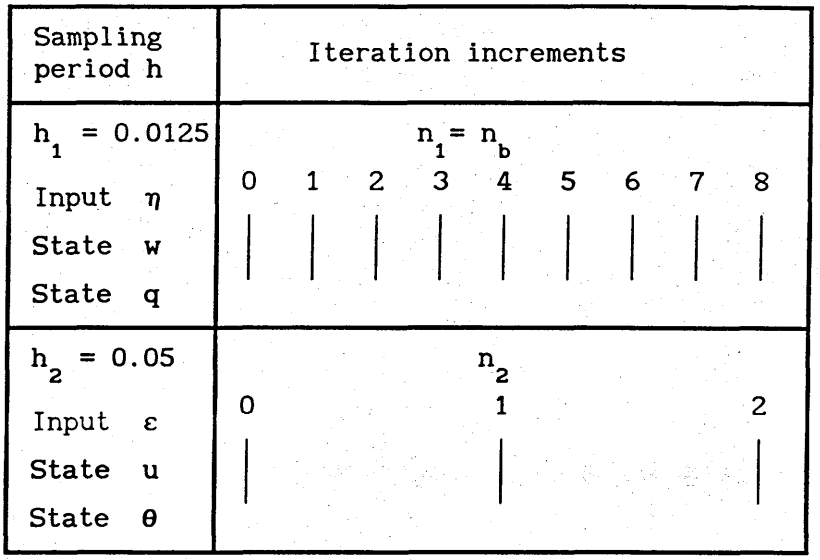

The DFC multirate sampling policy schedule

Fig.5.3

The dual-rate sampling policy, produced by the methods described above, confirms what flight control practitioners would expect; viz., the vertical speed state, w, and pitch-rate state, q, are associated with the "fast" short-period dynamics. The forward speed state, u, and pitch-attitude state, θ, are associated with the "slow" phugoid dynamics.

Confirmation of the suitability of the sampling policy is provided by a two parameter root-locus analysis, described in Section 4.3.4, and the criterion defined by Fig.3.2. In this case study, the analysis produces eight root-locus diagrams, one for each combination of input and output. To illustrate the application of the two parameter root-locus, Fig.5.4 shows the plot for the pitch-rate to elevator transfer-function, $q(z)/\eta(z)$.

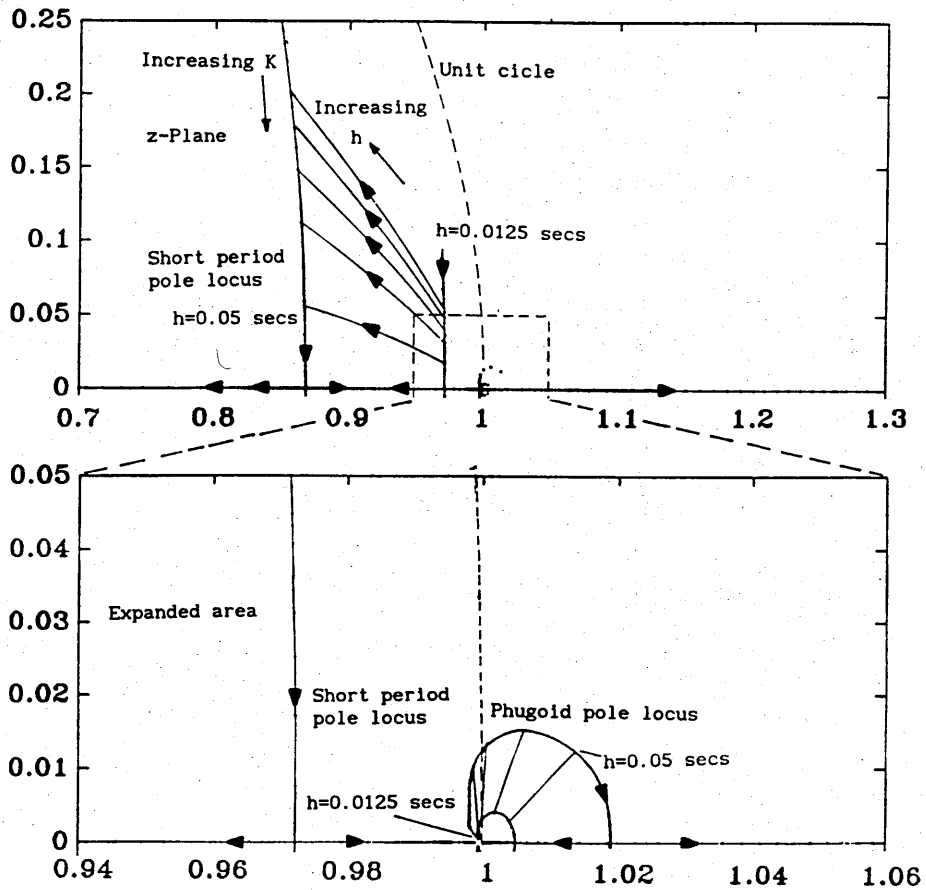

A two-parameter ($0 \leq K < \infty$, $0.0125 \leq h \leq 0.05$)

root-locus of the transfer-function $q(z)/\eta(z)$

Fig.5.4

The effect of multirate sampling on the state element covariance can be estimated by modifying the application of equation (3.9) in the following way:

The state elements are assumed to be reset to zero error at the instant they are sampled. In terms of the covariance equation (3.9), this infers that, if the state element x_i is reset, the i-th row and i-th column elements of G_{K+1} are also reset to zero.

Applying this procedure to the sampling policy of Fig.5.3 means that every 0.0125 seconds (h_1) of the covariance time history, the second

row and third column elements of G_{K+1} (the associated state elements are w and q) are reset to zero, and every 0.05 seconds (h_2) all the elements of G_{K+1} are reset to zero. The resulting multirate sampled-data state covariance time-history is shown in Fig.5.5.

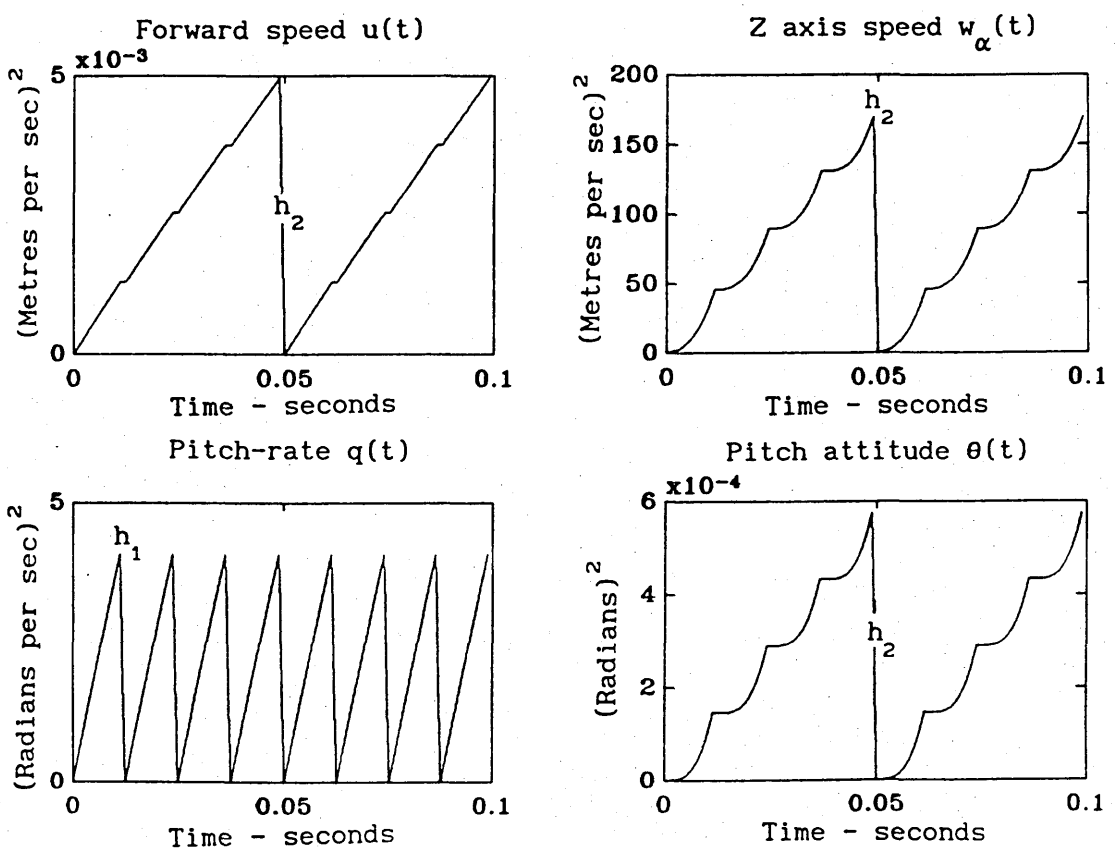

Time histories of the state element covariances produced by applying the multirate sampling policy to the solution of equation (3.9)

Fig.5.5

5.4 THE MULTIRATE SAMPLED-DATA STATE-SPACE MODEL

The open-loop, dual-rate, sampled-data model of the basic aircraft is cast in the form of equation (3.30) (Chapter 3). The components of this equation are as follows:[1]

The base sampling rate, $h_b = h_1 = 0.0125$ seconds.

The program period, $h_P = h_2 = 0.05$ seconds.

The parameters of k are $k_{0,3}$ and $k_{0,0}$, and $\rho = \frac{0.05}{0.0125} = 4$.

$$[\Phi] = \begin{bmatrix} 0.9992 & -0.0001 & -0.0011 & -0.1226 \\ 0.0006 & 0.9695 & 4.5561 & -0 \\ 0.0001 & -0.0019 & 0.9683 & -0 \\ 0 & -0 & 0.0123 & 1 \end{bmatrix} . \qquad (5.3)$$

$$[\Phi]^{\rho} = [\Phi]^4 = \begin{bmatrix} 0.9966 & -0.0005 & -0.0164 & -0.4897 \\ 0.0058 & 0.8337 & 16.4211 & -0.0011 \\ 0.0005 & -0.007 & 0.8294 & -0.0001 \\ 0 & -0.0002 & 0.0462 & 1 \end{bmatrix} . \qquad (5.4)$$

$$\begin{bmatrix} \rho_\Phi \end{bmatrix} = \begin{bmatrix} 4_\Phi \end{bmatrix} = \begin{bmatrix} \Phi^3 & \Phi^2 & \Phi^1 & I \end{bmatrix} . \qquad (5.5)$$

$$\Gamma = \int_0^{h_b} \exp(A\lambda)d\lambda = \int_0^{0.0125} \exp\left(\begin{bmatrix} -0.068 & -0.011 & 0 & -9.81 \\ 0.023 & -2.1 & 375 & 0 \\ 0.011 & -0.16 & -2.2 & 0 \\ 0 & 0 & 1 & 0 \end{bmatrix} \lambda \right) d\lambda . \qquad (5.6)$$

---

[1] All the calculations are processed to fourteen decimal places. However, for the purposes of a readable presentation, numbers are given to four decimal places. Hence, small value numbers are displayed as a signed zero.

$$\begin{bmatrix} B_1 & 0 & 0 & 0 & B_2 \\ 0 & B_1 & 0 & 0 & B_2 \\ 0 & 0 & B_1 & 0 & B_2 \\ 0 & 0 & 0 & B_1 & B_2 \end{bmatrix} = \begin{bmatrix} -0.41 & 0 & 0 & 0 & 1 \\ -77 & 0 & 0 & 0 & -0.09 \\ -61 & 0 & 0 & 0 & -0.11 \\ 0 & 0 & 0 & 0 & 0 \\ 0 & -0.41 & 0 & 0 & 1 \\ 0 & -77 & 0 & 0 & -0.09 \\ 0 & -61 & 0 & 0 & -0.11 \\ 0 & 0 & 0 & 0 & 0 \\ 0 & 0 & -0.41 & 0 & 1 \\ 0 & 0 & -77 & 0 & -0.09 \\ 0 & 0 & -61 & 0 & -0.11 \\ 0 & 0 & 0 & 0 & 0 \\ 0 & 0 & 0 & -0.41 & 1 \\ 0 & 0 & 0 & -77 & -0.09 \\ 0 & 0 & 0 & -61 & -0.11 \\ 0 & 0 & 0 & 0 & 0 \end{bmatrix} . \quad (5.7)$$

$$u_p(k) = u_4(k_{0,3}, k_{0,0}) = \begin{bmatrix} u_1(0) & u_1(1) & u_1(2) & u_1(3) & u_2(0) \end{bmatrix}^T . \quad (5.8)$$

Combining these function in the manner prescribed by (3.25) produces the form of state equation given in Chapter Three as (3.39a), where

$$\Phi_P = \begin{bmatrix} 0.9966 & -0.0005 & -0.0164 & -0.4897 \\ 0.0058 & 0.8337 & 16.4211 & -0.0011 \\ 0.0005 & -0.007 & 0.8294 & -0.0001 \\ 0 & -0.0002 & 0.0462 & 1 \end{bmatrix} , \quad (5.9)$$

and

$$\Lambda_P = \begin{bmatrix} 0.1928 & -0.1306 & -0.41 & -0.41 & 3.9966 \\ -848.4769 & -610.2654 & -352.5747 & -77 & -3.2142 \\ -53.3934 & -56.3656 & -58.9176 & -61 & -0.4139 \\ -2.1574 & -1.471 & -0.75 & 0 & -0.0079 \end{bmatrix} . \quad (5.10)$$

5.5 THE DIGITAL DESIGN PROCEDURE

The DFC design proceeds by mapping the multirate sampled-data equations of the basic CACT domain aircraft model to either the w-plane or w'-plane. The results of the DFC system, reported in Section 5.5.4 are produced by a w-plane design. The DFC is designed to perform two flight control functions; the first, is an inner-loop stability augmentation of the basic aircraft system, and the second is a speed-attitude decoupling control law.

The w-plane model of the basic multirate sampled-data aircraft model is computed through the time domain to w-plane algorithm, described by equations (4.19) to (4.22); the resulting quadruple is $(\mathbf{A}_w, \mathbf{B}_w, \mathbf{C}_w, \mathbf{D}_w)$, where

$$\mathbf{A}_w = \begin{bmatrix} -0.0017 & -0.0003 & -0.0002 & -0.2452 \\ 0.0007 & -0.0545 & 9.4655 & 0.0002 \\ 0.0003 & -0.004 & -0.057 & -0 \\ 0 & -0 & 0.0253 & 0 \end{bmatrix} , \qquad (5.11)$$

$$\mathbf{B}_w = \begin{bmatrix} -0.0059 & -0.0052 & -0.0037 & -0.0012 & 0.025 \\ 0.0292 & 1.9535 & 3.9638 & 6.0441 & 0.0229 \\ -0.4001 & -0.4093 & -0.4147 & -0.4162 & -0.003 \\ 0.0019 & 0.0069 & 0.0121 & 0.0173 & 0.0001 \end{bmatrix} . \qquad (5.12)$$

It is assumed that the state sampling operation is synchronised with the control action sampling, as described in Section 2.4.2; the components, $\mathbf{C}_w$ and $\mathbf{D}_w$, of the w-plane output equation are thus

$$\mathbf{C}_w = \begin{bmatrix} 1 & 0 & 0 & 0 \\ 0 & 1 & 0 & 0 \\ 0 & 0 & 1 & 0 \\ 0 & 0 & 0 & 1 \end{bmatrix} \qquad (5.13)$$

$$\mathbf{D}_w = \begin{bmatrix} 0.0031 & 0.004 & 0.0042 & 0.0034 & -0.0250 \\ 3.2585 & 1.5695 & -0.2291 & -2.1247 & 0.0032 \\ 0.3661 & 0.3812 & 0.3932 & 0.4018 & 0.0028 \\ 0.0074 & 0.0027 & -0.0021 & -0.0071 & 0 \end{bmatrix} . \qquad (5.14)$$

5.5.1 The Design of a Stability Augmentation System

The stability augmentation control-law is determined by applying a CACT domain optimal pole assignment procedure [5.3] to the w-plane model. The objective control function is selected to achieve compliance with the requirements of MIL-F-8785C, outlined in Table 5.1. In this case, the locations of the basic aircraft's CACT s-plane poles which meet the stability requirements are

$$s_{SP1} = -5.6 \pm j5.6 \quad \text{and} \quad s_{PH1} = -0.035 \pm j0.041.$$

The equivalent short-period and phugoid mode w-plane pole locations for the sampling-period, h_1=0.0125, are,

$$w_{SP1} = -0.0362 \pm j0.0363 \quad \text{and} \quad w_{PH1} = -.0002 \pm j0.0003.$$

Under the sampling-period, h_2 = 0.05 seconds, the same w-plane poles are mapped to

$$w_{SP1} = -0.1418 \pm j0.1381 \quad \text{and} \quad w_{PH1} = -0.0009 \pm j0.001.$$

The optimum state-feedback stability augmentation control matrix is computed through a standard CACT procedure. The distortion of the w-plane (when compared with the s-plane) places an additional restriction on the achievable pole positions. Identifying the general boundaries for pole placement is a significant problem and is clearly an area for further research. For the current design, the required pole locations are determined by trial. The resulting stability augmentation state feedback control matrix is given by

$$H_{w1} = \begin{bmatrix} 0 & 0.0006 & -0.1120 & -0.0001 \\ 0 & 0 & 0 & 0 \end{bmatrix} . \qquad (5.15)$$

The state-feedback matrix is examined to identify those elements can be set to zero. Although this practice produces a non-optimum controller, the result often removes the need for an actuator, or a sensor, or both, from the required control system. For the control-law in question, the element (1,3) is judged to be the only significant element in H_{w1}. The feedback control is reduced to applying the pitch-rate state element, q, onto the elevator. The feedback matrix is therefore recast as

$$H_{w1} = \begin{bmatrix} 0 & 0 & -0.12 & 0 \\ 0 & 0 & 0 & 0 \end{bmatrix} \quad . \qquad (5.16)$$

The resulting closed-loop system is analysed to ascertain the performance of the sub-optimal feedback control. A check is then made to determine whether the sub-optimal control law produces handling quality measures that compliant with the design specification. The w-plane stabilised system is given by

$$w\, X(w) \Big|_{h\,=\,0.0125} = \left[A_w - B H_{w1}\right] X(w) + BU(w) \quad . \qquad (5.17)$$

The closed-loop poles produced by (5.17) are

$$w_{SP1} = -0.0367 \pm j0.0429 \quad \text{and} \quad w_{PH1} = -.0002 \pm j0.0003.$$

The stability augmentation control is therefore implemented by closing a digital feedback loop from the pitch-rate state to the elevator. The sampling period required for this digital flight control activity is 0.0125 seconds.

5.5.2 The Design of a Speed-Attitude Decoupling Control Law

The final part of this exercise is concerned with the design of a digital control law that decouples the speed and attitude dynamics of the stabilised aircraft. A system decoupling algorithm [5.4] is applied to the stabilised w-plane aircraft model which, for this exercise, is defined for h_2=0.05 seconds. The CADT domain stabilised aircraft model is mapped from its defined form at h_1=0.0125 to h_2=0.05. The general procedure for this operation is described in Section 3.4. With a sampling period of 0.05 seconds, the w-plane model, on which the speed-attitude decoupling control is required, is given by

$$A_{Hw}\Big|_{h_2=0.05} = \begin{bmatrix} -0.0017 & -0.0003 & -0.0021 & -0.2452 \\ 0.0007 & -0.0545 & 10.9044 & 0.0002 \\ 0.0003 & -0.0040 & -0.2539 & -0 \\ 0 & -0 & 0.0299 & 0 \end{bmatrix} \qquad (5.18)$$

$$B_w\Big|_{h_2=0.05} = \begin{bmatrix} -0.016 & 0.025 \\ 11.9905 & 0.0229 \\ -1.6403 & -0.003 \\ 0.0382 & 0.0001 \end{bmatrix} \qquad (5.19)$$

$$D_w\Big|_{h_2=0.05} = \begin{bmatrix} 0.0147 & 0.025 \\ 2.4742 & 0.0032 \\ 1.5424 & 0.0028 \\ 0.0008 & 0 \end{bmatrix} . \qquad (5.20)$$

The state feedback matrix is produced by a standard CACT domain state decoupling design procedure [5.5]. Unlike the optimal pole placement technique, the CACT domain decoupling algorithm presents no w-plane application problems in this case study. The state-feedback control matrix which achieves the speed-attitude decoupling requirement is,

$$H_{w1} = \begin{bmatrix} 0 & 0 & -0.034 & -1.27 \\ 0.23 & 0 & 0 & 0 \end{bmatrix} . \qquad (5.21)$$

In addition to the state feedback, the speed-attitude decoupling control law includes a control input (elevator and thrust control) mixing function. This facet of the control law is automatically produced by the state element decoupling design procedure. The proposed control also includes a gain function on the elevator inceptor. This compensates for the loss of control sensitivity caused by the stability augmentation system.

5.5.3 The Digital Flight Controller

For the purposes of control law implementation, the w-plane controller must be mapped to the CADT domain. In this case study, the mapping does not change the purely gain **H** matrices. In the case of a dynamic controller, the inverse w-plane to discrete-time state-space mapping algorithms would be applied.

The proposed multirate digital control-law diagram is illustrated in Fig.5.6. The DFC terminology is noted on the diagram; that is, an iteration period, during which the control law is updated, is called a computing frame. The maximum time available for a computing frame is 0.0125 seconds; thus, a computing frame equates with the sampling period, h_1. The digital computing cycle consists of four frames and is clearly associated with the sampling period, h_2. The implicit assumption of the proposed controller is that the computational delay is small enough for the synchronous sampling assumption to remain valid.

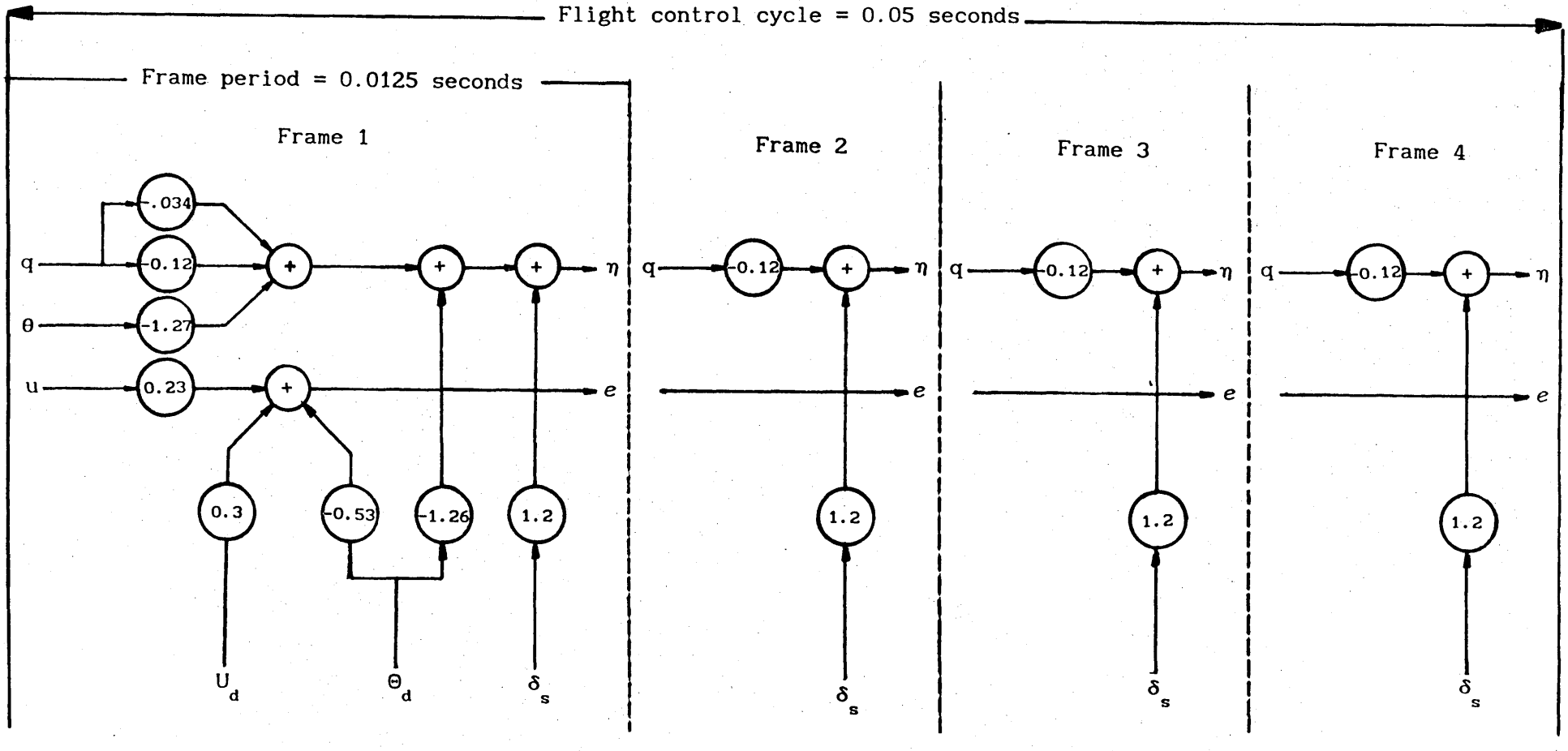

The multirate sampled-data SAS and attitude/speed decoupling control law

Fig.5.6

5.5.4 Test Results

The state vector time-history, following the application of a scaled (0.1 radian) unit doublet on the elevator, is given for each state of the decoupled, stability augmented aircraft, in Fig.5.7. The time histories indicate that a satisfactory stability performance is achieved with the multirate sampled-data control system.

An oscillation, which has a period equal to the sampling period, h_1, is particularly noticeable on the pitch-rate state. This oscillation is caused by the continuous-time dynamics of the basic aircraft. As the state element covariance analysis indicates, between the sampling instants, the basic aircraft state diverges from the control set-points or set-functions. The higher frequency response characteristic of the pitch-rate makes this state element more sensitive to the open-loop (intersample period) behaviour of the CACT dynamics of the basic aircraft. In a practical flight control system, the level of this sampling interference may be unacceptable. The level is reduced by selecting a smaller sampling period, h_1, for the stability augmentation control; this solution assumes that the pitch-rate state can be measured at an increased sampling frequency.

The published results of other DFC system designs [5.6] appear to be uncorrupted by the intersample oscillations that feature in this current design. At this stage it is only possible to speculate on this observation. One possibility, which is consistent with the operational DFC problems, described in Chapter One, is that the

analysis procedure used for this case study exposed the intersample oscillation, whereas the analysis applied in the reported DFC cases did not. Further work, employing hardware-in-the-loop simulations, is required in this area of DFC system design.

A comparison of two unirate sampled-data systems and the multirate sampled-data DFC system is summarised by the step response time-history characteristics, shown in Fig.5.8. These one-second time histories represent the CACT state element responses of the digitally controlled aircraft. The time responses are produced by applying a 0.1 radian step input to the elevator. The three curves produced for each of the four state elements represent three equivalent DFC systems, with each system incorporating a combined stability augmentation and speed-attitude decoupling control law. The two unirate systems, one operating with a 0.0125 second sampling period and the other with a 0.05 second sampling period, are compared with the multirate sampled-data DFC system produced in this case study.

The time histories are produced by pseudo analogue simulation [5.7] (a digital simulation with a simulation time step, Δt, much smaller than the shortest period in the DFC sampling policy; that is, $\Delta t << h_1$). The state element sampling and digital control functions are applied at the appropriate sampling instants, h_1 and h_2. The results represent the continuous-time response characteristics of the basic aircraft's state elements. The one-second time history curves show, once again, the intersample oscillation on the pitch-rate state element. The significant issue of these results is

the comparison of the two unirate sampled-data systems with the equivalent multirate sampled-data system. It is first observed that, as predicted by the two parameter root-locus, the dynamics of the sampled-data system is a function of the sampling rate. This observation underpins the recommendation to undertake a DFC design in the CADT domain. A second observation is the decreasing effectiveness of the control as the sampling period is increased. The multirate sampled-data system clearly represents a compromise between the two unirate systems.

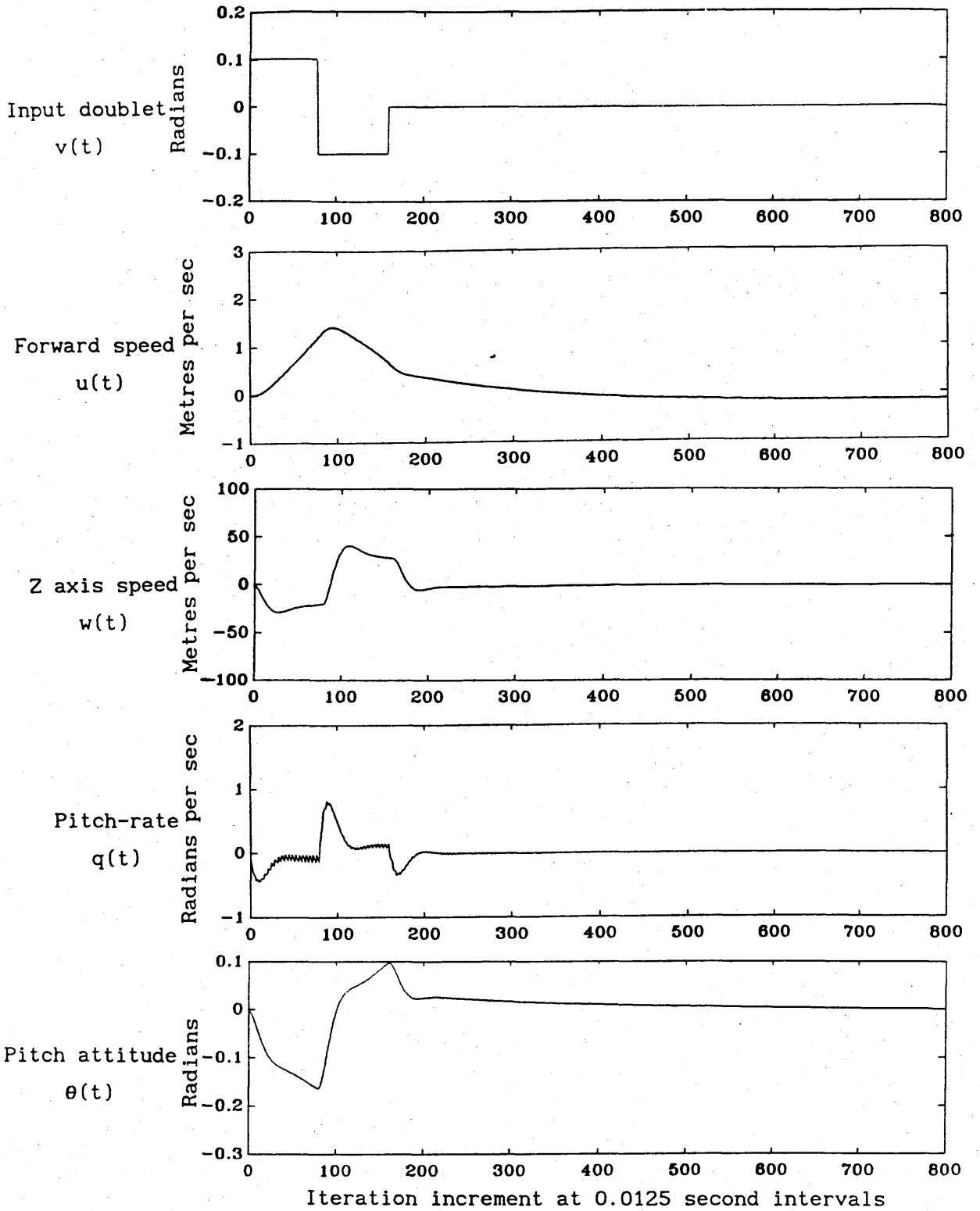

A ten second time-history of the stability augmented aircraft's state elements, produced by applying a scaled (±0.1 radian) unit doublet to the elevator.

Fig.5.7

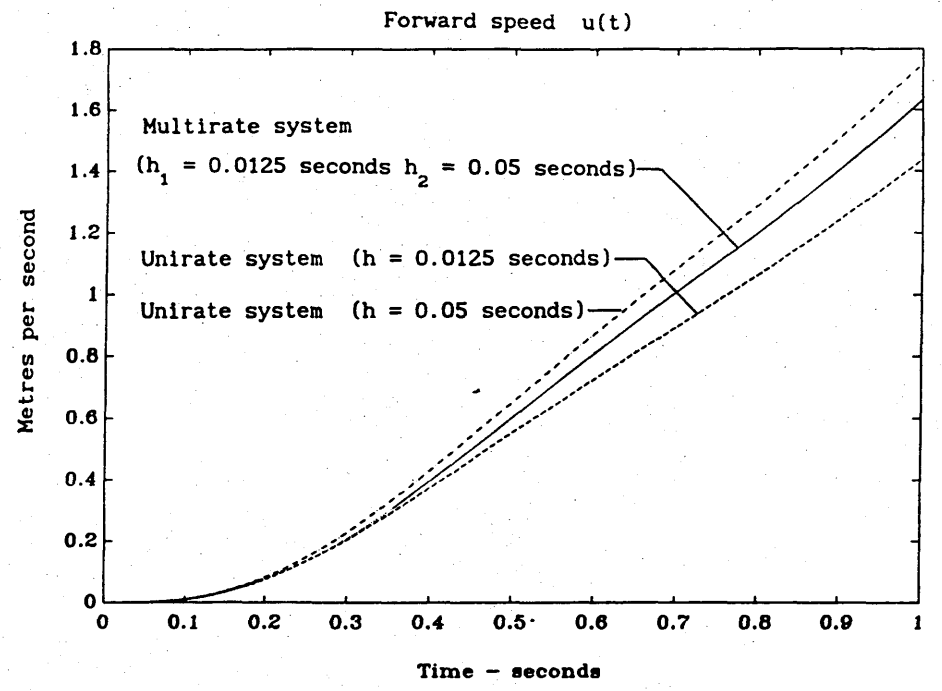

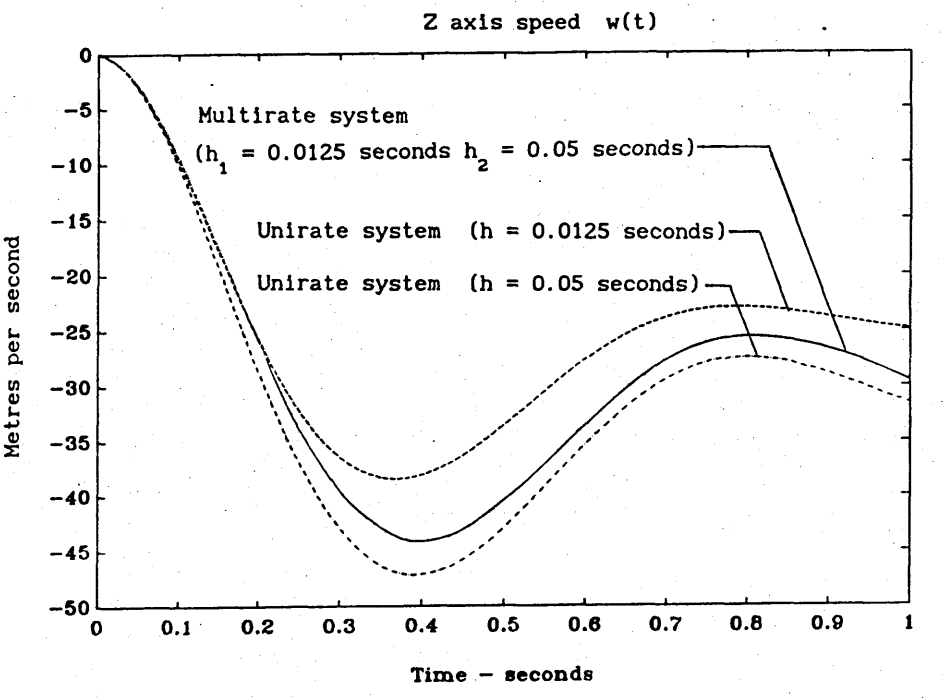

The CACT aircraft state (forward speed u(t) and vertical speed w(t)) step response produced by a 0.1 radian elevator control input

Fig.5.8a

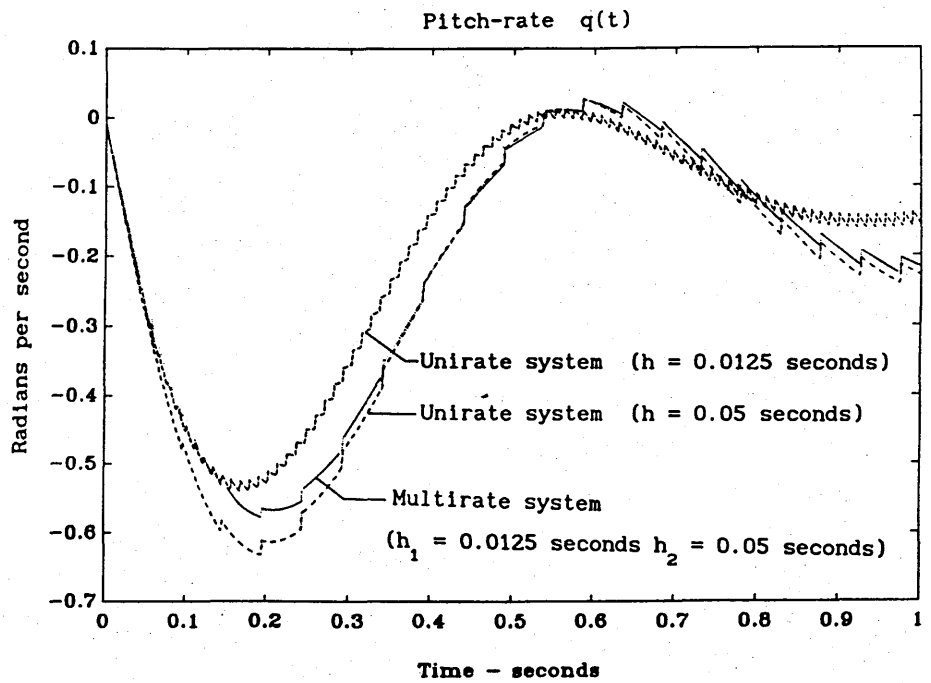

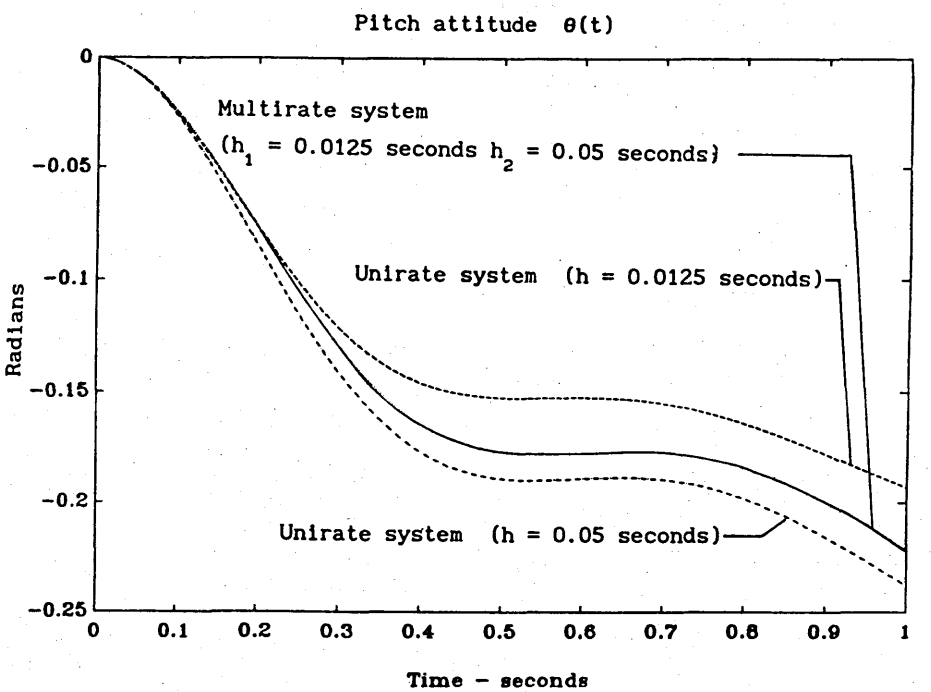

The CACT aircraft state (pitch-rate q(t) and pitch attitude θ(t))

step response produced by a 0.1 radian elevator control input

Fig.5.8b

5.6 SUMMARY

The results of the DFC stability augmentation and speed-attitude decoupling exercise, presented in this chapter, should only be regarded as a representation of a full DFC design process. Even in the case of this limited scale example, a considerable amount of work is required to establish, what is thought to be, a satisfactory flight control system. On the basis of this exercise, it can be concluded that the facility of the methodology proposed in this dissertation is suitable for practical DFC design.

Although the exercise only considers a design in the w-plane, the extension of the method to the w'-plane is readily deduced. For the selected sampling periods of this example, the w'-plane eigenvalues of the basic aircraft dynamics have numerical values that are, to four decimal places, identical to the s-plane eigenvalues.

A question that remains unanswered is: given a DFC system which is designed and analysed by the proposed methodology, will the resulting implementation avoid the difficulties that have been experienced with digital controllers designed by other methods? Although the results indicate the answer to this question is in the affirmative, a more positive conclusion requires further study. A specific aspect of this study will be the inclusion of the effects of data quantisation. The study will be expensive and will require both flight simulation and actual aircraft facilities.

CHAPTER SIX

CONCLUSIONS AND RECOMMENDATIONS FOR FURTHER RESEARCH

6.1 GENERAL CONCLUSIONS

The conclusions on the proposed Digital Flight Control (DFC) system design methodology are based on the results of the application exercise given in Chapter Five and the various examples presented in other sections of this dissertation.

The data-domain in which the dynamics of a mixed-data DFC system can be unified, for the purposes of flight control design and analysis, is the Continuous-Amplitude, Discrete-Time domain (CADT). A practical digital flight control system design model includes data elements which are continuous and discrete, in both amplitude and time. Thus, in addition to the CADT domain element, there is a Continuous-Amplitude, Continuous-Time data element which models the basic aircraft; a Discrete-Amplitude, Discrete-Time data element which is the digital flight control computer; and a Discrete-Amplitude, Continuous-Time data element which represents the flight control data on the output of the ZOH. The irony of this observation is that, in a practical implementation the CADT data domain exists only in a notional form within the structure of the Analogue-to-Digital converters. The three other domains exist in a physical sense.

A digital control system which retains the continuous amplitude characteristic of the data represents the classical concept of a sampled-data system. The design of sampled-data systems can be carried out on the basis of a unirate sampling policy, employing a direct digital design method. The advantage of the direct digital design method when compared with the emulation method is inferred by the results of the example, described in Appendix Two. While caution is required when drawing a general conclusion from the results of a specific case, the example supports the frequently asserted claim; viz., for a given control function, the direct digital design method yields a sampled-data control system with a lower sampling-rate than an equivalent sampled-data system which is designed by the emulation method.

A digital flight control system will, in general, require a multirate sampling policy. The two observations leading to this conclusion are:

(i) Flight control-data is associated with sensors and actuators that impose a variety of sampling-rates on a digital flight control system. By definition, a DFC system designed to accommodate a variety of sampling-rates is a multirate sampled-data system.

(ii) Data amplitude quantisation is a feature that distinguishes modern digital computer control systems from the classical sampled-data system. In terms of a given characteristic frequency, the minimum practical sampling-rate is defined by a

multiple (at least eight as defined in Fig 3.2) of the Nyquist rate. The effect of a quantisation process, is the imposition of a maximum limit to the sampling-rate. High dynamical order DFC systems, have several characteristic frequencies which are distributed over a wide spectrum. The consequence of a minimum sampling-rate (imposed by the Sampling Theorem) and maximum sampling-rate for each characteristic frequency is a DFC system with a multirate sampling policy.

The multirate sampling policy selection procedure, described in Chapter Three, is based specifically on the issues associated with the above item (ii). The selection procedure, which produces a multirate sampling policy, represents an interpretation of the basic aircraft's open-loop state covariance. The method gives an indication of intersample uncertainty on each state element of a multivariable system. A multirate sampling policy, which includes both state measurement and control-actuation sampling operations, is directly deduced from the variance time-history characteristic of each state element. The facility of the state covariance time history, in identifying a multirate sampling policy, establishes the technique as an appropriate procedure for the DFC design methodology. In association with z-plane pole-zero maps of the basic aircraft transfer-functions and the guidelines provided by the standard flight control design requirements, the sampling policy selection procedure offers a quantitative approach to this particular design task.

Preliminary studies revealed that the established multirate sampled-data system models are unsuitable for the objectives of the DFC system design methodology. An alternative formulation of a multirate sampled-data model, which addresses the requirements of the thesis, is described in Section 3.2. The assembly of a basic aircraft model for the purpose of DFC system design requires considerable assiduity if errors are to be avoided. It is believed that the assembly of the proposed multirate sampled-data model facilitates the goal of an error free DFC design.

The established multirate sampled-data system models are grouped into two basic forms. The first group comprises the z-plane transfer-function forms, developed by Sklansky [6.1] and Kranc [6.2] and the second group are the state-space, time-domain forms, which are epitomised by the Kalman and Bertram model [6.3]. Of these two established forms, the state-space model of Kalman and Bertram is the most suited to the requirements of the multivariable aircraft flight control system objectives of the thesis. However, an application study, described in a supplementary report, demonstrates that, although straight forward in principle, in practice the Kalman and Bertram model is complex and difficult to manage. While not explicitly discussed by Kalman and Bertram, it is considered that their model is directed towards multirate sampled-data system simulation, where it is intended to exercise a known digital controller configuration.

The multirate sampled-data system model developed for this thesis is assembled by inspection. The model is initially produced for the

equivalent, open-loop discrete-time system of the basic aircraft. A multirate structure of a digital feedback controller can also be defined and applied to the open-loop model using standard state-space matrix algebra. Two closely related forms of the model are described; one casts the multirate structure into the controls vector, and the other takes explicit account of the multirate sampling switch and ZOH functions by casting them as augmentation states to the basic open-loop model. The additional dynamics generated by a delay in computing the control data from the state data is easily accommodated by incorporating a delay operator at the input section of the plant model.

Although the w-plane and, in particular, the w'-plane are already established as suitable domains for unirate DFC system design, their potential has not been realised in the design of practical flight control systems. The major constraint on the practical application of both w planes is removed by the CADT state-space to w- and w'-plane transformation algorithms, described in Chapter Four. Both w domains are employed in the multirate sampled-data DFC design case study. Although of limited scope, the study demonstrates the utility of the w domain, for the design of a DFC system, which is bounded in a framework of a standard analogue flight control specification, namely MIL-F-8785C. In addition this study also indicates possible design techniques which will harmonise a DFC system implementation with the general requirements of MIL-F-8785C.

The CADT domain parameters, developed in Section 4.3, are presented as alternatives to the more commonly defined s-plane to z-plane

mappings. The main reason for developing these alternatives is to give a more natural image of the direct digital design performance measures. The two parameter root-locus gives a convenient, simultaneous parametric view of the sampling and gain changes. A reasonable presentation of a system's dynamics under multirate sampling policy is a feature of the two parameter root-locus.

The computational tasks of this thesis are undertaken in a MATLAB [6.4] computer aided design environment. The MATLAB package provides excellent facilities for processing the multirate sampled data model, and the algorithms for mapping between the time, z-plane w-plane and w'-plane. The simulation exercises of Chapter Five are are also the product of MATLAB processing. The collection of MATLAB subprograms combine to form a multirate sampled-data system design "toolbox".

6.2 TOPICS FOR FURTHER RESEARCH

The specification of piloted aircraft handling qualities, given in MIL-F-8785C is supported by a User Guide handbook [6.5]. The current version of this handbook gives no consideration to the digital-data implementation of flight control systems. The DFC design methods, described in this dissertation, could form the basis of a DFC supplement to the User Guide handbook.

By extending the transfer-function forms of aircraft handling qualities criteria to the state elements, a direct relationship

between the handling qualities requirements and the sampling policy could be established. The described method of selecting a multirate sampling policy is based on an assessment of the time history of state uncertainty. However, it may be more appropriate to consider the time rate-of-change of these state uncertainties.

A detailed study of the continuous-time state-space control system design techniques is required in the context of both the w- and w'-planes. A particular method, which has potential for directly synthesizing control laws that meet the aircraft handling qualities requirements specified by MIL-F-8785C, is Solheim's optimal pole placement technique [6.6].

The problems caused by amplitude quantisation require further study. The DFC methodology implicitly addresses the quantisation issue through the multirate sampling-policy approach. However, the methodology requires a practical technique for extending the design model to the DADT and DACT domains. A possible vehicle for this research task is the multirate sampled-data state-space model. The interference effects of multirate sampling are exposed on the time histories, as shown in the case study of Chapter Five.

The question of modelling the noise processes, both continuous and discrete, in mixed-data systems is still, largely, unanswered. It is felt that the current approach to the problem is based on a procedure which has become respectable through popular use, because it provides a quantitative design measure. As aircraft develop, an increased reliance is placed on active flight control systems to

maintain the structural integrity of the airframe and handling-quality requirements. For these aircraft developments, a better understanding of the nature of stochastic disturbances in digital flight control systems is required.

A multirate, sampled-data DFC system, incorporating all the flight control functions, and a redundant system architecture, has an implicit parallel structure. As such, the multirate DFC system is well placed to address the current developments in parallel processing DFC systems [6.7]. The methods described in this dissertation should be investigated for their application in the design of parallel computing DFC implementations.

For the practitioner, the only credible test of any engineering design, analysis, and implementation method is in its application in an engineering environment. The DFC design methodology proposed in this dissertation should be exercised in a practical environment to establish its utility as a general DFC system design technique. The resulting DFC systems will also require flight tests, to determine if the methodology avoids the deficiencies of the current digital flight control implementations, cited in Chapter One.

APPENDIX ONE

A BASIC AIRCRAFT MODEL FOR DFC DESIGN

A1.1 INTRODUCTION

This appendix gives details of a systematic method of organising the basic aircraft system into an analogue-data state-space model. In principle, once the states have been defined, the assembly of a state-space model is easily accomplished. In practice, the construction of a state-space model for a large complex aircraft system requires careful organisation. A model assembly, in which irregularities can be readily observed, facilitates the goal of an error free, flight control design, and thus accommodates the design methodology maxims prescribed in the thesis.

A1.2 A METHOD OF ASSEMBLING THE BASIC AIRCRAFT MODEL

The proposed method of assembling the state-space aircraft model approaches the task from the perspective of the flight control system design practitioner [A1.1]. In practice, the information required to model the total aircraft is produced from a variety of sources and is cast in a variety of different forms.

The complete, basic aircraft model consists of four subsystem groups. These are the actuators group, the sensors group, the

inceptors group and the vehicle group. The vehicle group is subdivided into rigid body dynamics and structural dynamics. An illustration of this arrangement is given in Fig.2.1 of Chapter Two. The development of the basic aircraft model starts with the non-linear, time-varying equations of the four subsystem groups. The first task is to combine the equations of the four subsystem models. The most convenient domain for modelling the Continuous-Amplitude, Continuous-Time (CACT) subsystem dynamics is the time-domain state-space. In practice, the vehicle system is naturally assembled as a collection of first and higher order differential equations. The high order equations are reduced to an equivalent set of first order equations.

The models, representing the dynamics of the actuators, sensors and inceptors are generally produced in a variety of forms. A typical representation is the single-input, single-output s-plane transfer-function. Of all the typical models, the transfer-function model requires the most effort to convert it to the common form. This is particularly true if the resulting independent variables are to be cast in terms of the physical coordinates [A1.2]. Standard methods are available for mapping state variables from one coordinate frame to another [A1.3].

In Section 2 of Chapter Two, three groups of non-linear time-varying equations are defined. These equations, repeated below as (A1.1a), (A1.1b) and (A1.1c), are described as the basic aircraft model.

$$\dot{\mathbf{x}}(t) = f(\dot{\mathbf{x}}(t),\mathbf{x}(t),\mathbf{u}(t),\mathbf{y}(t),t) \qquad \text{(A1.1a)}$$

$$\mathbf{y}(t) = g(\dot{\mathbf{x}}(t),\mathbf{x}(t),\mathbf{u}(t),\mathbf{y}(t),t) \qquad \text{(A1.1b)}$$

$$\mathbf{a}(t) = h(\dot{\mathbf{x}}(t),\mathbf{x}(t),\mathbf{u}(t),\mathbf{y}(t),t). \qquad \text{(A1.1c)}$$

The dimensions of the components in these equations are defined as follows: $\mathbf{x}(t)$ is a vector of m time dependent state functions, $\mathbf{u}(t)$ is a vector of q time dependent input functions and $\mathbf{y}(t)$ is a vector of p time dependent output functions. The functions f , g and h are non-linear. The linearising process is based on the equilibrium-condition, small-perturbation procedure [A1.4]. The equilibrium-condition also establishes time-invariance. The utility of the subsystem method is improved by explicitly including differential states, $\dot{\mathbf{x}}(t)$, in the right hand side functions. This feature is is discussed in more detail in the next section. The linearised equations are described in Section 2 of Chapter Two and are repeated below as equations (A1.2a), (A1.2b) and (A1.2c).

$$\dot{\mathbf{x}}(t) = \mathbf{F}_{\dot{\mathbf{x}}}\,\dot{\mathbf{x}}(t) + \mathbf{F}_{\mathbf{x}}\,\mathbf{x}(t) + \mathbf{F}_{\mathbf{y}}\,\mathbf{y}(t) + \mathbf{F}_{\mathbf{u}}\,\mathbf{u}(t) \qquad \text{(A1.2a)}$$

$$\mathbf{y}(t) = \mathbf{G}_{\dot{\mathbf{x}}}\,\dot{\mathbf{x}}(t) + \mathbf{G}_{\mathbf{x}}\,\mathbf{x}(t) + \mathbf{G}_{\mathbf{y}}\,\mathbf{y}(t) + \mathbf{G}_{\mathbf{u}}\,\mathbf{u}(t) \qquad \text{(A1.2b)}$$

$$\mathbf{a}(t) = \mathbf{H}_{\dot{\mathbf{x}}}\,\dot{\mathbf{x}}(t) + \mathbf{H}_{\mathbf{x}}\,\mathbf{x}(t) + \mathbf{H}_{\mathbf{y}}\,\mathbf{y}(t) + \mathbf{H}_{\mathbf{u}}\,\mathbf{u}(t). \qquad \text{(A1.2c)}$$

The subsystem form of block diagram model, which the above equations represent, is shown in Fig.A1.2. The diagram demonstrates the purpose of the interconnection equation (A1.2c).

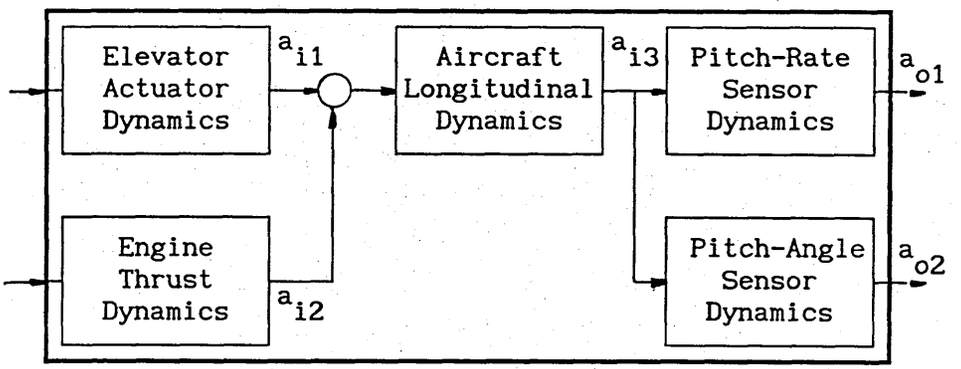

A subsystem block diagram, showing the elements of the internal and external system interconnection vector **a**

Fig.A1.1

A standard form of the linear, time-invariant, state-space model is given in Section 2 of Chapter Two by equations (2.3a) and (2.3b). These equations are repeated below as (A1.3a) and (A1.3b) respectively,

$$\dot{\mathbf{x}}(t) = \mathbf{A}\,\mathbf{x}(t) + \mathbf{B}\,\mathbf{u}(t) \qquad \text{(A1.3a)}$$

$$\mathbf{y}(t) = \mathbf{C}\,\mathbf{x}(t) + \mathbf{D}\,\mathbf{u}(t). \qquad \text{(A1.3b)}$$

The basic aircraft model of the digital flight control design methodology proposed for the thesis is cast in the form of equations (A1.3a) and (A1.3b). The equations, (A1.2a), (A1.2b) and (A1.2c), which are produced from the model assembly exercise, must be reformed into the state-space pair of (A1.3a) and (A1.3b). Rearranging equations (A1.2a) and (A1.2b) gives

$$[I - F_{\dot{x}}]\,\dot{x}(t) = F_x\,x(t) + F_y\,y(t) + F_u u(t) \qquad \text{(A1.4)}$$

$$[I - G_y]\,y(t) = G_{\dot{x}}\,\dot{x}(t) + G_x\,x(t) + G_u u(t) \quad . \qquad \text{(A1.5)}$$

By defining the two vectors

$$\begin{bmatrix} \dot{x}(t) \\ y(t) \end{bmatrix} \quad \text{and} \quad \begin{bmatrix} x(t) \\ u(t) \end{bmatrix} ,$$

equations (A1.4) and (A1.5) can be expressed as the matrix equation

$$\begin{bmatrix} I-F_{\dot{x}} & -F_y \\ -G_{\dot{x}} & I-G_y \end{bmatrix}\begin{bmatrix} \dot{x}(t) \\ y(t) \end{bmatrix} = \begin{bmatrix} F_x & F_u \\ G_x & G_u \end{bmatrix}\begin{bmatrix} x(t) \\ u(t) \end{bmatrix} \quad . \qquad \text{(A1.6)}$$

Rearranging equation (A1.6) gives

$$\begin{bmatrix} \dot{x}(t) \\ y(t) \end{bmatrix} = \begin{bmatrix} I-F_{\dot{x}} & -F_y \\ -G_{\dot{x}} & I-G_y \end{bmatrix}^{-1}\begin{bmatrix} F_x & F_u \\ G_x & G_u \end{bmatrix}\begin{bmatrix} x(t) \\ u(t) \end{bmatrix} \quad . \qquad \text{(A1.6)}$$

Evaluating the inverse, then multiplying out the matrix and vector terms produces the standard CACT matrix quadruple (A,B,C,D).

The interconnection vector is defined by substituting equation (A1.6) into (A1.2c) to give

$$a(t) = \left[[H_{\dot{x}}\ H_y] \begin{bmatrix} I - F_{\dot{x}} & -F_y \\ -G_{\dot{x}} & I - G_y \end{bmatrix}^{-1} \begin{bmatrix} F_x & F_u \\ G_x & G_u \end{bmatrix} + [H_x\ H_y] \right] \begin{bmatrix} x(t) \\ u(t) \end{bmatrix} \quad . \qquad \text{(A1.7)}$$

A1.3 REASONS FOR THE PROPOSED MODELLING METHOD

At first sight, it would appear that including a state differential term in the right-hand-side of the basic equations produces an unduly complicated method of model assembly. The utility of the technique is apparent, as a general method, by considering the incremental assembly of a complex system. This approach is typical of the standard methods of flight control system design [A1.5]. As an example, consider the block diagram model of an aircraft's longitudinal dynamics, shown in Fig.A1.2. This form of presentation of aircraft dynamics is used extensively in flight control systems work.

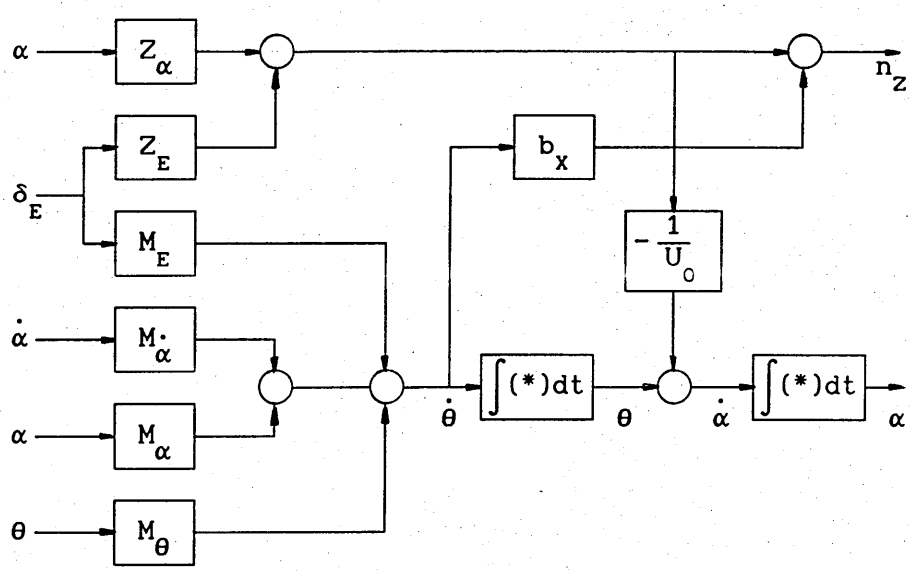

A partial diagram of an aircraft's longitudinal dynamics

Fig.A1.2

When states and state derivatives appear in a subsystem model as open loop inputs, as shown in the model of Fig.A1.2, then the procedure developed in this appendix provides a systematic method of assembling the state-space quadruple. This procedure accommodates the piecemeal assembly of a basic aircraft model, which is a typical approach to modern flight control system design. A common feature in flight system dynamics is the occurrence of an algebraic loop. Algebraic loops are formed as natural processes, as, for example, in the case of a missile guidance system [A1.6], or they can be deliberately introduced as a control law, as in the case of a washout function (a practical implementation of a differentiation function) [A1.7]. The assembly of a model which includes an algebraic loop is a systematic process for the method outlined above.

A1.4 A CADT MAPPING METHOD FOR RANK DEFICIENT SYSTEMS

The production of a rank deficient state matrix is caused by CACT domain dynamics that have the characteristics of open-loop integrators. The presence of an open-loop integrator, at the input of a system, is identified by a row of zeros in the state matrix, **A**. If the integrator is at the output then a column of zeros is produced in the state matrix. From basic matrix theory, a square matrix with a column or row of zeros is rank deficient and is therefore noninvertable. In the case of an open-loop integrator enclosed within a system, the determinant is once again zero but, unlike system's with an input or output integrator element, this

fact is not revealed by either a row or column of zeros in the **A** matrix. A technique that circumvents the singular matrix problem, and allows a CACT to CADT mapping without the need to solve the integral (2.15), is given below.

Consider the standard form of a state-space system model with an open-loop integrator at the output and a set of zero input augmentation states, as shown by the diagram of Fig.A1.3.

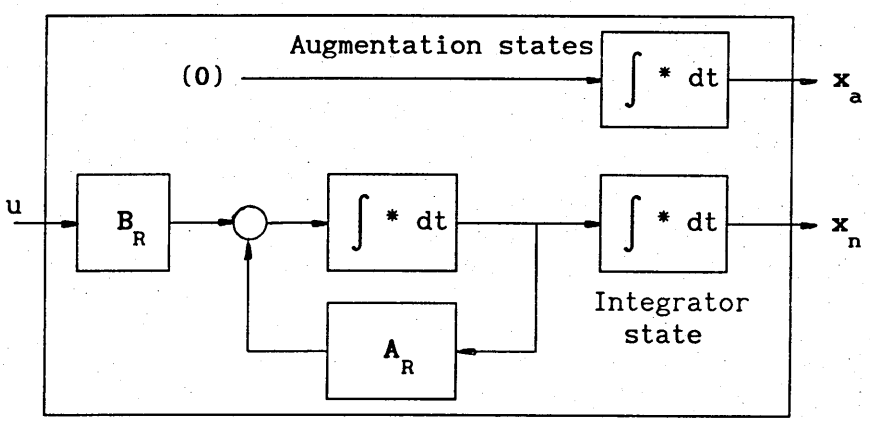

Standard form of a CACT system incorporating an integrator element

Fig.A1.3.

From Chapter Two, the state equation deduced from the model of Fig.A1.3. is given by

$$\dot{\mathbf{x}}(t) = \mathbf{A}\,\mathbf{x}(t) + \mathbf{B}\,\mathbf{u}(t). \qquad (2.3a)$$

For this system, assume $\mathbf{x}_n$ to be an m×1 state vector, with the nth element defined as the state open-loop integrator. The m×m state matrix, **A**, is partitioned into the form

$$\mathbf{A} = \left[\begin{array}{c|c} \mathbf{A}_R & \mathbf{0} \\ \hline \mathbf{0} \;\vdots\; 1 & \mathbf{0} \end{array}\right] \tag{A1.8}$$

where $\mathbf{A}_R$ is an (m-1)×(m-1) matrix and hence the dimensions of the zero sub-matrix in the last row is 1×(m-2). The n×q input matrix, **B**, is, in turn, partitioned into

$$\mathbf{B} = \begin{bmatrix} \mathbf{B}_R \\ \mathbf{0} \end{bmatrix} , \tag{A1.9}$$

where $\mathbf{B}_R$ has the dimensions (m-1)×q and the zero sub-matrix has the dimensions 1×q. The next step is to define an augmented state vector

$$\mathbf{x}_A = \begin{bmatrix} \mathbf{x} \\ \mathbf{x}_a \end{bmatrix} . \tag{A1.10}$$

The number of augmentation states is defined by the number of inputs q. The objective is to generate a (m+q)×(m+q) square matrix, $\mathbf{A}_a$, where

$$\mathbf{A}_a = \begin{bmatrix} \mathbf{A} & \mathbf{B} \\ \mathbf{0} & \mathbf{0} \end{bmatrix} . \tag{A1.11}$$

Evaluating the matrix function

$$\exp(\mathbf{A}_a h) = \exp\begin{bmatrix} \mathbf{A}h & \mathbf{B}h \\ \mathbf{0} & \mathbf{0} \end{bmatrix} \tag{A1.12}$$

gives

$$\exp(\mathbf{A}_a h) = \begin{bmatrix} \Phi & \Psi \\ \mathbf{0} & \mathbf{I} \end{bmatrix} . \qquad \text{(A1.13)}$$

where Φ and Ψ are equal to the expressions given in Chapter Two by equations (2.14) and (2.15), respectively. The method is also applicable to systems with non-synchronous sampling by replacing h with the output delay parameter, Δ, to yield Φ_Δ and Ψ_Δ in place of Φ and Ψ, respectively.

Proof of this result is obtained by recasting the state equation as a diagonal state matrix. The diagonalised state matrix and transformed **B** matrix are scaled by the sampling period, h, and substituted into equation (A2.12). The exponential matrix function is evaluated and compared with the Φ and Ψ matrices which are obtained by the direct application of equations (2.14) to (2.17).

A1.5 SUMMARY

This appendix describes a systematic method of assembling the CACT state-space quadruple for the purpose of the digital flight control system design methodology proposed in this dissertation. The method facilitates the model construction from subsystems in which state variables and derivatives of the state variables appear as inputs. The assembly of the basic aircraft's subsystem model is readily automated in a matrix manipulation, computer-aided-design environment. A technique to map a rank deficient CACT state matrix to the CADT domain, which avoids the need to solve a matrix integral, has also been exposed.

APPENDIX TWO

A STUDY OF DIGITAL DESIGN METHODS

A2.1 INTRODUCTION

The fundamental proposition of this thesis is that the design and analysis of a DFC system should be carried out in the CADT domain. In making this assertion, it is recognised that successful digital control systems have been designed through emulation and pseudo continuous methods by assuming high sampling-rates. However, the thesis proposes the direct digital design of DFC systems for the following reason. A claim, often made, is that a given control specification can be achieved at lower sampling-rate if it is designed in the CADT domain [A2.1]. This claim is widely asserted in the digital control literature but given without clear justification. This appendix presents a compelling argument that supports the "lower sampling-rate" claim of the direct digital design method.

The argument for direct-digital-design is made through a specific case study. Before the case study is considered, a general scheme for comparing the various digital control design methods is described in the next section.

A2.2 A COMPARISON OF DIGITAL SYSTEM DESIGN METHODS

Consider the mixed-data model shown below in Fig.A2.1. This model represents the generic arrangement of the basic aircraft and its DFC system. The flight control signals from the digital controller are coupled into the basic aircraft via a digital-to-analogue converter (DAC). An analogue-to-digital converter (ADC) forms part of the feedback-loop from the continuous-time system output to the digital controller input. The feedback-loop element, H_C, is implemented in the form of a program in the digital control computer.

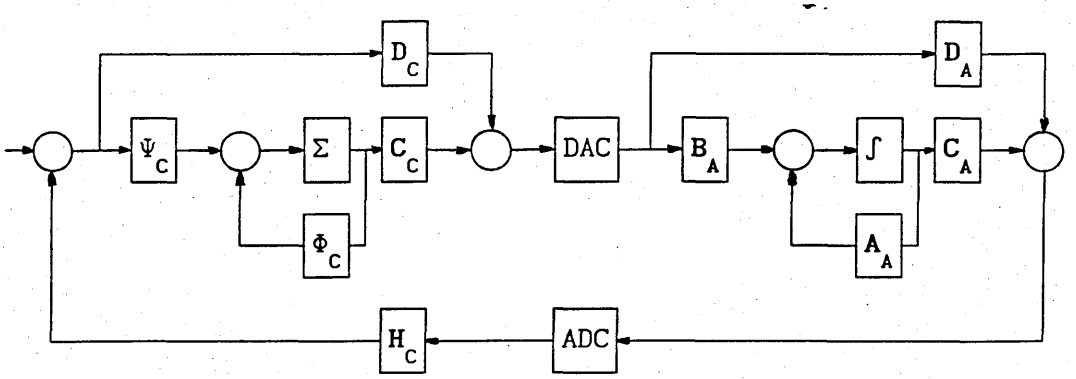

A general CACT system with digital control and output feedback

Fig.A2.1

The state-space equation for the system of Fig.A2.1, with the analogue-data elements recast in their equivalent discrete-time form, is given by

$$\begin{bmatrix} \mathbf{x}_A(n+1) \\ \mathbf{x}_C(n+1) \end{bmatrix} = \begin{bmatrix} \Phi_A - \Psi_A M^{-1} D_C H_C C_A & \Psi_A M^{-1} C_C \\ -\Psi_C N^{-1} H_C C_A & \Phi_C - \Psi_C N^{-1} H_C D_A C_C \end{bmatrix} \begin{bmatrix} \mathbf{x}_A(n) \\ \mathbf{x}_C(n) \end{bmatrix} + \begin{bmatrix} \Psi_A M^{-1} D_C \\ \Psi_C N^{-1} \end{bmatrix} \mathbf{v}(n), \tag{A2.1}$$

where $M = [I + D_C H_C D_A]$ and $N = [I + H_C D_A D_C]$.

The CACT elements, $\mathbf{A}_A$ and $\mathbf{B}_A$, are mapped to their equivalent discrete-time functions, Φ_A and Ψ_A, respectively, where

$$\Phi_A = \exp(\mathbf{A}_A h) \tag{A2.2}$$

$$\Psi_A = \int_0^h \exp(\mathbf{A}_A \lambda)\, d\lambda\, \mathbf{B}_A \quad . \tag{A2.3}$$

Assuming the sampling instants of the ADC and DAC coincide, then the terms, $\mathbf{C}_A$ and $\mathbf{D}_A$, of the continuous-data output equation, are unchanged by the continuous to discrete mapping.

The general state-space expression, given by equation (A2.1), forms the basis of an experimental procedure to compare the performance of a digital controller, designed by emulation methods with a controller designed by the direct-digital method.

A2.2.1 Experiments to Compare Digital Design Methods

An experimental procedure, used to compare the most common methods of DFC design, is outlined in this section. The procedure starts with a CACT system to which feedback control must be added. The benchmark for the experiment is the simulated performance of the system with an analogue controller. The performance measures used to compare the systems of each design method are closed-loop stability margin and disturbance attenuation. Both measures are investigated by taking the sampling rate as the base parameter. The experimental procedure is outlined in the diagram Fig.A2.2.

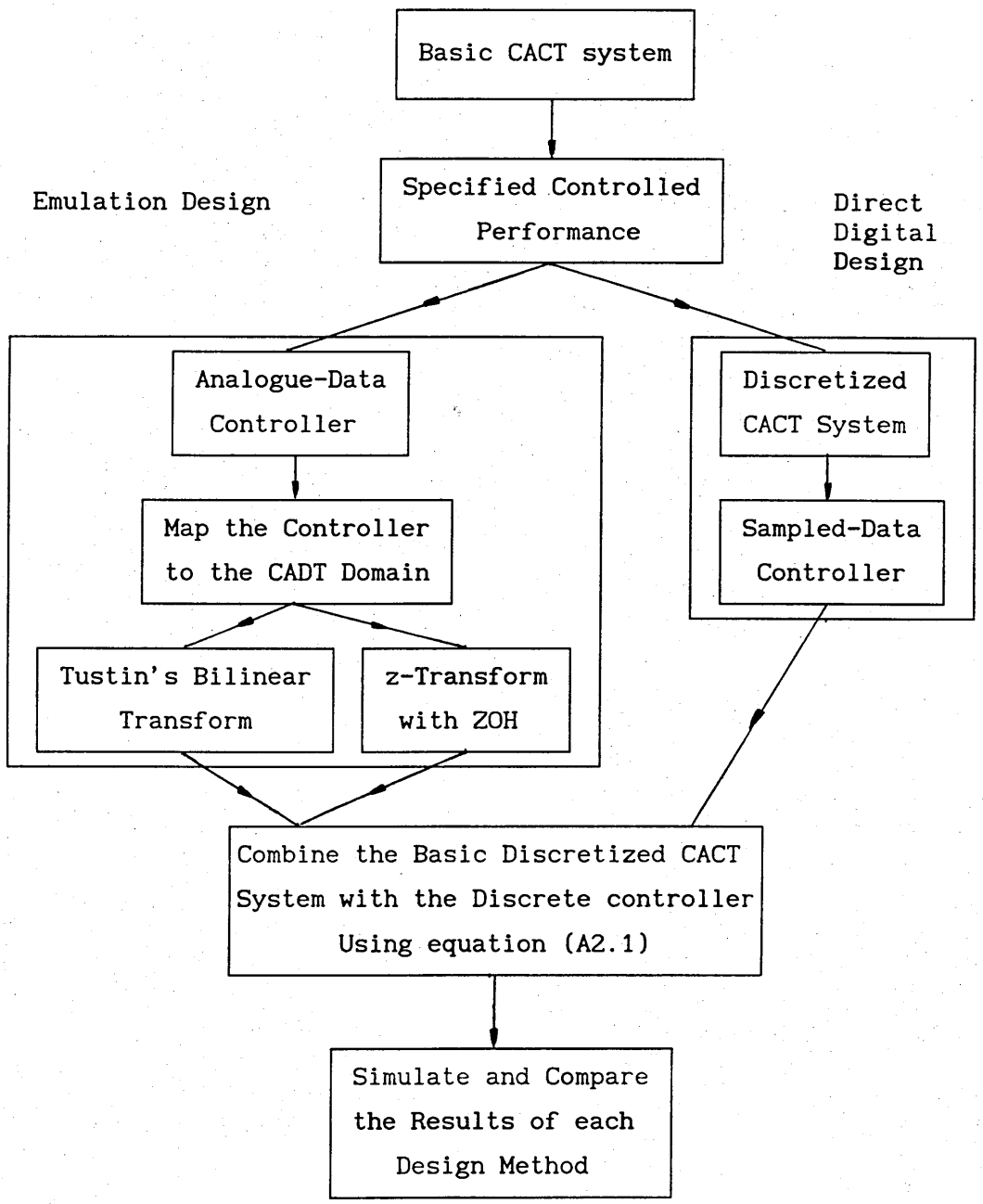

The procedure to compare the emulation design methods with the direct-digital-design method

Fig.A2.2

The experimental procedure, illustrated in Fig.A2.2, is exercised in the next section. Although trivial, the example exposes the lower sampling-rate advantage of the direct-digital-design method.

A2.3 THE EXPERIMENTS IN DIGITAL DESIGN METHODS

Consider a CACT system consisting of a simple integrator. In terms of the state-space quadruple, the matrices are cast as scalars and the values 0,1,1,0 are assumed for $\mathbf{A}_A, \mathbf{B}_A, \mathbf{C}_A$ and $\mathbf{D}_A$, respectively. A unity gain feedback controller is required to reduce the effects of a stochastic disturbance applied at the input of the CACT system. The stochastic disturbance is modelled as a white-noise source with zero-mean and standard deviation, σ. Further, the closed-loop dynamics are designed to have a damping ratio of 0.58. The analogue controller that meets the specification is given by

$$\dot{x}_2(t) = -x_2(t) + y(t). \qquad \text{(A2.4)}$$

The simple analogue system design produces the closed-loop model shown in Fig.A2.3.

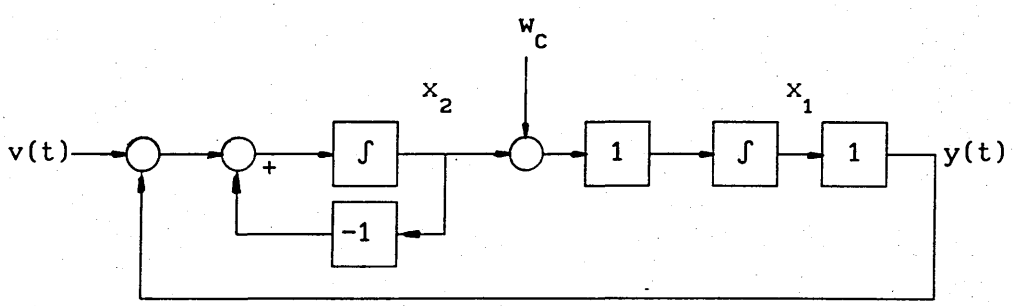

A closed-loop feedback and a dynamic controller

producing the specified damping ratio

Fig.A2.3

The state-space model for this system is given by

$$\begin{bmatrix} \dot{x}_1(t) \\ \dot{x}_2(t) \end{bmatrix} = \begin{bmatrix} 0 & 1 \\ -1 & -1 \end{bmatrix} \begin{bmatrix} x_1(t) \\ x_2(t) \end{bmatrix} + \begin{bmatrix} 0 \\ 1 \end{bmatrix} v(t) + \begin{bmatrix} 1 \\ 0 \end{bmatrix} w_c \qquad \text{(A2.5a)}$$

$$y(t) = x_1(t) \, . \qquad \text{(A2.5b)}$$

Using the analysis detailed in Appendix 5, the mean-square noise response at the output is given by (*c.f.* equation (A4.5))

$$G_c = \mathcal{E}\left(\begin{bmatrix} x_1(t) \\ x_2(t) \end{bmatrix} \begin{bmatrix} x_1(t) & x_2(t) \end{bmatrix} \right) = \begin{bmatrix} g_{11} & g_{12} \\ g_{21} & g_{22} \end{bmatrix} \, , \qquad \text{(A2.6)}$$

where $\mathcal{E}\left(\ * \ \right)$ is the expectation operator. A convenient form of the definition (A2.6) is to expand it as a Lyapunov equation, which is given by (*c.f.* equation (A4.6))

$$\begin{bmatrix} 0 & 1 \\ -1 & -1 \end{bmatrix} \begin{bmatrix} g_{11} & g_{12} \\ g_{21} & g_{22} \end{bmatrix} + \begin{bmatrix} g_{11} & g_{12} \\ g_{21} & g_{22} \end{bmatrix} \begin{bmatrix} 0 & -1 \\ 1 & -1 \end{bmatrix} + \begin{bmatrix} 1 \\ 0 \end{bmatrix} w_c^2 \begin{bmatrix} 1 & 0 \end{bmatrix} = [0] \, . \qquad \text{(A2.7)}$$

Solving equation (A2.7) for the four elements of G_c gives

$$g_{11} = w^2 \, , \quad g_{12} = -\frac{w^2}{2} = g_{21} \quad \text{and} \quad g_{22} = \frac{w^2}{2} \, .$$

The statistical response associated with the system output is therefore given by

$$Y_{CN} = C \, G_c C^T \, . \qquad \text{(A2.8)}$$

The next step is to embark on the design of the digital controller. Following the emulation procedure there, are two possible methods available. The first method is to form an equivalent discrete-data model of the analogue controller using Tustin's bilinear transform (equation 2.10). Substituting the parameters of the analogue controller, **A** =-1, **B** = 1, **C** = 1 and **D**= 0, into the Tustin transform gives

$$\Phi_T = \frac{1 - \frac{h}{2}}{1 + \frac{h}{2}} \qquad \text{(A2.9)}$$

$$\Psi_T = \left(\frac{h}{1 + \frac{h}{2}}\right)^2 \qquad \text{(A2.10)}$$

$$C_T = 1 \qquad \text{(A2.11)}$$

$$D_T = \left(\frac{\frac{h}{2}}{1 + \frac{h}{2}}\right) . \qquad \text{(A2.12)}$$

The alternative method for mapping the controller model to the CADT domain is by the z-transform with a ZOH. This mapping gives

$$\Phi_z = \exp(-h) \qquad \text{(A2.13)}$$

$$\Psi_z = 1 - \exp(-h) \qquad \text{(A2.14)}$$

$$C_z = 1 \qquad \text{(A2.15)}$$

$$D_z = 0. \qquad \text{(A2.16)}$$

With a sampling period h, the equivalent discrete-time system for the integrator is obtained by evaluating (*c.f.* equations (2.22) and (2.24))

$$\exp\left(\begin{bmatrix} 0 & h \\ 0 & 0 \end{bmatrix}\right) = \begin{bmatrix} 1 & h \\ 0 & 1 \end{bmatrix} = \left[\begin{array}{c|c} \Phi_A & \Psi_A \\ \hline 0 & 1 \end{array}\right].$$

Using equation (A2.1) to combine the equivalent discrete system model with the controller model produced by the Tustin transform, and omitting the disturbance input, gives the Tustin equivalent state equation as

$$\begin{bmatrix} x_A(n+1) \\ x_C(n+1) \end{bmatrix} = \left[\begin{array}{c|c} 1 - \dfrac{\frac{h^2}{2}}{\left(1 + \frac{h}{2}\right)} & \dfrac{h}{1 - \frac{\frac{h}{2}}{1 + \frac{h}{2}}} \\ \hline \dfrac{-h}{\left(1 + \frac{h}{2}\right)^2} & \end{array}\right] \begin{bmatrix} x_A(n) \\ x_C(n) \end{bmatrix} + \left[\begin{array}{c} \dfrac{\frac{h^2}{2}}{\left(1 + \frac{h}{2}\right)} \\ \hline \dfrac{h}{\left(1 + \frac{h}{2}\right)^2} \end{array}\right] v(n). \qquad \text{(A2.17)}$$

Applying the same procedure for the z-transform controller model gives

$$\begin{bmatrix} x_A(n+1) \\ x_C(n+1) \end{bmatrix} = \left[\begin{array}{c|c} 1 & h \\ \hline -(1-\exp(-h)) & \exp(-h) \end{array}\right] \begin{bmatrix} x_A(n) \\ x_C(n) \end{bmatrix} + \begin{bmatrix} 0 \\ 1-\exp(-h) \end{bmatrix} v(n) \quad . \quad \text{(A2.18)}$$

A2.3.1 Stability Measured Against Sampling Period

Computing the characteristic equation for both the Tustin derived, and z-transform derived, systems reveals the stability characteristic for a varying sampling-period, h. The sampling-period root-locus of the control system designed with the Tustin transform progresses out of the z-plane unit disc when the sampling-period exceeds two seconds. In the the case of the control system designed using the z-transform, the sampling-period root-locus leaves the unit disc when the sampling period exceeds one second.

The two stability test results, for the systems produced by the non-direct-digital-design methods, are compared with the stability of an equivalent controller, produced by the direct-digital-design method. For the purpose of comparison, the controller designed by the direct-digital method is specified to produce a system with closed-loop dynamics that are equivalent to the original CACT system given by equation (A2.5). The combined CADT domain sampled-data model of the basic CACT system and the proposed digital controller is assembled through equation (A2.18) to give

$$\begin{bmatrix} x_1(nh+h) \\ x_2(nh+h) \end{bmatrix} = \exp\left(\begin{bmatrix} 0 & 1 \\ -1 & -1 \end{bmatrix} h\right) \begin{bmatrix} x_1(nh) \\ x_2(nh) \end{bmatrix} + \int_0^h \exp\left(\begin{bmatrix} 0 & 1 \\ -1 & -1 \end{bmatrix} \lambda\right) d\lambda \begin{bmatrix} 0 \\ 1 \end{bmatrix} v(t) \ . \tag{A2.19}$$

From equation (A2.19), the z-plane transfer function is computed for increasing values of h. The sampling-period z-plane root-locus remains within the unit circle for all values of h. The

sampling-period root-locus diagrams shown in Fig.A2.4 give an obvious comparison of the three design methods in terms of the system stability.

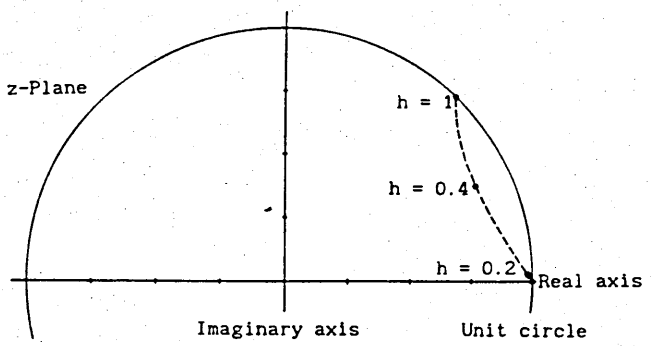

Emulation Design via z Transforms

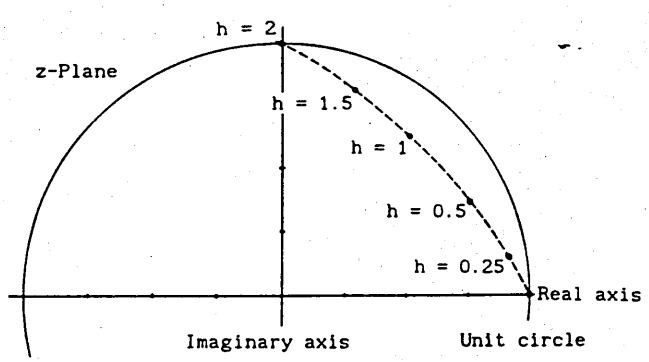

Emulation Design via the Tustin Bilinear Transform

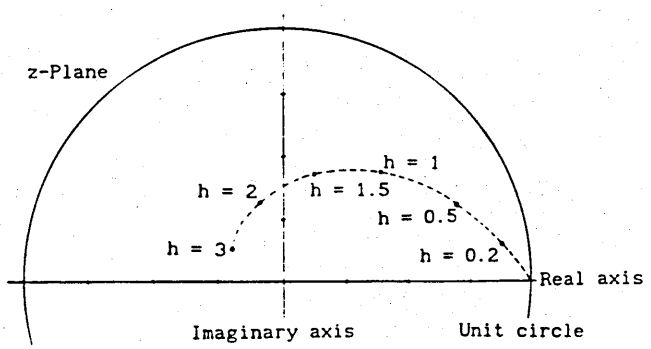

Direct Digital Design

The sampling-rate z-plane root-locus diagrams of equivalent digital control systems designed by the direct method and emulation methods

Fig.A2.4

A2.3.2 Disturbance Measured Against Sampling Period

Consider a discrete system, which has a state matrix, Φ, and a controls matrix, Ψ. If the system is excited by a white noise signal, it is shown in Appendix Four that the covariance matrix, $\mathbf{G}_d$, is given by (*c.f.* equation (A4.11))

$$\mathbf{G}_d = \Phi \mathbf{G}_d \Phi^T + \mathbf{Q}_d \quad , \tag{A2.20}$$

where

$$\mathbf{Q}_d = \int_0^h \exp(\mathbf{A}_A \lambda) w_C(\lambda)\, d\lambda \quad . \tag{A2.21}$$

In this example $\mathbf{A}_A = 0$, then $\mathbf{Q}_d$ is given by

$$\mathbf{Q}_d = \begin{bmatrix} hw_C^2 & 0 \\ 0 & 0 \end{bmatrix} . \tag{A2.22}$$

The next task is to evaluate equation (A2.20) for the three design methods; that is, for the Tustin transform, the z-transform and the direct-digital-design method, where Φ is obtained from equations (A2.17), (A2.18) and (A2.19), respectively. In each case, the computation is repeated for different values of sampling period, h. Applying equation (A2.6) to these discrete-time results gives the sampled-data system output noise as

$$Y_{DN} = \mathbf{C}\, \mathbf{G}_d \mathbf{G}^T . \tag{A2.23}$$

The normalised noise response is defined as

$$Y_{NN} = 20 \log \left(\frac{Y_{DN}}{Y_{CN}} \right)^{\frac{1}{2}} \quad . \tag{A2.24}$$

For each design method, the result of equation (A2.24) is plotted against a base of sampling period, as shown in Fig.A2.5. The plotted results clearly illustrate that, to achieve a given noise performance, the emulation design methods require a higher sampling rate than the the direct-digital-design method. Differentiating equation (A2.22) with respect to h gives a measure of the noise sensitivity as a function of the sampling rate.

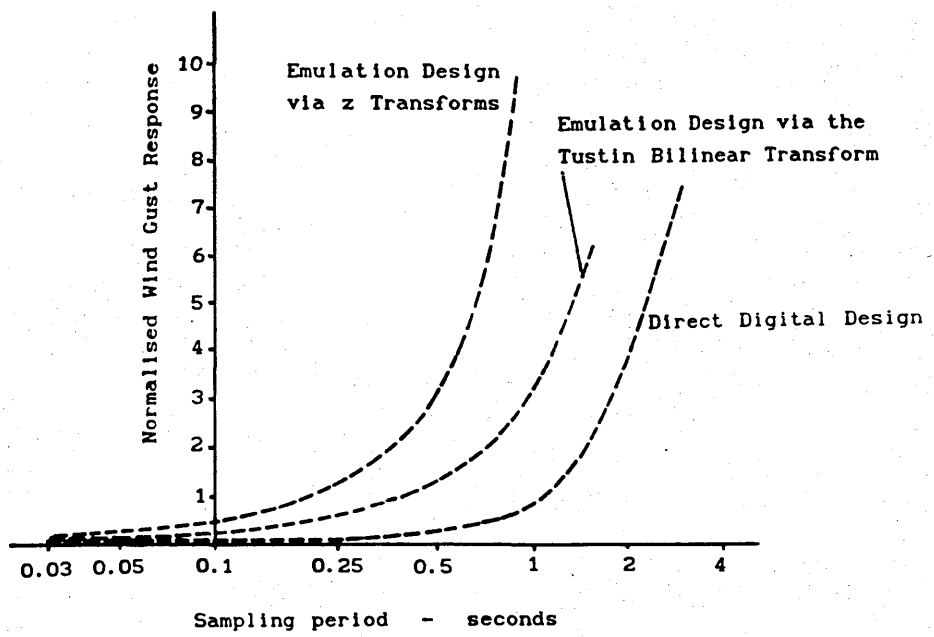

The normalised wind gust disturbance response of equivalent digital control systems designed by the direct method and emulation methods

Fig.A2.5

A2.4 SUMMARY

This appendix has offered an argument to support the method of direct-digital-design of a mixed-data control system. The argument is based on the results obtained from an analysis of a particular system configuration. The results, while exposing interesting comparisons, must be treated with caution when drawing general conclusions. The analysis technique is, however, general and can be extended to compare emulation and direct-digital-design methods for higher-order, mixed-data systems. The analysis, which produces the normalised gust response against sampling period, forms the basis of the sampling rate selection procedure employed in Chapter Three.

APPENDIX THREE

SAMPLING, QUANTISATION AND DATA RESOLUTION

A3.1 INTRODUCTION

This appendix presents an example to demonstrate the relationship that exists between the sampling-rate, the quantisation noise and the digital-data wordlength of a sampled-data, digitally controlled CACT system. The purpose of the example is to support the specific arguments of Chapter Three.

A3.2 THE PROBLEM STATEMENT

Consider the discrete-data model of a sampled-data system shown in Figure A3.1.

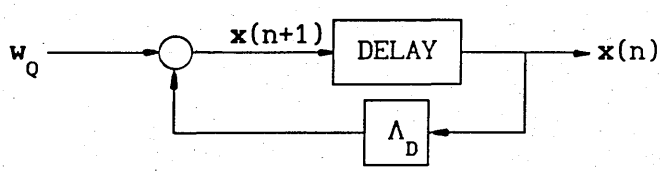

The discrete-data model for quantisation noise analysis

Fig.A3.1

Without loss of generality, it can be assumed that the discrete-data model is cast in the modal form, given by

$$\mathbf{x}(n+1) = \Lambda_D\, \mathbf{x}(n) + \mathbf{w}_Q \quad , \qquad (A3.1)$$

where Λ_D is a discrete, m×m, diagonal state-matrix, produced by mapping a CACT domain m×m diagonal matrix, Λ, by the function $\exp(\Lambda h)$. If the input function, $\mathbf{w}_Q$, is a white noise quantity representing the quantisation noise then, using the analysis developed in Appendix Four, the steady-state condition of the mean square quantisation error is given by

$$\mathbf{G}_{CS} = \exp(\Lambda h)\ \mathbf{G}_{CS}\ \exp(\Lambda^T h) + \mathbf{Q}_N \quad , \qquad (3.2)$$

where the matrix $\mathbf{G}_{CS}$ is the output noise covariance, with elements usually denoted as σ_X^2 and $\mathbf{Q}_N$, is an m×m diagonal matrix whose elements values represent the "strength" of the quantisation-noise.

A3.3 SAMPLING, QUANTISATION AND DATA RESOLUTION COMPROMISES

In the case of a mixed-data system, where the CACT to DADT domain interfaces are implemented with ADC and DAC devices, and the CACT domain data is represented as a W-bit digital-data vector, it can be shown, [A3.1], that the matrix $\mathbf{Q}_N = \left[\mathbf{I}\right]\frac{(2^{-W})^2}{12}$, where $\frac{(2^{-W})^2}{12} = \sigma_W^2$, and I is an m×m identity matrix. Substituting these two quantities into (A3.2) gives

$$\mathbf{I}\ \sigma_X^2 = \exp(\Lambda h)\ \sigma_X^2\ \exp(\Lambda^T h) + \mathbf{I}\ \sigma_W^2 \quad . \qquad (A3.3)$$

With the parameters of (A3.3) expressed in the modal form, the equation can be reformed as

$$\left[\exp(\Lambda h)\right]^2 \sigma_X^2 - \mathbf{I}\ \sigma_X^2 + \mathbf{I}\ \sigma_W^2 = 0 \quad . \qquad (A3.4)$$

If a noise amplification factor is defined as

$$\eta = \frac{\sigma_x}{\sigma_w} \quad , \tag{A3.5}$$

then equation (A3.4) can be reformed to give

$$\left[\exp(\Lambda h)\right]^2 = I - I\frac{1}{\eta^2} \quad . \tag{A3.6}$$

The purpose of the analysis is served by considering the particular case of a system with distinct eigenvalues. It is recalled that a system with distinct eigenvalues has a diagonal modal-form state-matrix, thus the states are uncoupled and the analysis can be performed on scalar equations. A single row of (A3.6) represents one dynamic mode and produces a scalar equation given by

$$\exp(\lambda h) = \sqrt{1 - \frac{1}{\eta^2}} \quad . \tag{A3.7}$$

Expanding the exponential function as a series and truncating the result after the first order term gives

$$1 + \lambda h \cong \sqrt{1 - \frac{1}{\eta^2}} \quad . \tag{A3.8}$$

Solving (A3.8) for h gives

$$h = \frac{1}{\lambda}\left(-1 \pm \sqrt{1 - \frac{1}{\eta^2}} \right) \quad . \tag{A3.9}$$

Since λ is a pole of the system, it is clear that if the noise amplification term is constant then, as the pole moves towards zero, h tends to infinity. For the purposes of selecting a sampling-rate,

it can be seen that, for a constant noise amplification, the sampling-period, h, must be increased as the pole location is reduced.

Expressing the noise amplification in terms of $\frac{(2^{-W})^2}{12}$ and σ_x leads to a relationship between sampling-rate, quantisation-noise and wordlength. Rearranging equation (A3.7) and substituting the quantisation-noise expression for σ_w gives

$$\frac{(2^{-W})^2}{12} = \sigma_x\left[1 - (1 + \lambda h)^2\right] \quad . \qquad \text{(A3.10)}$$

Solving (A3.10) for the word-length, W, gives

$$W = \frac{1}{\log(2)} \log\left\{ \frac{1}{\sqrt{12}\ \sigma_x \sqrt{(\lambda h)^2 + 2\lambda h}} \right\} \quad . \qquad \text{(A3.11)}$$

This expression indicates that, for a given level of output noise, σ_x, a reduction in the sample period will require an increase in the data-conversion process wordlength W. It is also clear that for a constant output noise level and sampling period, a decrease in the pole location must be matched by an increase in the data-conversion wordlength.

A3.4 SUMMARY

The analysis presented in this appendix exposes the relationship between sampling-rate and amplitude-quantisation, in terms of the data wordlength, and the effect they have on the noise level in a digital data system. The clear relationship, that higher

sampling-rates require higher data wordlengths in order to achieve a given quantisation, is a feature that distinguishes the modern concept of a sampled-data system from the classical sampled-data system.

APPENDIX FOUR

NOISE PROCESSES AND SAMPLED-DATA SYSTEMS

A4.1 INTRODUCTION

This appendix presents a method for including a continuous noise process in a sampled-data system model. In the context of an aircraft digital flight control system, the typical noise processes are the continuous air-turbulence disturbances impinging on the airframe and the amplitude quantisation noise which is an inherent feature of digital computer control. The sampled-data noise model is developed by progressing an argument from both the purely continuous and purely discrete noise model cases. The form of system implicitly considered in this appendix is the generic aircraft model illustrated in Fig.2.1 of Chapter 2.

A4.2 NOISE PROCESSES IN CONTINUOUS-TIME SYSTEMS

The basic system for which the continuous-time noise process is defined is shown in Fig.A4.1 and modelled by the state-equation

$$\dot{\mathbf{x}}(t) = \mathbf{A}\,\mathbf{x}(t) + \mathbf{B}_N \mathbf{w}_C(t), \qquad \text{(A4.1)}$$

where $\mathbf{x}(t)$ and $\mathbf{A}$ are interpreted in the usual deterministic system sense. The matrix $\mathbf{B}_N$ couples the white noise process $\mathbf{w}_C(t)$ into the

system state. For engineering purposes, equation (A4.1) is respectable; in a rigorous sense, it should be interpreted as a stochastic differential equation of the form

$$\mathbf{dx}(t) = \mathbf{A}\,\mathbf{x}(t)d(t) + \mathbf{B}_N d\beta(t), \qquad \text{(A4.2)}$$

where $\mathbf{dx}(t)$ and $d\beta(t)$ are differential operators of the state vector, $\mathbf{x}(t)$, and Brownian motion input vector, $\beta(t)$, respectively. Equation (A4.2) is the proper form because $\beta(t)=\int w(t)$ but $w(t) = d\beta(t)/dt$ does not exist [A4.1]. The purpose of this appendix is served without further reference to this interpretation.

In formal terms the properties of white noise are defined as

$$\mathcal{E}\left([w_C(t)]\right) = 0 \qquad \text{(A4.3)}$$

$$\mathcal{E}\left([w_C(t)][w_C(\tau)]^T\right) = Q_C\delta(t-\tau)\ , \qquad \text{(A4.4)}$$

where $\mathcal{E}\left(\ *\ \right)$ is the expectation operator and δ is the Dirac delta function. The covariance state matrix is defined as

$$G_C = \mathcal{E}\left([\mathbf{x}(t)][\mathbf{x}(t)]^T\right)\ . \qquad \text{(A4.5)}$$

In terms of the system parameters, the steady-state covariance matrix G_D is found by solving the equation

$$\mathbf{A}\,G_C + G_C\mathbf{A}^T + \mathbf{B}_N Q_C \mathbf{B}_N^T = 0. \qquad \text{(A4.6)}$$

The development of equation (A4.6) is a well documented process and is given in detail in [A4.1].

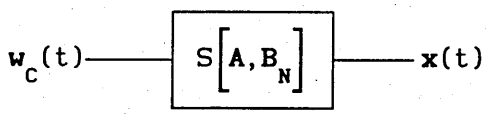

A continuous-time system driven by white noise

Fig.A4.1

A4.3 NOISE PROCESSES IN DISCRETE-TIME SYSTEMS

This section considers the definition of a model for the case of a discrete system being exercised by a discrete noise process. The arrangement for this case is shown in Fig.A4.2 and modelled by the discrete state-equation

$$\mathbf{x}(n+1) = \Phi\mathbf{x}(n) + \Psi_N \mathbf{w}_D(n). \qquad \text{(A4.7)}$$

The properties of the discrete noise data $\mathbf{w}_D$ are defined as

$$\mathcal{E}\left([w_D]\right) = 0 \qquad \text{(A4.8)}$$

$$\mathcal{E}\left([w_D]_i [w_D]_j^T\right) = Q_D \, \delta_{ij} \quad , \qquad \text{(A4.9)}$$

where $\mathcal{E}\left(\ * \ \right)$ is the expectation operator. The discrete state covariance matrix is defined as

$$G_D = \mathcal{E}\left([\mathbf{x}\,][\mathbf{x}\,]^T\right) \quad . \qquad \text{(A4.10)}$$

In terms of the discrete system parameters, the covariance matrix is expressed by the equation

$$G_D(n+1) = \Phi\, G_D(n)\Phi^T + \Psi_N Q_D \Psi_N^T. \qquad \text{(A4.11)}$$

Details of the development of equation (A4.11) are given in [A4.1]

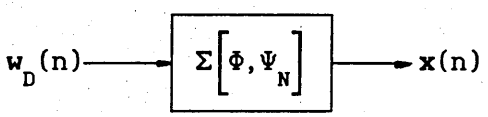

A discrete system driven by discrete noise

Fig.A4.2

A4.4 THE EQUIVALENT DISCRETE MODEL FOR A SAMPLED-DATA SYSTEM

The development of a practical design model of a sampled-data system, which includes continuous noise data sources as inputs to the analogue-data elements, is based on the approach employed to model deterministic systems. Although in a rigorous sense this approach is questionable, a convincing theory of noise processes in a mixed-data system appears not to have been developed. The basis of the generally accepted sampled-data noise model is a continuous system, S, embedded in a discrete system, Σ; the arrangement is shown in the diagram of Fig.A4.3. In this model, the process noise vector, $\mathbf{w}_c(t)$, and the measurement noise vector, $\mathbf{v}_c(t)$, are directly applied to the input and output of S, respectively. A continuous measurement noise, $\mathbf{v}_c(t)$, can be redefined as a sequence of discrete vectors and therefore becomes an input to the discrete system Σ. The continuous system output is sampled every h units of time, so the ADC clocking rate is given by $\frac{1}{h}$.

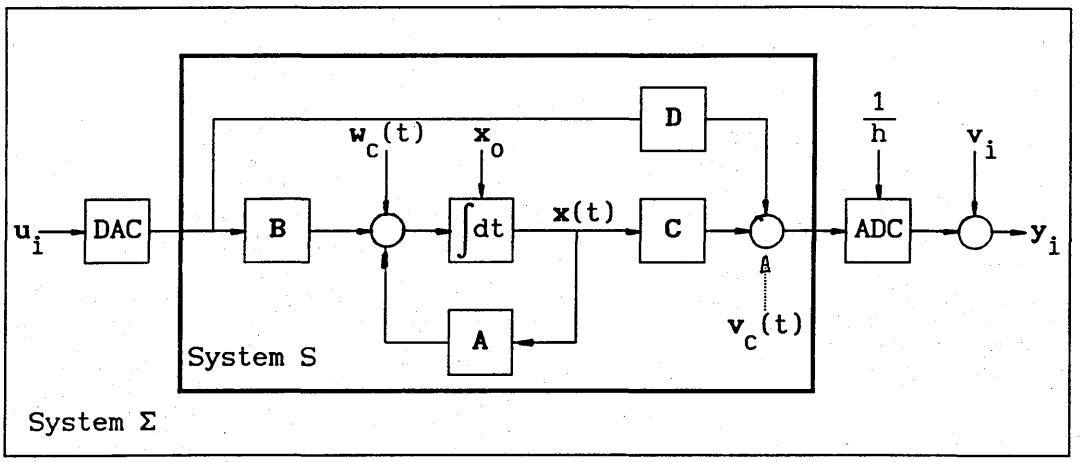

The definition model of the sampled-data stochastic system

Fig.A4.3

The process model, S, represents the basic CACT domain system and any augmentation states needed to make the process noise, $\mathbf{w}_c$, white. If the measurement noise, $\mathbf{v}_c$, occurs within S so that it is processed by the ADC then it is standard practice [A4.2] to calculate the statistics of the resulting noise sequence emerging from the ADC and call this sequence $\mathbf{v}_i$. If $\mathbf{v}_i$ is not white then augmentation is carried out on the equivalent discrete-time system.

A white measurement noise vector, $\mathbf{v}_c$, with a covariance defined as $\mathbf{R}_c\delta$ is applied to the input of the ADC. The resulting output sequence, $\mathbf{v}_i$, can be considered as white, [A4.3], with a covariance given by

$$\mathbf{R}_D = \frac{\mathbf{R}_c}{h}. \qquad \text{(A4.12)}$$

The physical interpretation of equation (A4.12) is obscure and this is one reason that the procedure described in the previous paragraph is adopted.

The equivalent CADT domain state-space model of the system illustrated in Fig.A4.3 is given by

$$\mathbf{x}(i+1) = \Phi\,\mathbf{x}(i) + \Psi\,\mathbf{u}(i) + \mathbf{w}_D(i) \qquad \text{(A4.13a)}$$

$$\mathbf{y}(i) = \mathbf{C}_D\mathbf{x}(i) + \mathbf{D}_D\mathbf{u}(i) + \mathbf{v}(i) \qquad \text{(A4.13b)}$$

On the assumption that the members of $\mathbf{u}_i$ arrive at the DAC at the same instant the ADC is clocked, then the quadruple terms of (A4.13) are given by

$$\Phi = \exp(\mathbf{A}h), \qquad \text{(A4.14)}$$

$$\Psi = \int_0^h \exp(\mathbf{A}\lambda)d\lambda\ \mathbf{B}, \qquad \text{(A4.15)}$$

$$\mathbf{C}_D = \mathbf{C}, \qquad \text{(A4.16)}$$

$$\mathbf{D}_D = \mathbf{D}. \qquad \text{(A4.17)}$$

The noise term $\mathbf{w}_D(i)$ is given by

$$\mathbf{w}_D(i) = \int_{(i-1)h}^{ih} \exp(\mathbf{A}\lambda)\ \mathbf{w}_D(\lambda)d\lambda. \qquad \text{(A4.18)}$$

The discrete process-noise covariance is defined by equation (A4.9). From (A4.18), it is deduced that

$$\mathbf{Q}_D = \int_0^h \exp(\mathbf{A}\lambda)\ \mathbf{Q}_C\exp(\mathbf{A}^T\lambda)\ d\lambda. \qquad \text{(A4.19)}$$

From (A4.19), it is observed that for a high sampling-rate, $\mathbf{Q}_D = h\mathbf{Q}_C$.

A4.4.1 The Covariance Matrix of Sampled-Data Noise

This section examines the effect that sampling has on a continuous system's output-data covariance. The basic model on which the analysis is carried out is shown in Fig.A4.4 as a subset of the system given above.

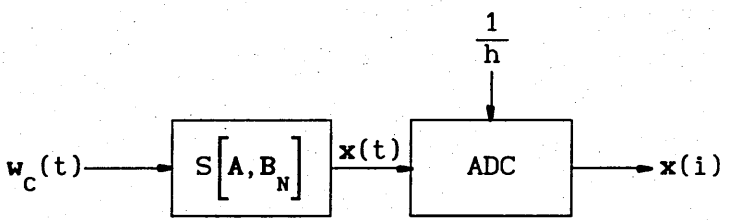

A continuous-time system driven by white noise and sampled by an ADC

Fig.A4.4

The objective is to find a mapping function for the continuous covariance matrix, G_C, given in (A4.6), that will generate an equivalent sampled-data covariance matrix, G_D, for the arrangement shown in Fig.A4.4.

For G_C to be finite, the state matrix **A** must have open, left-half-plane eigenvalues so that A^{-1} exists. The procedure to find the mapping between G_C and G_D starts with the solution of Q_D, where matrix Q_D is defined by (A4.19). The arrangement shown in Fig.A4.4 implies that the noise is also processed by the coupling matrix, B_N. The modification to Q_D, given by (A4.19), is easily deduced to account for this generalisation. The modified equation for Q_D is given by

$$Q_d = \int_0^h \exp(A\lambda)\ B_N Q_c\ B_N^T \exp(A^T\lambda)\ d\lambda. \qquad (A4.20)$$

Integrating (A4.20) by parts yields

$$\int_0^h \exp(A\lambda)\ B_N Q_C B_N^T \exp(A^T\lambda)\ d\lambda = \left[\left[\exp(A\lambda)\ B_N Q_C B_N^T\right]\ A^{-T}\exp(A^T\lambda)\right]_0^h - \int_0^h \left[A\ \exp(A\lambda)\ B_N Q_C B_N^T\right] A^{-T}\exp(A^T\lambda)\ d\lambda. \tag{A4.21}$$

Evaluating the limits of (A4.21) produces

$$Q_D = \left[\exp(Ah)\ B_N Q_C B_N^T \exp(A^T h) - B_N Q_C B_N^T - A\ Q_D\right] A^{-T}. \tag{A4.22}$$

Post-multiplying both sides of (A4.22) by A^T and rearranging to separate the terms Q_D and Q_C gives

$$A\ Q_D + Q_D A^T = \exp(Ah)\ B_N Q_C B_N^T \exp(A^T h) - B_N Q_C B_N^T . \tag{A4.23}$$

From the discrete system covariance (A4.11), Q_D is given as

$$Q_D = G_D - \Phi\ G_D \Phi^T \tag{A4.24}$$

and from (A4.14),

$$\Phi = \exp(Ah). \tag{A4.14}$$

Substituting (A4.14) and (A4.24) into (A4.23) gives

$$A\ G_D - A\ \exp(Ah)\ G_D\ \exp(A^T h) + G_D A^T - \exp(Ah)\ G_D\left(\exp(A^T h)\right)A^T = \exp(Ah)\ B_N Q_C B_N^T \exp(A^T h) - B_N Q_C B_N^T . \tag{A4 25}$$

Functions of the same matrix commute, therefore Aexp(Ah) and $\left(\exp(A^T h)\right)A^T$ terms can be recast as $\left(\exp(Ah)\right)A$ and $A^T\exp(A^T h)$,

respectively, to allow (A4.25) to be written as

$$\mathbf{A}\,\mathbf{G}_D + \mathbf{G}_D\mathbf{A}^T + \mathbf{B}_N\mathbf{Q}_C\mathbf{B}_N^T - \exp(\mathbf{A}h)\left[\mathbf{A}\,\mathbf{G}_D + \mathbf{G}_D\mathbf{A}^T + \mathbf{B}_N\mathbf{Q}_C\mathbf{B}_N^T\right]\exp(\mathbf{A}^T h) = \mathbf{0}. \tag{A4.26}$$

Given that exp(**A**h) has full rank and is not equal to a unit matrix I, it is seen that equation (A4.26) is satisfied if

$$\mathbf{A}\,\mathbf{G}_D + \mathbf{G}_D\mathbf{A}^T + \mathbf{B}_N\mathbf{Q}_C\mathbf{B}_N^T = \mathbf{0}. \tag{A4.27}$$

Comparing (A4.27) with (A4.6) gives the interesting result of

$$\mathbf{G}_D = \mathbf{G}_C. \tag{A4.28}$$

which implies that sampling does not change the covariance of **x**.

A4.5 SUMMARY

This appendix has outlined the development of an approach to map stochastic system parameters between the CACT and CADT domains under the operation of a ZOH sampled-data scheme. It should, however, be realised that only plausible arguments have been presented. A complete and definitive approach to the problem of stochastic modelling in aircraft DFC systems is not available and is the subject of current research [A4.4].

APPENDIX FIVE

MODELLING A MULTIRATE SAMPLED-DATA SYSTEM MODEL

A5.1 INTRODUCTION

This appendix gives an example to demonstrate the procedure, developed in Chapter Three, of assembling a multirate sampled-data system model. The example builds a state-feedback closed-loop model with a dual-rate sampling policy. The model and resulting multirate digital control system are compared to an identical system that is designed by the alternative method of Kalman and Bertram, which is described in detail in reference [A5.1].

A5.2 THE PROBLEM STATEMENT

Consider the system illustrated in Fig.A5.1, where both the CACT system's inputs and the digital feedback loops are partitioned for the application of a dual-rate sampling policy.

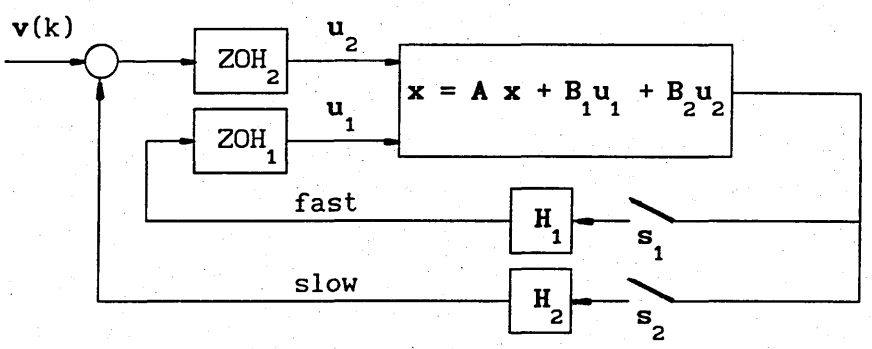

The model of a dual-rate sampled-data system with state-feedback

Fig.A5.1

The model of this dual-rate system is obtained directly by the methods described in Chapter Three. The sampling rates are selected for a policy of 2^{ρ}, where ρ is an integer. That is, from an iteration increment rate of, say, one time-unit, the next sampling rate is two time-units and the next is four time-units and so on.

A5.2.1 The Assembly of the Closed-Loop Sampled-Data Model

The state equation for the dual-rate system, with a sampling policy of $h_p = 2^{\rho}h_b$, is given by

$$\mathbf{x}(nh_p + h_p) = \left[\Phi_{\rho} \right] \mathbf{x}(nh_p) + \left[\Psi_{\rho} \right] \mathbf{v}_{\rho}(nh_p) \quad . \qquad (A5.1)$$

The state coefficient matrix is given by

$$\left[\Phi_\rho \right] = \Big[[\Phi + \Psi_1 H_1]^\rho + [\Phi + \Psi_1 H_1]^{\rho-1} \Psi_2 H_2 + \ldots .$$

$$\ldots + [\Phi + \Psi_1 H_1]^{\rho-2} \Psi_2 H_2 + [\Phi + \Psi_1 H_1] \Psi_2 H_2 + [I\ ] \Psi_2 H_2 \Big] \quad , \quad (A5.2)$$

and the inputs coefficient matrix is given by

$$\left[\Psi_\rho \right] = [\Phi + \Psi_1 H_1]^{\rho-1} \Psi_2 + [\Phi + \Psi_1 H_1]^{\rho-2} \Psi_2 + \ldots .$$

$$\ldots . + [\Phi + \Psi_1 H_1] \Psi_2 + [I\ ] \Psi_2 \quad . \quad (A5.3)$$

The matrix terms Φ , Ψ_1 and Ψ_2 have the usual interpretation under the assumption of a ZOH sampling process and are given by

$$\Phi = \exp(A h_1) \quad , \quad (A5.4)$$

$$\Psi_1 = \int_0^{h_1} \exp(A\lambda)\, d\lambda\, B_1 \quad , \quad (A5.5)$$

$$\Psi_2 = \int_0^{h_2} \exp(A\lambda)\, d\lambda\, B_2 \quad . \quad (A5.6)$$

In this final part of the example, the application of these equations is illustrated using the system introduced to demonstrate the modified Kalman and Bertram method given in [A5.1] For convenience, this system model is summarised in Fig.A5.2.

The continuous time system model

$$\begin{bmatrix} x_1(t) \\ x_2(t) \end{bmatrix} = \begin{bmatrix} 0 & 0 \\ 0 & -1 \end{bmatrix} \begin{bmatrix} x_1(t) \\ x_2(t) \end{bmatrix} + \begin{bmatrix} 1 \\ 0 \end{bmatrix} u_1(t) + \begin{bmatrix} 0 \\ 1 \end{bmatrix} u_2(t)$$

The sampling policy

Iteration Increments n			
n_b = 0	h_b	1	h_b 2
n_1 = 0	h_1	1	h_1 2
n_2 = 0	h_2		1
n_3 = 0	h_p		1

The feedback system

$$\begin{bmatrix} u_1 \\ u_2 \end{bmatrix} = \begin{bmatrix} 0 & H_2 \\ H_1 & 0 \end{bmatrix} \begin{bmatrix} x_1 \\ x_2 \end{bmatrix} + \begin{bmatrix} 1 \\ 0 \end{bmatrix} v(nh_1)$$

with $H_1 = -1$ and $H_2 = +1$

The sampled-data state equation

$$\begin{bmatrix} x_1(nh + h) \\ x_2(nh + h) \end{bmatrix} = \begin{bmatrix} 1 & 0 \\ 0 & \exp(-h) \end{bmatrix} \begin{bmatrix} x_1(nh) \\ x_2(nh) \end{bmatrix}$$

$$+ \begin{bmatrix} h & 0 \\ 0 & 1-\exp(-h) \end{bmatrix} \begin{bmatrix} 1 \\ 0 \end{bmatrix} u_1(nh) + \begin{bmatrix} h & 0 \\ 0 & 1-\exp(-h) \end{bmatrix} \begin{bmatrix} 0 \\ 1 \end{bmatrix} u_2(nh)$$

A summary of the multirate sampled-data system model from [A5.1]

Fig.A5.2

For the open-loop model, the equivalent discrete matrix terms of the CACT system are evaluated using equations (A5.4), (A5.5) and (A5.6), and are given by

$$\Phi = \begin{bmatrix} 1 & 0 \\ 0 & \exp(-h_1) \end{bmatrix} \tag{A5.7}$$

$$\Psi_1 = \begin{bmatrix} h_1 & 0 \\ 0 & 1-\exp(-h_1) \end{bmatrix} \begin{bmatrix} 1 \\ 0 \end{bmatrix} + \begin{bmatrix} h_1 \\ 0 \end{bmatrix} \tag{A5.8}$$

$$\Psi_2 = \begin{bmatrix} h_1 & 0 \\ 0 & 1-\exp(-h_1) \end{bmatrix} \begin{bmatrix} 0 \\ 1 \end{bmatrix} + \begin{bmatrix} 0 \\ 1-\exp(-h_1) \end{bmatrix} \tag{A5.9}$$

The state feedback matrices are given as

$$H_1 = [0 \ -1] \tag{A5.10}$$

$$H_2 = [1 \ \ 0]. \tag{A5.11}$$

Substituting these equations into the dual-rate state model defines the closed-loop system given by

$$\begin{bmatrix} x_1(nh_P + h_P) \\ x_2(nh_P + h_P) \end{bmatrix} = \left[\begin{bmatrix} 1 & 0 \\ 0 & \exp(h_1) \end{bmatrix} + \begin{bmatrix} h_1 \\ 0 \end{bmatrix} [0 \ -1] \right]^2 \begin{bmatrix} x_1(nh_P) \\ x_2(nh_P) \end{bmatrix}$$

$$+ \left[\begin{bmatrix} 1 & 0 \\ 0 & \exp(h_1) \end{bmatrix} + \begin{bmatrix} h_1 \\ 0 \end{bmatrix} [0 \ -1] + \begin{bmatrix} 1 & 0 \\ 0 & 1 \end{bmatrix} \right] \begin{bmatrix} 0 \\ 1-\exp(-h_1) \end{bmatrix} [1 \ 0] \begin{bmatrix} x_1(nh_P) \\ x_2(nh_P) \end{bmatrix}$$

$$+ \left[\begin{bmatrix} 1 & 0 \\ 0 & \exp(h_1) \end{bmatrix} + \begin{bmatrix} h_1 \\ 0 \end{bmatrix} [0 \ -1] + \begin{bmatrix} 1 & 0 \\ 0 & 1 \end{bmatrix} \right] \begin{bmatrix} 0 \\ 1-\exp(-h_1) \end{bmatrix} [1 \ 0] \ \mathbf{v}(nh_P) \quad . \tag{A5.12}$$

Multiplying out the matrices of equation (A5.12) gives

$$\begin{bmatrix} x_1(nh_P + h_P) \\ x_2(nh_P + h_P) \end{bmatrix} = \begin{bmatrix} 1-h_1(1-\exp(-h_1) & -h_1(1+\exp(-h_1) \\ 1-\exp(-2h_1) & \exp(-2h_1) \end{bmatrix} \begin{bmatrix} x_1(nh_P) \\ x_2(nh_P) \end{bmatrix}$$

$$\begin{bmatrix} -h_1(1+\exp(-h_1) \\ 1-\exp(-2h_1) \end{bmatrix} \mathbf{v}(nh_P) \quad .(A5.13)$$

A5.3 SUMMARY

The application of sampled-state feedback control to the Continuous-Amplitude, Continuous-Time system, shown in Fig.A5.1, results in the closed-loop state-equation (A5.13). This result is identical to the one produced by the modified Kalman-Bertram method [A5.1]. In the above case, the approach starts with an open-loop system and progresses to the closed-loop model. By apparently reversing the Kalman-Bertram method, the proposed approach is aligned to conventional flight control system design techniques. In this respect, the facility of the above method appears to offer an advantage for the particular requirements of DFC design. A further advantage of the above approach appears from the structure of the of matrix equations used to develop the multirate sampled-data model. The visibility of the physical system, throughout the development of the control system, is greater than that offered by other multirate modelling methods. It is therefore claimed that the proposed digital control system design methodology meets the requirements of the design maxims of the thesis.

APPENDIX SIX

MULTIVARIABLE w-PLANE AND w'-PLANE MODELS

A6.1 INTRODUCTION

This appendix supports the discussion presented in Section 4.2 of Chapter Four. In that chapter, the w-plane and w'-plane system models were defined. The relationship between the CADT system quadruple, (Φ,Ψ,C_D,D_D) and the w-plane and w'-plane quadruples, (A_w,B_w,C_w,D_w) and $(A_{w'},B_{w'},C_{w'},D_{w'})$, respectively, are given. These relationships are developed in this appendix.

A6.2 MAPPING THE CADT STATE-SPACE MODEL TO THE w-PLANE

By definition, the bilinear transform maps the w-plane from the z-plane. However, if an equivalent CADT model is obtained directly from the CACT state-space equations, the w-plane is effectively cast in terms of the discrete-time quadruple (Φ,Ψ,C_D,D_D). Under these conditions, the algorithm developed in this section can be regarded as a time-domain to w-plane mapping.

The bilinear transform that maps the w-plane from the z-plane is

$$z = \frac{1 + w}{1 - w} \quad . \tag{A6.1}$$

Substituting (A6.1) into the z-plane state-space equation,

$$z\,X(z) = \Phi\,X(z) + \Psi\,U(z) \qquad \text{(A6.2a)}$$

$$Y(z) = C_D X(z) + D_D U(z)\ , \qquad \text{(A6.2b)}$$

and adopting a minor abuse of notation[1] , gives

$$\left(\frac{1+w}{1-w}\right)X(w) = \Phi\,X(w) + \Psi\,U(w) \qquad \text{(A6.3a)}$$

$$Y(w) = C_D X(w) + D_D U(w)\ . \qquad \text{(A6.3b)}$$

As a first step, the product of the scalar form of the bilinear transform and the state vector is recast as a matrix equation.

$$\left(\frac{1+w}{1-w}\right)X(w) = [I - wI]^{-1}[I + wI]X(w)\ . \qquad \text{(A6.4)}$$

Substituting equation (A6.4) into (A6.3a) and premultiplying both sides by [I - wI] gives

$$[I + wI]X(w) = [I - wI]\Phi\,X(w) + [I - wI]\Psi\,U(w)\ . \qquad \text{(A6.5)}$$

Collecting the state vector, $\left(X(w)\right)$, on the left hand side, multiplying out the bracketed terms and factorising to isolate w gives

$$\left[w[I + \Phi] + [I - \Phi]\right]X(w) = [I - wI]\Psi\,U(w)\ . \qquad \text{(A6.6)}$$

---

[1] The strict notation is $X\left(\frac{1+w}{1-w}\right)$ but in the interest of simplicity the notation X(w) has been adopted throughout this text.

Taking $[I + \Phi]$ as a common factor gives

$$[I + \Phi]\left[wI + [I + \Phi]^{-1}[I - \Phi]\right]X(w) = [I - wI]\Psi\, U(w) \quad . \quad \text{(A6.7)}$$

The next objective is to isolate a single term containing the transform variable, w. This is most readily achieved by rearranging the right hand side of equation (A6.7) and adding the term

$$\left[[I + \Phi]^{-1}[I - \Phi] - [I + \Phi]^{-1}[I - \Phi]\right] = 0 \quad ,$$

$$[I + \Phi]\left[wI + [I + \Phi]^{-1}[I - \Phi]\right] X(w) =$$

$$-\left[\left[wI + [I + \Phi]^{-1}[I - \Phi]\right] - \left[I + [I + \Phi]^{-1}[I - \Phi]\right]\right]\Psi\, U(w) \quad . \quad \text{(A6.8)}$$

Taking the term $[I + \Phi]^{-1}$ outside the second bracket of the right hand side of equation (A6.8) gives

$$[I + \Phi]\left[wI + [I + \Phi]^{-1}[I - \Phi]\right] X(w) =$$

$$-\left[\left[wI + [I + \Phi]^{-1}[I - \Phi]\right] - [I + \Phi]^{-1}\, 2I\right]\Psi\, U(w) \quad . \quad \text{(A6.9)}$$

Premultiplying both sides of equation (A6.9) by

$$\left[wI + [I + \Phi]^{-1}[I - \Phi]\right]^{-1}[I + \Phi]^{-1}$$

gives

$$X(w) = -\left[\left[wI + [I + \Phi]^{-1}[I - \Phi]\right]^{-1}[I + \Phi]^{-1}\left[wI + [I + \Phi]^{-1}[I - \Phi]\right]\right.$$

$$\left.-\left[wI + [I + \Phi]^{-1}[I - \Phi]\right]^{-1}[I + \Phi]^{-1}[I + \Phi]^{-1}2I\right]\Psi\, U(w) \quad .$$

(A6.10)

Using the two matrix relationships

$$wI\ [I + \Phi] = [I + \Phi]\ wI$$

$$[I - \Phi][I + \Phi] = [I + \Phi][I - \Phi] \quad ,$$

the term $[I + \Phi]^{-1}$ in the first part of the right hand side of equation (A6.10) commutes to the left to give

$$\mathbf{X}(w) = \left[\left[wI + [I + \Phi]^{-1}[I - \Phi]\right]^{-1} 2\ [I + \Phi]^{-2}\Psi - [I + \Phi]^{-1}\Psi\right] \mathbf{U}(w) \ . \tag{A6.11}$$

Substituting equation (A6.11) into the w-plane output equation gives

$$\mathbf{Y}(w) =$$

$$\mathbf{C}_D\left[\left[wI + [I + \Phi]^{-1}[I - \Phi]\right]^{-1} 2[I + \Phi]^{-2}\Psi - [I + \Phi]^{-1}\Psi\right] \mathbf{U}(w) + \mathbf{D}_D\mathbf{U}(w). \tag{A6.12}$$

The relationship between the w-plane quadruple and the CADT quadruple is found by comparing equation (A6.12) with the w-plane transfer-function. From the w-plane state-space equations given in Chapter Four by (4.13), the w-plane matrix transfer-function is given as

$$\mathbf{Y}(w) = \mathbf{C}_w[I - \mathbf{A}_w]^{-1}\mathbf{B}_w\ \mathbf{U}(w) + \mathbf{D}_w\ \mathbf{U}(w) \quad . \tag{A6.13}$$

A comparison of the coefficient matrices of equation (A6.12) and equation (A6.13) gives the w-plane quadruple. In summary, the w-plane quadruple, in terms of the CADT state-space quadruple, is

given by

$$A_w = -[I + \Phi]^{-1}[I - \Phi] \quad , \tag{A6.14}$$

$$B_w = 2[I + \Phi]^{-2}\Psi \quad , \tag{A6.15}$$

$$C_w = C_D \quad , \tag{A6.16}$$

$$D_w = - C_D[I + \Phi]^{-1}\Psi + D_D \quad . \tag{A6.17}$$

The inverse mapping functions are directly deduced from these four equations and are given by

$$\Phi = [I + A_w][I - A_w]^{-1} \quad , \tag{A6.18}$$

$$\Psi = 2[I - A_w]^{-2}B_w \quad , \tag{A6.19}$$

$$C_D = C_w \quad , \tag{A6.20}$$

$$D_D = C_w[I - A_w]^{-1}B_w + D_w \quad . \tag{A6.21}$$

A6.3 MAPPING THE CADT STATE-SPACE MODEL TO THE w'-PLANE

The w'-plane, defined in terms of the w-plane, is given as

$$w = \frac{h}{2}w' \quad . \tag{A6.22}$$

Substituting equation (A6.22) into (A6.12) gives

$$Y(w') =$$

$$C_D\left[\left[w'I + \frac{2}{h}[I+\Phi]^{-1}[I-\Phi]\right]^{-1}\frac{4}{h}[I+\Phi]^{-2}\Psi - [I+\Phi]^{-1}\Psi\right] U(w') + D_D U(w') \quad .$$

6.23)

Comparing the coefficient matrices of equation (A6.23) with the matrix coefficients of equation (A6.13) gives the w'-plane quadruple. In summary, the w'-quadruple, in terms of the CADT state-space quadruple, is given by the following equations:

$$\mathbf{A}_{w'} = -\frac{2}{h}[\mathbf{I} + \Phi]^{-1}[\mathbf{I} - \Phi] \quad , \tag{A6.24}$$

$$\mathbf{B}_{w'} = \frac{4}{h}[\mathbf{I} + \Phi]^{-2}\Psi \quad , \tag{A6.25}$$

$$\mathbf{C}_{w'} = \mathbf{C}_D \quad , \tag{A6.26}$$

$$\mathbf{D}_{w'} = -\mathbf{C}_D[\mathbf{I} + \Phi]^{-1}\Psi + \mathbf{D}_D \quad . \tag{A6.27}$$

The inverse mapping functions deduced from these equations are

$$\Phi = [\mathbf{I} + \frac{h}{2}\mathbf{A}_{w'}][\mathbf{I} - \frac{h}{2}\mathbf{A}_{w'}]^{-1} \quad , \tag{A6.28}$$

$$\Psi = 2[\mathbf{I} - \frac{h}{2}\mathbf{A}_{w'}]^{-2}\frac{h}{2}\mathbf{B}_{w'} \quad , \tag{A6.29}$$

$$\mathbf{C}_D = \mathbf{C}_{w'} \quad , \tag{A6.30}$$

$$\mathbf{D}_D = \mathbf{C}_{w'}[\mathbf{I} - \frac{h}{2}\mathbf{A}_{w'}]^{-1}\frac{h}{2}\mathbf{B}_{w'} + \mathbf{D}_{w'} \quad . \tag{A6.31}$$

A6.4 SUMMARY

The algorithms developed in this appendix provide a convenient and efficient method for directly mapping a CACT state-space quadruple to the w- and the w'-planes.The algorithms avoid the generation of the cumbersome transfer-functions that usually occur with the single-input single-output transfer-function mapping method.

APPENDIX SEVEN

ANALYSIS TECHNIQUES FOR DIRECT DIGITAL DESIGN

A7.1 INTRODUCTION

The z-plane performance criteria, for sampled-data control systems, are usually defined from a one-to-one mapping of the s-plane to the z-plane. Alternative criteria, that suits the direct digital design methods prescribed in this thesis, are developed by applying the arguments used to establish CACT frequency domain criteria to a CADT system. As a basis for comparison, a brief review of the CACT domain performance criteria is given in the next section.

A7.2 A REVIEW OF CACT DOMAIN DESIGN AND ANALYSIS CRITERIA

Consider the CACT domain linear, time-invariant state-equation

$$\dot{\mathbf{x}}(t) = \mathbf{A}\,\mathbf{x}(t) + \mathbf{B}\,\mathbf{u}(t) \quad . \qquad \text{(A7.1)}$$

The poles of the system, described by (A7.1), are the eigenvalues of the state matrix **A**. In terms of the s-plane, the eigenvalues are the zeros of the characteristic equation, given by the determinant of [sI-A]. In the case of dynamical systems, the concepts of bandwidth and natural frequency are often ambiguous, particularly when the order of the system is greater than two. This ambiguity also applies to the performance measures listed in Fig.A7.1.

However, the performance of higher order systems can often be deduced by considering the natural-frequency, damping-ratio, etc, associated with the lowest frequency mode (a technique usually referred to as dominant pole approximation). The s-plane performance criteria, used as design guides for pole placement techniques and performance analysis, are summarised in Fig.A7.1 and defined on the s-plane diagram of Fig.A7.2.

Frequency	ω_s
Decrement per unit time	σ_s
Decrement per unit cycle	$f(\zeta_s)$
Natural frequency	ω_{ns}
Resonance frequency	ω_{ms}
Resonance magnification	m_s

Performance measures for s-plane pole placement and analysis

Fig.A7.1

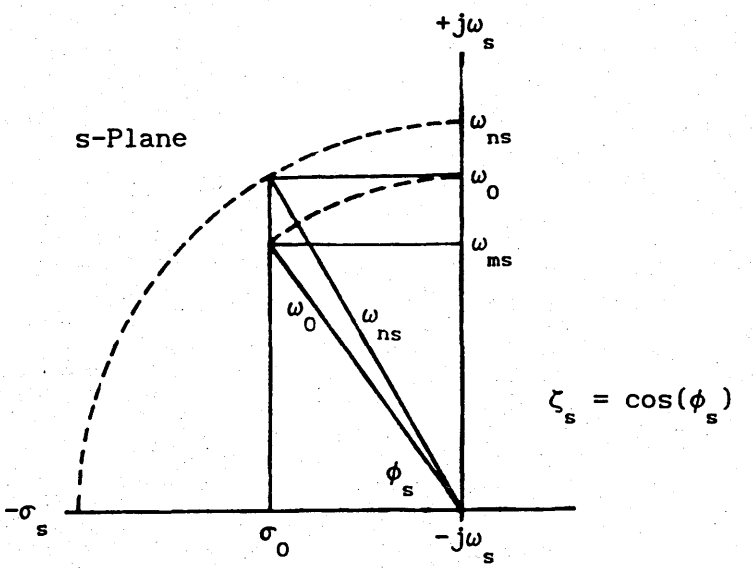

Performance and analysis criteria defined on the s-plane

Fig.A7.2

The three parameters, ω_s, σ_s, and $f(\zeta_s)$, listed in Fig.A7.1, are measures associated with the zero-input characteristics of a given system. The other three parameters are defined on the s-plane shown in Fig.A7.2.

A7.3 THE DEVELOPMENT OF CADT DOMAIN DESIGN AND ANALYSIS CRITERIA

The CADT z-plane analysis criteria, described in this section, are developed by observing the equivalence between CACT and CADT system parameters. The first observation, which forms the basis of the criteria development, is the previously described equivalence of the CACT state equation (A7.1) and the CADT state-equation given as

$$\mathbf{x}_D(n+1) = \Phi\, \mathbf{x}_D(n) + \Psi\, \mathbf{u}(n) \quad . \tag{A7.2}$$

The s-plane analysis criteria are primarily concerned with a system's characteristic equation; therefore, without compromising generality, the criteria can be developed by considering a zero-input modal state model. For the CACT system of (A7.1), this is given by

$$\dot{\mathbf{x}}_M(t) = \Lambda\, \mathbf{x}_{MO} \quad , \tag{A7.3}$$

where $\mathbf{x}_M(t) = \mathbf{M}\, \mathbf{x}(t)$ and $\Lambda = \mathbf{M}^{-1}\mathbf{A}\, \mathbf{M}$, and the matrix $\mathbf{M}$ is a modal transformation which produces the diagonal form of the state matrix. The i-th modal state is therefore given by

$$\dot{x}_i(t) = \exp(\lambda_i t)\, x_{io} \quad . \tag{A7.4}$$

In general, λ_i is a complex number, so equation (A7.4) can be written as

$$\dot{x}_i(t) = \exp(\sigma_s t)\, \exp(j\omega_s t)\, x_{i0} \quad , \qquad \text{(A7.5)}$$

where the real and imaginary components of λ_i are σ_s and ω_s, respectively.

For the CADT system given by the state equation (A7.2), the associated zero-input modal form is given by

$$\mathbf{x}_{DM}(n) = \left[\Lambda_D\right]^n \mathbf{x}_{DMO} \quad . \qquad \text{(A7.6)}$$

With a discrete-system inverse modal matrix, $\mathbf{M}_D$, the modal state vector is $\mathbf{x}_{DM}(n) = \mathbf{M}_D\mathbf{x}(n)$ and the matrix $\Lambda_D = \mathbf{M}_D^{-1}\Phi\ \mathbf{M}_D$. The i-th modal state of the CADT system is therefore given by

$$x_{Di}(n) = (\lambda_{Di})^n\, x_{Di0} \quad . \qquad \text{(A7.7)}$$

In general, λ_{Di} is a complex number, so equation (A7.7) can be written as

$$x_{Di}(n) = r^n \exp(j\phi n)\, x_{Di0} \quad . \qquad \text{(A7.8)}$$

The CADT domain criteria, that have equivalent roles to the CACT domain criteria listed in the table of Fig.A7.1, are deduced by comparing equations (A7.5) and (A7.8). The two CADT domain parameters, sample-number, n, and envelope-frequency, ϕ, are

equivalent to the CACT parameters, t and ω, respectively. These observations are interpreted in the following paragraphs.

A synchronous sequence of samples, with members, u(n), represents, for example, instantaneous values of a continuous periodic function which has a time period, T. The frequency of this periodic function can be interpreted as the envelope-frequency of the sample sequence. The number of data samples taken during the period, T, of the notional continuous function, is μ; this parameter is referred to as the samples-per-envelope-cycle. For the case illustrated in Fig.A7.3, μ=6 samples-per-envelope-cycle.

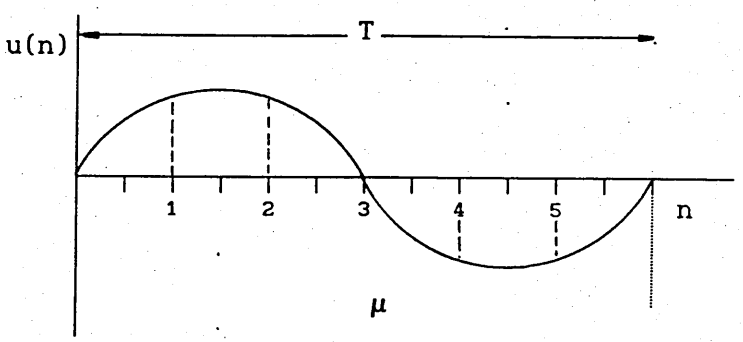

Sinusoidal envelope of discrete samples

Fig.A7.3

It should be noted that the ratio $\frac{\mu}{n}$ for $0<n\leq\mu$ need not necessarily be an integer. From Fig.A7.3, it can be seen that the values of the discrete sample sequence are given by

$$u(n) = \sin\left(\frac{2\pi n}{\mu}\right) \quad . \qquad (A7.9)$$

Defining $\phi = \frac{2\pi}{\mu}$ and substituting this relationship into equation (A7.9) gives $u(n) = \sin(\phi n)$. For a CACT model with complex

eigenvalues given by ($\sigma_s \pm j\omega_s$), the envelope-cycle is ω_s. An important issue associated with this concept is that to satisfy Shannon's sampling theorem the parameter $\mu \geq 2$. The samples-per-envelope-cycle locus is plotted within the unit circle of the z-plane. Each sample-per-envelope-cycle produces a radial line, projecting from the origin of the z-plane, as shown in Fig.4.8 of Chapter Four.

Comparing, again, the modal forms of the zero-input CACT and CADT state-equations, (A7.5) and (A7.8), respectively, it is seen that the rate of decay of the CACT domain system is governed by the function, $\exp(\sigma_s)$, and the rate of decay of the CADT domain system is governed by the parameter, r. These two parameters are both referred to as the decrement-per-unit-time. On the s-plane, a CACT system's modes converge to the zero-state for negative values of σ_s and diverge for positive values of σ_s. Modes are in a steady-state condition for all time when σ_s is zero. In the case of a CADT domain system defined in a z-plane, it is seen that modes converge to a zero-state for values of r less than unity and diverge for values of r greater than unity. When r has is unity, the CADT domain mode is steady-state for all time.

A7.3.1 Damping Factor in the CADT Domain

The damping factor, ζ, gives a measure of the stability characteristics of CACT domain systems. The damping factor is related to the decrement-per-time parameter through the function

$$\sigma_s = - \frac{\zeta}{\sqrt{1 - \zeta^2}} \omega_s \quad . \qquad \text{(A7.10)}$$

Radial lines of constant damping factors can be plotted on the s-plane, as shown in Fig.A7.2. In terms of the s-plane axes, σ_s and ω_s, a constant damping line is given by a constant ratio ratio of σ_s to ω_s; this ratio is called the damping-per-unit-cycle. The zero-input, CACT domain, modal form of the state equation (A7.5) can be recast to give ζ in terms the damping-per-unit-cycle ratio. The parallel operation in the CADT domain is based on equation (A7.8) and defines a set of contours on the z-plane. These contours are equivalent to the constant decrement radials of the s-plane.

To define a CADT parameter which can be regarded as equivalent to the CACT domain damping factor, consider the CACT zero input modal state equation (A7.5), recast in the form

$$x_i\left(\frac{p_s}{\omega_s}\right) = \exp\left(\frac{\sigma_s}{\omega_s}\right)\exp(jp_s)\, x_{i0} \quad , \qquad \text{(A7.11)}$$

where $p_s = \omega_s t$. The equivalent parameter in the CADT domain is defined as p_D where $p_D = \phi\, n$. Substituting p_D into equation (A7.8) gives

$$x_{Di}\left(\frac{p_D}{\phi}\right) = (r)^{\frac{1}{\phi}} \exp(jp_D)\, x_{Di0} \quad . \qquad \text{(A7.12)}$$

From the CACT domain equation (A7.11), the decrement-per-unit-cycle is given by

$$f(\zeta_s) = \frac{\sigma_s}{\omega_s} \quad , \qquad \text{(A7.13)}$$

where the function, $f(\zeta_s) = \tan\left(\arccos(\zeta_s)\right)$. Comparing this parameter with the equivalent term in equation (A7.12) gives the CADT domain decrement-per-unit-cycle as

$$\gamma = \left(r\right)^{\frac{1}{\phi}} \quad . \tag{A7.14}$$

As shown by Fig.4.9, in Chapter Four, the CADT constant value decrement-per-cycle z-plane contours produce a family of logarithmic spirals. These spirals converge on two points. For an infinite sampling-rate, the convergence point is z(1,j0). For zero sampling-rate (a meaningless notion), the contours meet at z(0,j0). In progressing towards the zero sampling rate limit, the contours make successive crossings of the negative real z axis for μ=2k, and the positive real axis for μ=2(k+1) for k=1, 2, 3, ...∞.

It is observed that the decrement-per-envelope-cycle contours defined in this section have the same logarithmic spiral form as the s-plane damping factor contours when they are mapped onto the z-plane. However, it should be noted that the z-plane contours illustrated in Fig.4.9 are directly defined for the CADT domain and therefore have a different interpretation to similar contours produced by an s-plane to z-plane mapping. The different interpretation arises because the geometrical basis for both sets of contours is the origin of their respective planes. In addition,the s-plane origin, s(0,j0), maps to z(1,j0) and not to the origin of the z-plane.

In the CACT domain, σ_s can have either a positive or negative value. For negative values of σ_s , as the decrement-per-cycle ratio becomes smaller, the damping factor tends to zero. The equivalent to σ_s in the CADT domain is the radial vector r of equation (A7.12), which can only have positive values. The interpretation of r in terms of σ_s is that $0<r<1$ corresponds to $\sigma_s<0$. For digital control system design in the CADT domain, r is the appropriate parameter for measuring stability.

A7.3.2 Natural-Frequency and Resonance in the CADT Domain

The three CACT domain parameters of natural-frequency, ω_{ns}, resonance-frequency, ω_{ms}, and resonance-magnification, m_s, are important measures in the specification and assessment of control systems. As in the case of the damping factor described above, the natural-frequency and resonance parameters can be mapped from the s-plane to a z-plane. Details of the s-plane to z-plane mapping method are well documented [A7.1]. The concepts of natural-frequency and resonance, based on the direct CADT domain definition, are developed in this section.

The CACT domain system performance parameters can be defined by considering the s-plane geometry associated with a complex pole-pair. The development of equivalent CADT domain parameters can be achieved by following the s-plane geometry with a corresponding z-plane geometry, as shown in Fig.A7.4.

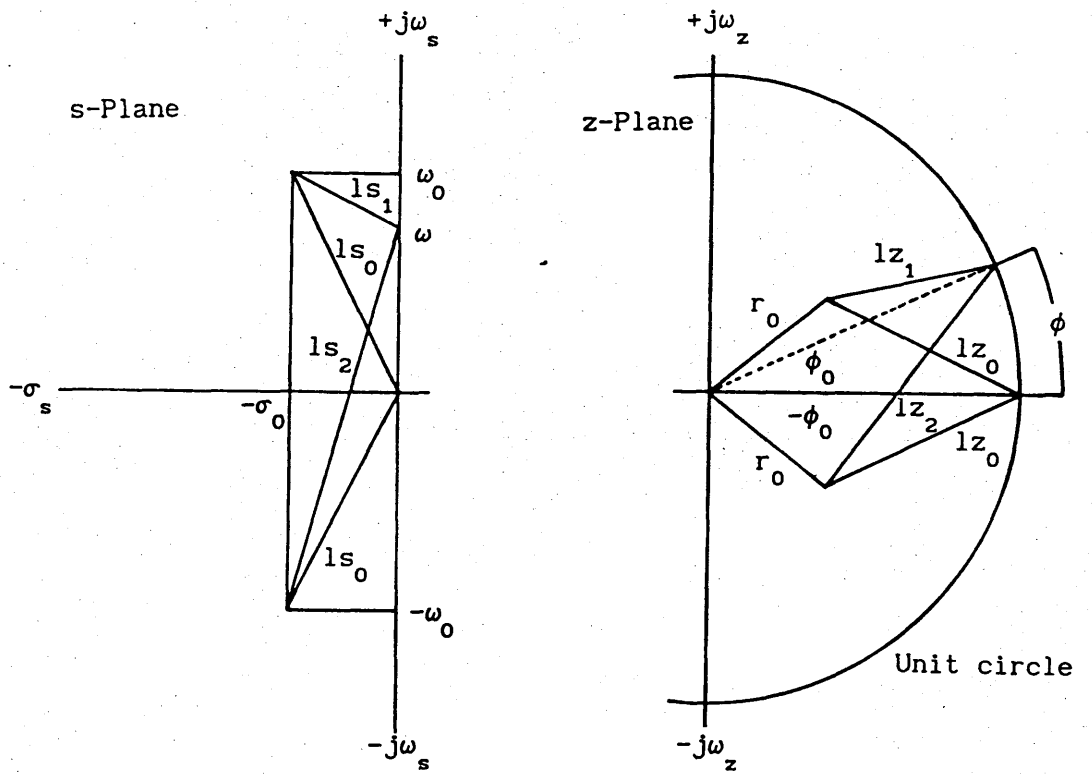

s-plane z-plane

The s- and z-plane geometries of a pole-pair which are applied in the definition of the control system performance parameters

Fig.A7.4

To examine the CADT concepts of natural frequency and resonance, consider the CADT domain second order system given as

$$F(z) = \frac{1}{\left(z - r_o \exp(j\phi_o)\right)\left(z - r_o \exp(-j\phi_o)\right)} \quad . \qquad (A7.15)$$

If the system modelled by equation (A7.15) is stable and is processed in discrete-time within the time frame of the primary iteration rate, then the complex pole-pair is mapped onto the z-plane, as shown in Fig.A7.4.

The concept of frequency response and its associated parameters is based on the geometry of Fig.A7.6 and the product of the magnitudes of vectors, lz_1 and lz_2, where lz_1 is given by

$$lz_1 = \left|\exp(j\phi) - r_0\exp(j\phi_0)\right| \qquad \text{(A7.16)}$$

and lz_2 is given by

$$lz_2 = \left|\exp(j\phi) - r_0\exp(-j\phi_0)\right| \quad . \qquad \text{(A7.17)}$$

To facilitate the development of the CADT domain z-plane frequency response criteria, the variable, ϕ, is replaced by

$$\phi = 2\ \arctan(\omega_w) \quad . \qquad \text{(A7.18)}$$

This, apparently obscure substitution, is a direct consequence of the w-plane frequency response, which is discussed in Section 4.2 of Chapter Four.The z-plane contours of natural frequency, (ϕ_n), and resonance magnification, (m_z), are shown in Chapter Four by Fig.4.10 and 4.11, respectively. These two sets of contours are defined in terms of the z-plane geometry of Fig.A7.4b and were derived from the w-plane parameters described in Chapter Four.In terms of the z-plane geometry, the contours for these two parameters, together with the z-plane definition of resonance frequency, (ϕ_m), are given by

$$\phi_n = \arccos\left(\frac{2r_o}{1 + r_o^2} \cos(\phi_o) \right) \quad , \qquad \text{(A7.19)}$$

$$m_z = \frac{(1 + r_o^2) - 2r_o \cos(\phi_o)}{(1 - r_o^2) \sin(\phi_o)} \quad , \qquad \text{(A7.20)}$$

$$\phi_m = \arccos\left(\frac{1 + r_o^2}{2r_o} \cos(\phi_o) \right) \quad . \qquad \text{(A7.21)}$$

A7.4 SUMMARY

The CADT domain analysis criteria described in this appendix represents the appropriate measures for the assessment of a mixed-data DFC system. The direct discrete domain definitions of the criteria establish the techniques as suitable measures for analysing both sampled-data and purely discrete-data systems.

REFERENCES

CHAPTER ONE

[1.1] Fraser, D. C. "Aircraft Control Systems - A projection to the Year 2000" *IEEE Control Systems Magazine*. Feb 1985. pp.11-13.

[1.2] Moran, W. A. "(A) Operational and Developmental Experience With the F/A-18A Digital Flight Control System" *AGARD FMP Symposium on Active Control Systems - Review, Evaluation and Projections*. Oct 1984 pp.12A.1-12A.13.

[1.3] Tischler, M. B. "Digital Control of Highly Augmented Combat Rotorcraft" NASA Tech Memo 88346. May 1987 pp.2-4.

[1.4] McRuer, D., Johnston, D. E., Myers, T. T. "A Perspective on Superaugmented Flight Control, Advantages and Problems: *AGARD FMP Symposium on Active Control Systems - Review, Evaluation and Projections*. Oct 1984 pp.3.1-3.16.

[1.5] Goodchild, C. "The Digital Control of an Aircraft Using Multirate sampling" Cranfield Institute of Technology, M.Sc Thesis 1980.

[1.6] Tischler, M. B. *ibid* [1.3] pp.15 and 16.

[1.7] Powers, B. G. "Active Control Technology Experiences With the Space Shuttle in the Landing Regime" NASA TM-85910. Oct 1984.

[1.8] Burton, R., Kneeland, B. T., Wagner, T. A. "(B) Operational and Developmental Experience With The F/A-18A Digital Flight Control System" *AGARD FMP Symposium on Active Control Systems Review, Evaluation and Projections*. Oct 1984 pp.12B.1-12B.5.

[1.9] Chalk, C. R. "Excessive Roll Damping Can Cause Roll Ratchet" *Jounal of Guidance, Control and Dynamics* Vol.6 No.3 p.218.

[1.10] Johnston, D. E., McRuer, D. "Investigation of Limb-Side Stick Dynamic Interaction With Roll Control" *Jounal of Guidance, Control and Dynamics*. Vol.10, No.2 Mar-Apr 1987, pp.178-186.

[1.11] Smith, T. D., Yeo, C. J., Marshall, R. E. W. "Ground and Flight Testing on the Fly-By-Wire Jaguar Equipped With A Full Time Quadruplex Digital Integrated Flight Control System" *AGARD GCP Conference Proceedings No.321*. Oct 1982 pp.23.1-23.20.

[1.12] Fraser, D. C. *ibid* [1.1]

[1.13] Mulcare, D. B., Ness, W. G., Davis, R. M. "Analytical Design and Assurance of Digital Flight Control System Structure" *AIAA Jounrnal on Guidance and Control,* Vol.7 No.3 May-Jun 1984, pp.329-337.

[1.14] Joshi, Dinesh. S., Kesler, D. F., Johnson, E. H. "Development and Application of Digital Control for Tactical Aircraft Flutter Suppression" *AGARD GCP Conference Proceedings* No.321. Oct 1982 pp.19.1-19.14.

[1.15] Kidd, W. M. "The Development of Design Techniques for the Digital Flight Control of Remotely Piloted Vehicles" Cranfield Instsitute of Technology, M.Sc Thesis 1979.

[1.16] Goodchild, C. *ibid* [1.5]

[1.17] Tichler, M. B. *ibid* [1.3] pp.19 and 20.

[1.18] Oz, H., Meriovitch, L., Johnson, C. R. "Some Problems Associated With Digital Control of Dynamical Systems" *AIAA Journal Guidance and Control*. Vol.3 No.6 Nov-Dec 1980 pp.523-528.

[1.19] Tretter, S. A. "*Introduction to Discrete-Time Signal Processing*" Wiley 1976, pp.14-16.

[1.20] Anon. "MIL-F-8785C Flying Qualities of Piloted Airplanes" USA DoD Military Specification. Nov 1980.

[1.21] Powell, D. J., Katz, P. "Sample Rate Selection for Aircraft Digital Control" *AIAA Journal*. Vol.13, No.8, Aug 1975 pp.975-979.

[1.22] Kranc, G. M. "Multirate Sampled Systems" Dept of Electrical Engineering, Columbia University New York, Technical Report No T-14/B May 1956.

[1.23] Kalman, R. E., Bertram, J. E. "A Unified Approach to the Theory of Sampling Systems" *Journal of the Franklin Institute*" May 1959. pp405-436.

[1.24] Araki, M., Yamamoto, K. "Multivariable Multirate Sampled-Data Systems" State-Space Description, Transfer Characteristics and Nyquist Criterion" *IEEE Trans on Automatic Control*. Vol. AC-31, No.2, Feb 1986 pp.145-154.

[1.25] Goodchild, C. "The Application of Kalman and Bertram's Unified Methods of Modelling Sampled-Data Systems for the Simulation of Multirate Sampled-Data DFC Systems" Glasgow University Dep of Aerospace Engineering Report August 1990.

[1.26] Whitbeck, R. F. and Hofmann, L. G. "Digital Control Law Synthesis in the w' Domain" *AIAA Journal Guidance and Control*. Vol.1 No.5 Sept-Oct 1978 pp.319-326.

[1.27] Tichler, M. B. *ibid* [1.3] p148.

[1.28] Moler, C., Little, J., Bangert, S.: PC-MATLAB Version 3.2-PC User Guide. The Math Works Inc June 1987.

CHAPTER TWO

[2.1] Johannes, R. P., Thompson, G. O. "B-52 Control Configured Vehicles Program" *AGARD Conference Proceedings* No.137Sept 1973 pp.23.1-23.10.

[2.2] McCormick, B. W. "*Aerodynamics and Flight Mechanics*" Wiley 1979 Appendix A3 p.629.

[2.3] Fermelia, A., Gyorog, D. A., Flanigan, V.J. "Helicopter Motion: Equation Linearization" *IEEE Transactions on Aerospace and Electronic Systems*. Vol. AES-12 No.6 Nov 1976 pp767-791.

[2.4] Bakken, J. T. "Implementation of Fly-By-Wire/Fly-By-Light Experimental Flight Control Systems in Helicopters" *Presentation at the National Specialists Meeting on Flight Controls and Avionics. The American Helicopter Society*, Cherry Hill, N.J., Oct 1987.

[2.5] Tretter, S. A. *ibid* [1.19] Chapter Three, pp23-28.

[2.6] Tretter, S. A. *ibid* [2.5] p23.

[2.7] Tretter, S. A. *ibid* [2.5] p24.

[2.8] Dotson, W. P., Wilson, J. H. "A Digital-To-Analog Conversion Circuit Using Third Order Polynomial Interpretation" NASA Technical Report TR R-382, Feb 1972.

[2.9] Bakken, J. T. *ibid* [2.4].

[2.10] Schmid, H. "*Electronic Analog to Digital Conversions*" Van Nostrand Reinhold 1970.

[2.11] Sheingold, D. H., Ed. "*Analog-Digital Conversion Notes*" Analog Devices 1977.

[2.12] Tou, J. T. "*Digital and Sampled-Data Control Systems*" McGraw-Hill, 1959, p.130.

[2.13] Houpis, C. H., Lamont, G. B. "*Digital Control Systems - Theory, Hardware, Software*" McGraw-Hill, 1985 p191.

[2.14] Harvey, C. A., Pope, R. E. "Design Techniques For Multivariable Flight Control Systems" *AGARD GCP Agardograph* No.251 Jul 1981.

[2.15] Boucher, A. R., Cox, C. S., Doonan, A. "Sampling Time Selection and its Effect od Direct Digital and Adaptive Control Algorithm Implementation" *IEE Computing and Control Division PG-C9 Colloquium.* Digest No 1989/73. 9th May 1989. pp.5.1-5.7.

[2.16] Kuo, B. C. "*Digital Control Systems*" Holt, Rinehart and Winston. 1980 Chapter 3.

[2.17] Tou, J. T. "*Digital and Sampled-Data Control Systems*" McGraw-Hill, 1959, p.146.

[2.18] Tustin, A. "A Method of Analyzing the Behavior of Linear Systems in Terms of Time Series" *Proceedings of the IEE* Vol.94 Pt.2A, 1947 pp.130-142.

[2.19] Szalai, K. J. "Flight Test Experience with the F-8 Digital Fly-By-Wire System" NASA Technical Memorandum TM X-3409, Aug 1976 pp.199-253.

[2.20] Kwakernaak, H., Sivan, R. "*Linear Optimal Control Systems*" Wiley, 1972 pp.443-447.

[2.21] Fulmer, E. P. "Computation of the Matrix Exponential" *American Mathematical Monthly*, Vol.82 1975 pp.156-159.

[2.22] Moler, C., Van Loan, C. "Nineteen Dubious Ways To Compute The Exponential Matrix" *SIAM Review* Vol.20 No.4 Oct 1978, pp.801-836.

[2.23] Laub, A. J. "Numerical Aspects of Control Design Computations" *AGARD Lecture Series* No.128 Jul 1983 pp.5.1-5.16.

[2.24] Anon. "TSIM, Non Linear Dynamic Simulation Package, User Guide" Cambrige Control March 1986.

CHAPTER THREE

[3.1] Sklansky, J. "Network Compensation of Error Sampled Feedback Systems" Dept of Electrical Engineering, Columbia University, Ph.D. Dissertation 1955.

[3.2] Kranc, G. M. *ibid* [1.22].

[3.3] Kalman, R. E., Bertram, J. E. *ibid* [1.23].

[3.4] Araki, M., Yamamoto, K. *ibid* [1.24].

[3.5] Phillips, C. L., Nagle, H. T. "*Digital Control System Analysis and Design*" Prentice-Hall, 1984 pp.428-441.

[3.6] Isermann, R. "*Digital Control Systems*" Vol.1, 2nd Edition. Springer-Verlag 1989 pp151-154.

[3.7] Powell, D. J., Katz, P. *ibid* [1.21].

[3.8] Tretter, S. A. *ibid* [1.19].

[3.9] Jamshdi, M., Malek-Zavarei, M. "*Linear Control Systems; A Computer Aided Approach*" Pergamon Press 1986 pp.163-175.

[3.10] Goodchild, C. "Engineering Logbooks" GEC Research Laboratory Records. August 1976 to August 1984.

[3.11] Kalman, R. E., Ho, Y. C., Narendra, K. S. "Controllability of Linear Dynamical Systems" *Contribution, Differential Equations* Vol.1 1961 pp.189-213.

[3.12] Goodchild, C. *ibid* [1.5].

[3.13] Sklansky, J. *ibid* [3.1].

[3.14] Kranc, G. M. *ibid* [1.22].

[3.15] Kalman, R. E., Bertram, J. E. *ibid* [1.23].

[3.16] Araki, M., Yamomoto, K. *ibid* [1.24].

[3.17] Berg, M. C. "Design of Multirate Digital Control Systems" Ph.D Dissertation. Stanford University 1986.

[3.18] Goodchild, C. *ibid* [1.25].

[3.19] Franklin, G. F., Powell, J. D. "*Digital Control of Dynamic Systems*" Addison Wesley 1980 pp.171-177.

[3.20] Goodchild, C. *ibid* [1.25].

CHAPTER FOUR

[4.1] Anon. *ibid* [1.20].

[4.2] Goodchild, C. *ibid* [1.5].

[4.3] Whitebeck, R. F., Hofmann, L. G. *ibid* [1.26]

[4.4] Szalai, K. J. "Flight Test Experience with the F-8 Digital Fly-By-Wire System" NASA Technical Note TD-7843. Feb 1975 pp.127-180.

[4.5] Kidd, W. M.: *ibid* [1.14].

[4.6] Franklin, G. F. "Fundamentals of Analysis for Digital Control Systems" *AGARD Lecture Series* No.128 Computer-Aided Design and Analysis of Digital Guidance and Control Systems. Sept 1983 pp.2.1-2.15.

[4.7] Kidd, W. M.: *ibid* [1.15].

[4.8] Moler, C., Little, J., Bangert, S.: *ibid* [1.28].

[4.9] Laub, A. J.: Numerical Aspects of Control Design Computations. *ibid* [4.6] pp.5.1-5.16.

[4.10] Franklin, G. F. *ibid* [4.6].

[4.11] Tretter, S. A. *ibid* [1.18].

[4.12] Franklin, G. F. *ibid* [4.6].

CHAPTER FIVE

[5.1] Solheim, O. A. "Some Integrity Problems in Optimal Control" *AGARD Conference Proc* No.137 Sept 1973 pp.4.1-4.10.

[5.2] Falb, P. L., Wolovich, W. A. "Decoupling in the Design and Synthesis of Multivarible Control Systems" *IEEE Trans Auotomatic Control*, AC Dec 1967.

[5.3] Aitken, J. C. "An Investigation of Two Alternative Methods of Lateral Control System Design" Cranfield Institute of Technology M.Sc Thesis 1980.

[5.4] Kailath, T. "*Linear Systems Theory*" Prentice-Hall 1980, Chapter Two Section 2.4 pp137-138.

[5.5] Falb, P. L., Wolovich, W. A. *ibid* [5.2].

[5.6] Harschburger, H. E., Moomaw, R. F. "Experience with the F/A-18 Digital Flight Control System" *IEEE/AIAA 5th Digital Avionics Systems Conference*. Nov 1983.

[5.7] Goodchild, C. "Sampled-Data Control System Analysis Techniques Implemented With Small Digital Computers" Marconi Research Centre ITM 81/122 Nov 1981.

CHAPTER SIX

[6.1] Sklansky, J. *ibid* [3.1].

[6.2] Kranc, G. M. *ibid* [1.22].

[6.3] Kalman, R. E., Bertram, J. E. *ibid* [1.23].

[6.4] Moler, C., Little, J., Bangert, S. *ibid* [1.28].

[6.5] Moorhouse, D. J., Woodcock, R. J. "Background Information and User Guide For MIL-F-8785C, Military Specification - Flying Qualities of Piloted Aircraft" Flight Dynamics Laboratory AFWAL-TR-81-3109, Wright-Patterson Air Force Base. May 1981.

[6.6] Solheim, O. A.: *ibid* [5.1].

[6.7] Fleming, P. J., Garcia Nocetti, D. F., Thompson, H. A. "Implementation of a Transputer-Based Flight Controller". *IEE Conf Proc Control 88*. Oxford April 1988 pp.719-724.

APPENDIX ONE

[A1.1] Goodchild, C. *ibid* [3.10].

[A1.2] Schultz, D. G., Melsa, J. L. "*State Functions and Linear Control Systems*". McGraw-Hill 1967 pp.7-68.

[A1.3] Chen, C. T. *ibid* [3.6] pp.25-64.

[A1.4] Hsu, J. C., Mayer, A. U. "*Modern Control Principles and Applications*. McGraw-Hill 1968 pp.131-179.

[A1.5] Roskam, J. "*Airplane Flight Dynamics*" Roskam Publishing 1979.

[A1.6] Shepherd, J. T., Stollery, J. L., Lipscombe, J. M. "The Effect of Guidance and Control on Missile Design" AGARD Short Course Notes. Rome 1979 pp.6.13-6.16.

[A1.7] Blakelock, J. H. "*Automatic Control of Aircraft and Missiles*" Wiley 1965 pp.138-139.

APPENDIX TWO

[A2.1] Powell, D. J., Katz, P.: *ibid* [1.21].

APPENDIX FOUR

[A4.1] Maybeck, P. S. "*Stochatic Models Estimation and Control Vol.1*" Academic Press 1979. pp.163-170.

[A4.2] Leondes, C. T. "*Advances in Control Systems Vol.3*" Academic Press 1966. p.243.

[A4.3] Gelb, A. (Ed) "*Applied Optimal Estimation*: MIT Press 1974 pp.75-79.

[A4.4] McRuer, D., Johnston, D. E., Meyers, T. T.: *ibid* [1.4].

APPENDIX FIVE

[A5.1] Goodchild, C.: *ibid* [1.25].

APPENDIX SEVEN

[A7.1] Tustin, A.: *ibid* [2.18].